

Winter 2013

Attachment Ability and Melanoma Inhibitory Activity mRNA Expression Level Changes in Murine B16-F10 Melanoma Cells Post Nanosecond Electric Pulses

Hongxia Jia
Old Dominion University

Follow this and additional works at: https://digitalcommons.odu.edu/biomedicalsciences_etds



Part of the [Cell Biology Commons](#), [Medical Biotechnology Commons](#), and the [Molecular Biology Commons](#)

Recommended Citation

Jia, Hongxia. "Attachment Ability and Melanoma Inhibitory Activity mRNA Expression Level Changes in Murine B16-F10 Melanoma Cells Post Nanosecond Electric Pulses" (2013). Doctor of Philosophy (PhD), Dissertation, , Old Dominion University, DOI: 10.25777/jzr8-gn86
https://digitalcommons.odu.edu/biomedicalsciences_etds/47

This Dissertation is brought to you for free and open access by the College of Sciences at ODU Digital Commons. It has been accepted for inclusion in Theses and Dissertations in Biomedical Sciences by an authorized administrator of ODU Digital Commons. For more information, please contact digitalcommons@odu.edu.

ATTACHMENT ABILITY AND MELANOMA INHIBITORY
ACTIVITY MRNA EXPRESSION LEVEL CHANGES IN MURINE
B16-F10 MELANOMA CELLS POST NANOSECOND ELECTRIC
PULSES

by

Hongxia Jia

Bachelor of Clinical Medicine, Master of Internal Medicine, June 2008, Nankai
University, Tianjin, China

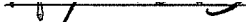
A Dissertation Submitted to the Faculty of
Old Dominion University in Partial Fulfillment of the
Requirements for the Degree of

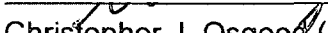
DOCTOR OF PHILOSOPHY


BIOMEDICAL SCIENCES


OLD DOMINION UNIVERSITY
December 2013

Approved by: 


R. James Swanson (Director)


Christopher J. Osgood (Member)


Lesley H. Greene (Member)


Shu Xiao (Member)

ABSTRACT

ATTACHMENT ABILITY AND MELANOMA INHIBITORY ACTIVITY MRNA EXPRESSION LEVEL CHANGES IN MURINE B16-F10 MELANOMA CELLS POST NANOSECOND ELECTRIC PULSES

Hongxia Jia
Old Dominion University, 2013
Director: Dr. R. James Swanson

The effects of high-voltage nanosecond electric pulses (nsEPs) on metastatic melanoma are still unclear. Hence, we applied one, two, three, and four 300 ns 40 kV/cm pulses to murine B16-F10 melanoma cells. Cell attachment ability was determined by comparing the number of floating cells and the percentage of attached cells. Melanoma inhibitory activity (MIA) is a secretory protein that is highly correlated with the malignancy and metastasis of malignant melanomas. We used MIA as our target to evaluate the effect of nsEPs on metastasis. Pulsed (experimental) and unpulsed (control) cells were incubated at 37°C under a 5% CO₂ atmosphere. To determine cell attachment ability, the culture medium supernatant and attached cells were collected at 6, 12, 18, and 24 h after a single pulse. The live, dead, and total floating cells in the culture medium supernatant were counted. In addition, the live, dead, and total attached cells were counted after multiple pulses. Total RNA was extracted from the attached cells and reverse transcribed into cDNA. The MIA mRNA expression levels were measured using the cDNA template via quantitative real-time PCR, with β -actin as the internal control. The experiment was repeated three times (n=3). The results show that a single pulse did not affect the cell attachment ability, cell morphology, and the MIA mRNA expression levels (P=0.8058). Two pulses significantly decreased the cell attachment ability (P=0.014), cell viability (P<0.0001), and changed the cell morphology, but did not change the MIA mRNA expression. The three-pulse and the four-pulse treatments significantly decreased the cell attachment ability (P=0.004, 0.00002, respectively), cell viability (P<0.0001), changed the cell morphology, and increased the MIA mRNA expression levels within the first 12 h (P=0.041, 0.001, respectively). These indices were almost normal at 24 h after pulsing. We speculate that the two-, three-, and four-pulse treatments would be optimal for treating melanoma metastasis, whereas the

single pulse treatment was not. Therefore, nsEPs provides a great opportunity for treating metastatic melanomas.

To my lovely husband Qiu
and Molly,
who have enriched my life
more than I ever could have imagined.

ACKNOWLEDGMENTS

I would like to thank my parents and my parents-in-law for their generous financial aid to our family, which allowed me study overseas and stay together with my husband and my daughter. Although they are not rich, they contributed money and clothes to us as much as they could. Words are not enough to express my thanks and love for them.

I am fortunate to have Dr. R. James Swanson as my academic advisor and mentor. He is a generous, kind, humorous, considerate, open-minded, and knowledgeable teacher and a good friend. He likes to inspire students to discover their research interests and support them with his endless knowledge, encouragement, and research supply, and even financial aid. I feel very lucky and grateful to be his student. Words do not sufficiently express my thanks to him.

I would like to thank my committee members, Dr. Christopher J. Osgood, Dr. Lesley H. Greene, and Dr. Shu Xiao for their time and valuable inputs. I would also like to extend my thanks to Dr. Lesley H. Greene for giving me the precious opportunity to rotate in her lab, which helped me broaden my knowledge and enhance my practical skills.

I would also like to thank Dr. David Gauthier providing research consumables and NanoDrop 2000 spectrophotometer for measuring the RNA purity and concentration, the gel electrophoresis apparatus, and the gel imaging system for RNA integrity and real-time PCR product size identification. I am thankful to Dr. Wayne L. Hynes for providing research consumables and the Bio-Rad iCycler™ Thermal Cycler for reverse transcription and Bio-Rad MiniOpticon™ Real-Time PCR Detection System for quantitative real-time PCR. I also appreciate Dr. Robert E. Ratzlaff for providing the low-speed centrifuge machine for cell collection. I also appreciate Dr. Shu Xiao, Dr. Yeong-Jer (Jack) Chen, and Dr. Muhammad Arif Malik for assisting me and adjusting the pulsing device. I also owe thanks to Dr. Kathryn F. Simmons for providing the ordering assistance for my endless order sheets.

I greatly appreciate Dr. R. James Swanson, Dr. Douglas J. Mills, Dr. Ralph W. Stevens, and Dr. Emilia Oleszak for supervising me teaching in the Gross Anatomy and Laboratory, the Human Cadaver Dissection and Laboratory, the Advanced Human Physiology and Laboratory, the General Biology lab, Human

Anatomy and Physiology Laboratory, and the Histology Laboratory. Their valuable knowledge and guidance of teaching techniques helped me a lot and inspired me to teach Advanced Human Physiology Lecture. They are good teachers and friends. I am blessed to have them as my supervisors.

I am truly grateful to Nardos Sori, Fang Li, Liang Yu, Yiling Chen, Bo Liu, Anthony Nanajian, Sylvere Ngabonziza, Elizaveta Svyatova, Logan Reddy, Philip Tan, Katherine Tan, Khalid Alarid, Rebecca Rough, David Britt, Janna Grubbs, Tyler Balak, Suresh Patthipati, Lakshmi Chekur, Lauren Browning, Feng Ding, Tao Huang, Kerry Lee, Nobel Egekwu, Chelsea Wright, Sharon Vaturi, Dorothy Yordt, and the others I have not mentioned. I am so happy to have these friends in ODU. I greatly appreciate their help during class, teaching, and research. They helped me have a wonderful time in ODU.

Nomenclature

7-AAD	7-aminoactinomycin D
ANOVA	analysis of variance
ATCC	American Type Culture Collection
bp	base pair(s)
CAMs	cell adhesion molecules
CD-RAP	cartilage-derived retinoic acid-sensitive protein
cDNA	complementary DNA
Cq	quantification cycle
DMEM	Dulbecco's modified Eagle's medium
DMSO	dimethyl sulfoxide
EDTA	ethylenediaminetetraacetic acid
FBS	fetal bovine serum
IHC	immunohistochemistry
J	Joule
kDa	kilodalton
MIA	melanoma inhibitory activity
mRNA	messenger RNA
NRT control	no reverse transcription control
nsEPs	nanosecond electric pulses
nsPEFs	nanosecond pulsed electric fieldsx
nt	nucleotide(s)
NTC	no template control
PBS	phosphate buffered saline
PCR	polymerase chain reaction
PI	propidium iodide
qPCR	quantitative PCR
RCF	relative centrifugal force
RPM	revolutions per minute
rRNA	ribosomal RNA
RT	reverse transcription
RT-qPCR	reverse transcription-quantitative PCR
SH3	Src homology 3

Src	sarcoma
VPD450	Violet Proliferation Dye 450

TABLE OF CONTENTS

	Page
LIST OF TABLES	xii
LIST OF FIGURES	xiv
 Chapter	
1. INTRODUCTION	1
1.1 CANCER MALIGNANCY	1
1.2 MELANOMA	1
1.3 MELANOMA INHIBITOR ACTIVITY (MIA)	2
1.4 TREATMENT OF METASTATIC MALIGNANT MELANOMA	3
1.5 nsEPS	5
1.6 nsEPS EFFECT ON CELL MEMBRANE	6
1.7 METHOD FOR MEASURING CHANGES IN ATTACHMENT ABILITY	6
1.8 CELL ATTACHING PROCESS	8
1.9 METHOD FOR MEASURING MIA mRNA EXPRESSION LEVEL ...	10
1.10 METHOD FOR MEASURING PCR EFFICIENCY	11
1.11 STATISTICAL METHOD FOR ANALYZING THE RESULTS	12
1.12 SIGNIFICANCE	13
1.13 INNOVATION	13
2. MATERIALS AND METHODS	15
2.1 EXPERIMENTAL DESIGN	15
2.2 CELL CULTURE	16
2.3 CELL COUNTING/VIABILITY ASSAY	18
2.4 PULSE GENERATORS	19
2.5 NANOSECOND PULSED ELECTRIC FIELD TREATMENT	23
2.6 SAMPLE COLLECTION FOR RNA EXTRACTION	23
2.7 LONG-TERM CELL VIABILITY TEST	26
2.8 TOTAL RNA EXTRACTION AND DNA ELIMINATION	26
2.9 PURITY AND QUANTIFICATION OF RNA	27
2.10 TOTAL RNA INTEGRITY TEST	28
2.11 RNA REVERSE TRANSCRIPTION	29
2.12 QUANTITATIVE REAL-TIME PCR	30
2.13 STATISTICS	32
3. RESULTS	34
3.1 CELL ATTACHMENT ABILITY TEST AFTER A SINGLE PULSE ...	34
3.2 CELL MORPHOLOGY AFTER A SINGLE PULSE	46
3.3 LONG-TERM VIABILITY TEST AFTER MULTIPLE PULSES	50

3.4	CELL ATTACH ABILITY AFTER MULTIPLE PULSES	61
3.5	CELL MORPHOLOGY AFTER MULTIPLE PULSES	64
3.6	RNA QUALITY CONTROL AND REAL-TIME PCR QUALITY CONTROL.....	69
3.7	DETERMINING REAL-TIME PCR AMPLIFICATION EFFICIENCY ..	76
3.8	MIA mRNA EXPRESSION LEVEL AFTER A SINGLE PULSE.....	84
3.9	MIA MRNA EXPRESSION LEVEL AFTER MULTIPLE PULSES	92
4.	DISCUSSION	102
4.1	CELL ATTACH ABILITY CHANGES AFTER nsEPS	102
4.2	CELL MORPHOLOGY CHANGES AFTER nsEPS.....	103
4.3	LONG-TERM VIABILITY TEST AFTER nsEPS.....	104
4.4	PCR EFFICIENCIES	104
4.5	MIA MRNA EXPRESSION LEVEL AFTER nsEPS	105
5.	CONCLUSIONS	108
	REFERENCES	110
	APPENDIX.....	118
	VITA.....	119

LIST OF TABLES

Table	Page
1 Composition of Complete Growth Medium (500 mL) Receipt	16
2 Genomic DNA Elimination Reaction Components	30
3 Reverse Transcription Reaction Components	30
4 Quantitative Real-Time PCR Reaction Components	31
5 Thermal Cycling Protocol	32
6 Number of Floating Cells and Cell Viability in the Growth Media	35
7 Rank of the Number of Live Cells in the Growth Media after a Single Pulse, Two-Way Fixed ANOVA Table	38
8 Rank of the Number of Dead Cells in the Growth Media after a Single Pulse, Two-Way Fixed ANOVA Table	39
9 Rank of the Total Number of Cells in the Growth Media after a Single Pulse, Two-Way Fixed ANOVA Table	39
10 Rank of Long-term Total Cell Viability (%) after Multiple Pulses, Two-Way Fixed ANOVA Table	51
11 Rank of Total Number of Live Cells after Multiple Pulses, Two-Way Fixed ANOVA Table	55
12 Natural Log Transformation of the Total Number of Dead Cells after Multiple Pulses, Two-Way Fixed ANOVA Table	59
13 Rank of the Percentage of Attached Cells after Multiple Pulses, Two-Way Fixed ANOVA Table	62
14 Purity and Concentrations of the Extracted Total RNA	72
15 Mean C _q Values of β -actin and MIA cDNA after a Single Pulse	84
16 Calibrated MIA mRNA Expression Level after a Single Pulse	86
17 Rank of MIA mRNA Expression Levels after a Single Pulse, Two-way Fixed ANOVA Table	88

18	Multiple Comparisons (Tukey's) Test	89
19	Mean C_q Values of β -actin and MIA cDNA after Multiple Pulses	92
20	Calibrated MIA mRNA Expression Level after Multiple Pulses (6 h and 12 h)	94
21	Calibrated MIA mRNA Expression Level after Multiple Pulses (18 h and 24 h)	95
22	Raw $-\Delta C_q$ of MIA mRNA Expression Level after Multiple Pulses, Two-way Fixed ANOVA Table	98
23	Multiple Comparisons (Tukey's) Test for Different Time Points	99
24	Multiple Comparisons (Tukey's) Test for Multiple Pulses	99

LIST OF FIGURES

Figure	Page
1 Solution Structure of Human MIA protein	4
2 Cell Attachment Process	9
3 Experimental Design Flow Chart	15
4 Pulse Forming Network	19
5 Single Pulse Generator	21
6 Multiple Pulses Generator	22
7 Samples arranged in a 24-well plate for single pulse	24
8 Samples arranged in a 24-well plate for multiple pulses	25
9 Interaction Plot of the Number of Live Cells between Treatments and Time Points after a Single Pulse	40
10 Number of Floating Live Cells after a Single Pulse	41
11 Interaction Plot of the Number of Dead Cells between the Treatments and the Time Points after a Single Pulse	42
12 Number of Floating Dead Cells after a Single Pulse	43
13 Interaction Plot of the Number of Dead Cells between the Treatment and the Time Points after a Single Pulse	44
14 Total Number of the Floating Cells after a Single Pulse	45
15 Cell Morphology after a Single Pulse	47
16 A Second Set of Cell Morphology Photographs	49
17 Long-term Total Cell Viability Interaction Graph after Multiple Pulses ...	52
18 Long-term Total Cell Viability after Multiple Pulses	53
19 Long-Term Total Number of Live Cells after Multiple Pulses	56
20 Long-Term Total Number of Live Cells after Multiple Pulses	57

21	Long-Term Total Number of Dead Cells after Multiple Pulses	60
22	Percentage of Attached Cells after Multiple Pulses	63
23	Cell Morphology at 6 h after Multiple Pulses	65
24	Cell Morphology at 12 h after Multiple Pulses	66
25	Cell Morphology at 18 h after Multiple Pulses	67
26	Cell Morphology at 24 h after Multiple Pulses	68
27	Gel Image of the RNA Sample and quantitative Real-time PCR product	70
28	Adjusted Gel Image to Show MIA Band	71
29	The NRT Negative Control and the NTC Negative Control	74
30	Melting Curve Analysis	75
31	Determination of Individual Amplification Efficiency Using LinRegPCR .	77
32	Box Plot of Amplification Efficiencies, Determined by LinRegPCR	78
33	Real-time PCR Amplification Efficiency Determined by qpcR	81
34	β -actin Real-Time PCR Amplification Efficiency	82
35	MIA Real-Time PCR Amplification Efficiency	83
36	MIA mRNA Interaction Graph	90
37	MIA mRNA expression levels (calibrated with β -actin) after a Single Pulse	91
38	MIA mRNA Interaction Graph after Multiple Pulses	100
39	MIA mRNA Expression Level (calibrated to β -actin) after Multiple Pulses	101

CHAPTER 1

INTRODUCTION

1.1 CANCER MALIGNANCY

The diagnosis of cancer malignancy is based on anaplasia, invasiveness, and metastasis (Mostofi et al., 1999). Anaplasia is the dedifferentiation of normal cells, wherein they loss structural and functional differentiation, and fail to develop recognizable growth patterns. Invasiveness is the ability to infiltrate and destroy the surrounding tissue. The invasiveness of cancer cells is related to intercellular adhesion (Turner and Sherratt, 2002). Metastasis is the movement of cancer cells from one original tissue or organ to other tissues or organs. Various types of cancer have different metastatic levels (Vinay et al., 2004).

1.2 MELANOMA

1.2.1 GENERAL CHARACTERISTICS OF MELANOMA

Melanomas are a malignant skin cancer derived from melanocytes. Melanomas are less common than other skin cancers, but they account for the majority of skin cancer deaths. Melanomas mainly occur in skin, but they can occur in any tissue that contains melanocytes. Melanomas derived from melanocyte. Most melanomas are dark pigmented, because of the melanin secreted by abnormal melanocytes. However, some melanomas called melanotic melanomas, are unpigmented.

The incidence rates of melanoma among Caucasians is 31.6 per 100,000 men and 19.9 per 100,000 women, much higher than Black and Asians/Pacific Islanders at 2 per 100,000 men or women (Howlader et al., 2012). Although the incidence rates of most cancer sites are decreasing, the incidence rates of melanomas among men and women are increasing (Siegel et al., 2013). About 61,300 cases of melanoma *in situ* are expected to be diagnosed in 2013 (Siegel et al., 2013).

1.2.2 MELANOMA METASTASIS

Numerous reports have shown the increasing incidence of melanoma metastasis and recurrence in both children and adolescents in Western Countries (Kopf et al., 1982; Rigel et al., 1996; Hoang and Eichenfield, 2000; Yeung, 1994). Sufficient evidence from case studies have shown that human melanoma metastasize to various organs in the human body, including the bladder (Toledano et al., 2009), brain (Cemil et al., 2008; Takahashi et al., 1990), breasts (Loffeld and Marsden, 2005), colon (Lesur et al., 2009), heart (Chrissos et al., 2008; Houmsse et al., 2004), liver (Arunkumar et al., 2001), lungs (Shin et al., 2011), nerves (Hashemi et al., 2009), penis (Kurul et al., 2006), placenta (Perret-Court et al., 2010), spleen (Buzbee and Legha, 1992), thyroid gland (Punda et al., 2010), and uterus (Luxman et al., 1997), among others. The most frequent target organs of metastases are the bones, brain, liver, and lungs (Langley and Fidler, 2011). The median survival for metastatic melanomas is very poor, only ranging from 2 to 8 months (Jemal et al., 2008) with only 5% of all patients surviving more than 5 years. Thus, metastatic melanomas are one of the most uncontrollable and mentally devastating cancers.

1.3 MELANOMA INHIBITOR ACTIVITY (MIA)

1.3.1 FUNCTION OF MIA

The growth of human malignant melanoma cells can be regulated by autocrine and paracrine growth factors in a culture supernatant (Bogdahn et al., 1989). MIA protein has been isolated from the culture supernatant of human melanoma cells lines and it potently suppresses the growth of malignant melanoma cells by inhibiting DNA synthesis and causing cell rounding (Blesch et al., 1994). MIA mRNA was reported as expressed in non-metastatic melanoma cell lines but was absent in highly metastatic cell lines (van Groningen et al., 1995). However, subsequent analyses have shown contrasting results. High serum MIA levels correspond to high malignancy and metastasis in malignant melanoma patients (Bosserhoff et al., 1997a). In mice, the invasion of lung metastasis is strictly correlated with levels of MIA secretion (Bosserhoff et al., 2001). MIA overexpression is correlated with higher rates of extravasation and invasion (Guba et al., 2000).

MIA has been independently identified from primary bovine chondrocytes and cartilage tissue as cartilage-derived retinoic acid-sensitive protein (CD-RAP), which is necessary for cartilage development and maintenance (Dietz and Sandell, 1996). Hence, the term MIA/CD-RAP refers to MIA. MIA is involved in malignant melanoma progression and spread by mediating cellular detachment from extracellular matrix proteins, including fibronectin (Bosserhoff et al., 2003) and integrin (Bauer et al., 2006). MIA is also expressed in breast cancer (Bosserhoff et al., 1999), gastric cancer (Aung et al., 2005), and pancreatic cancer (El Fitori et al., 2005). Low doses of MIA enhance mesenchymal stem cell migration, whereas high doses inhibit cell migration (Tscheudschilsuren et al., 2006). Extremely low levels of MIA mRNA are present in various normal and neoplastic cell types (De Vries et al., 1999).

MIA is a highly specific and sensitive marker for clinically follow-up and therapy monitoring (Bosserhoff and Buettner, 2002). Thus, we choose to evaluate MIA as a mediator for melanoma malignancy and metastasis.

1.3.2 STRUCTURE OF MIA

The human MIA precursor has 131 amino acids. The secreted MIA is 11 kDa, consisting of 108 amino acids, and forms a small globular protein via two intramolecular disulfide bonds (Blesch et al., 1994). Src (sarcoma) homology 3 (SH3) is a small protein containing 64-77 amino acids. They form five or six β -strands producing two anti-parallel β -sheet. Multidimensional NMR shows that MIA adopts Src homology 3 (SH3) domain-like folds: two perpendicular, antiparallel, three-strand, and 5-strand β -sheets (Stoll et al., 2001). MIA has a single-domain. The solution structure of human MIA protein is shown in Figure 1. The PDB ID of human MIA protein is 1K0X. The folded core of MIA is rigid; however, several loops that connect the β -sheets have increased mobility, indicating the extended interactions of SH3 domains (Stoll et al., 2003). The mouse MIA gene is 1.5 kbp and consists of four exons (Bosserhoff et al., 1997b). Mature mouse MIA has 130 amino acids. MIA dimerization was recently found to be correlated with functional activity (Schmidt et al., 2012).

1.4 TREATMENT OF METASTATIC MALIGNANT MELANOMA

The most common treatment of melanoma is resection. For unresectable

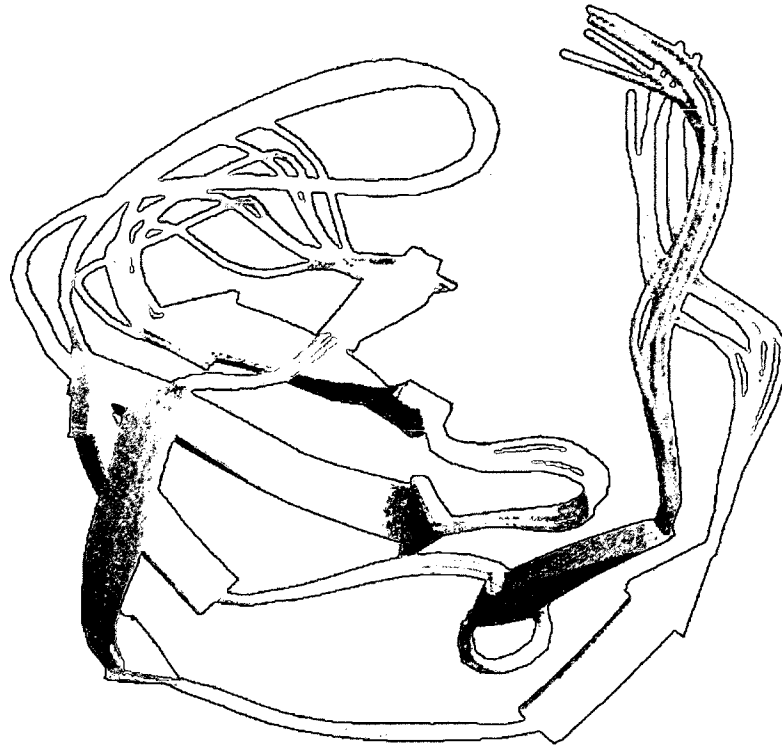


Figure 1. Solution Structure of Human MIA protein

Human MIA protein has 7 β -sheets. It contains a SH3 subdomain. The N- and C-terminal end have about 20 amino acids each which fold toward the SH3 subdomain. The picture was obtained from Protein Data Bank.

malignant melanomas, other treatments that are clinically used include single drug and multidrug chemotherapy (e.g., dacarbazine, hydroxyurea), immunotherapy (e.g., interleukin-2, interferon- α), and biochemotherapy (e.g., dacabazin/interferon- α combination)(Mouawad et al., 2010).

Considering that the incidence of melanoma deaths continues to increase despite the wide availability of surgical and chemical treatments and heightened concerns regarding patient with tumor survival, novel treatments for inhibiting metastasis progression, prolonging patient survival, and enhancing quality of life are urgently necessary.

New alternative approaches using electric pulse treatment are being explored.

Electrochemotherapy is an alternative treatment that combines drug therapy with microsecond-scale electric pulses, which causes electroporation (Kubota et al., 2005). Irreversible electroporation is a non-thermal tumor ablation therapy that uses continuous microsecond-scale pulses to permanently permeabilize the cell membrane (Al-Sakere et al., 2007). Another treatment uses nsEPs to induce apoptosis within the cancer cells (Schoenbach et al., 2007).

1.5 nsEPS

nsEPs are pulses with nanosecond durations. nsEPs have pulse rise times that are much shorter than the redistribution time of plasma membrane lipid bilayers. Thus, nsEPs penetrate the cell membrane and probable most organelle membranes (Nuccitelli et al., 2009b). nsEPs cause small pores in the membrane without significant heating. A single 300 ns electric pulse only deposits 0.2 Joule (J) of energy and penetrates the membranes without significantly heating the melanoma (Nuccitelli et al., 2006).

nsEPs generate intense nanosecond pulsed electric fields (nsPEFs), which are widely used in many bioelectric applications (Romeo et al., 2010), for example manipulating lipid nanopores in the cell membrane (Pakhomov et al., 2009). One report showed that nsPEFs accelerate platelet aggregation (Zhang et al., 2008). Our colleagues have also shown that murine B16-F10 melanoma cells under nsPEFs therapy die through a combination of electrical effects (major) and thermal effects (minor to negligible) (Xiao et al., 2011). Our previous research showed that nsPEFs therapy initiates apoptosis in melanomas, achieving completed remission without recurrence in mice (Nuccitelli et al., 2009a). Despite the remarkable progression of nsPEFs research, metastatic data on the link between the nsPEFs and malignant melanoma are still lacking. Thus, we selected murine B16-F10 melanoma cells and the similar pulse condition (300 ns duration, 40 kV/cm power, but not 100 pulse number, 17 Hz lower frequency) (Nuccitelli et al., 2009a) to study the changes in cancer malignancy or metastasis at the low pulse numbers of, one, two, three, and four pulses *in vitro*. We chose fewer pulses for the following reasons:

1. The final goal of this research is to determine a new method for treating metastatic melanoma. If this method works, both metastatic melanoma cells and normal tissue cells would necessarily be pulsed *in vivo*. We

expect that metastatic melanoma cells would be killed or inhibited, whereas the normal tissues would not.

2. To our knowledge, this study is the first to measure MIA after high-voltage nsPEs treatment. We expect one of three possible results: inhibition, stimulation, or no effect on MIA mRNA expression. Although, we hope to show an inhibitory effect from this method, no effect would be a better finding than stimulation because such a result would indicate that pulses at least do not further aggravate melanomas.
3. In terms of research feasibility, pulsed melanoma cells must remain alive so that total RNA may be extracted from melanoma cells, and MIA mRNA expression can be measured. Based on the cell viability under similar pulse conditions, 10 pulses would significantly increase trypan blue cell intake (Ford et al., 2010). Thus, pulses fewer than 10 should suitably advance our research.

1.6 nsEPS EFFECT ON CELL MEMBRANE

nsEPs cause long-lasting (minutes) cell membrane permeabilization in mammalian cells and the gradual recovery could take 15 min (Pakhomov et al., 2007a). Unlike classical electroporation conditions, nsEPs causes fewer and smaller pores, as well as more rapid resealing rates (Beebe et al., 2003). The maximum pore size of the cell membrane after nsEPs treatment is around 1 nm (Pakhomov et al., 2009). This small pore size would not allow trypan blue go through. Thus, nsEPs do not trigger the cell membrane to immediately uptake the membrane-impermeable marker dyes, such as trypan blue and propidium iodide (Pakhomov et al., 2007b; Thomas Vernier et al., 2004). Thus, trypan blue can be used to test cell integrity and viability tests are still valid if all the pores are resealed.

1.7 METHOD FOR MEASURING CHANGES IN ATTACHMENT ABILITY

Several methods are available for testing cell adhesion and attachment ability. One method is called centrifugal force-based adhesion assays (Angres et al., 1996). This assay tests cells bond for adhesion ability. A cell monolayer is formed at the bottom of the microtiter well. Radioactively labeled cells are seeded into the monolayer by centrifugation. Another microtiter with growth medium is

mounted on top of the first microtiter, forming a sealed chamber. Afterward, the sealed chamber is incubated, inverted, and centrifuged to dislocate the unbound radioactively labeled cells from the monolayer. The sealed chamber is then frozen and clipped into top, middle, and bottom layers. The radioactivity in the three layers is measured, and the percentage of bound cells indicates the adhesion ability.

The other method is using a standard physical agitation procedure to test cell detachment ability (Zhu et al., 2002). This assay tests cell detachment for adhesion ability. A layer of cell adhesion molecules, such as collagen I and collagen IV, are spread on the surface of cell culture plate. Cells are seeded into the plate and incubated for 24 h. The plate is then placed on a motorized shaking table at 40 hertz for 10 min to 50 min. Afterward, the detached cells are collected from the growth medium and counted using 3-(4,5-Dimethylthiazol-2-yl)-2,5-diphenyltetrazolium bromide (MTT), which turns purple if the cells are alive and yellow if the cells are dead. The percentage of cells that remain attached indicates the adhesion ability.

The third method involves measuring the percentage of attached live cells among the total number of live cells. The total number of cells includes the floating cells in the growth media and the attached cells on the cell culture plate. Cell number is counted using trypan blue on a hemocytometer. Trypan blue is a large blue hydrophilic dye with two azo chromophores. Trypan blue is an acid tetrasulfonated negatively charged dye. Trypan blue cannot enter cells unless their cell membranes are broken. Clear or unstained cells indicate intact cell membranes. The blue stained cells indicate damaged cell membranes. Normally, trypan blue is used as a vital stain because live cells exclude trypan blue outside the membrane, whereas dead cells allow trypan blue to penetrate the cell. Thus, the trypan blue exclusion test is called trypan blue viability test. However, in some special circumstances, such as pore formation, trypan blue intake does not indicate cell death. Trypan blue can enter the cell if the pore is large enough. Hence, the trypan blue exclusion test is called trypan blue uptake test. The pores may last for several seconds, or minutes. The duration of pores formed by nsEPs is still under development.

Cell adhesion includes cell attachment and cell detachment. The first two adhesion assays determine cell detachment ability. The last adhesion assay tests

cell attachment ability. In this study, we tested cell attachment ability using the last adhesion test method. The number of live, dead, and total floating cells and the percentage of live attached cells among the total live cells were used to examine the changes in cell attachment ability after nsEPs.

1.8 CELL ATTACHING PROCESS

Changes in cell shape were observed during cell division based on the time-lapse video recording of the dividing cells (Piel et al., 2001) (Figure 2). The just-attached cells were round, and the cell contents moved from the center to one end and then from one end to the opposite end, forming a spindle shape. Afterward, the cell contents move from one end to the other end, forming an umbrella shape. The cell began to grow and the cell contents spread out to more area, forming a stellate or polygonal shape. Some cell contents move from one process to another process, which leave the old processes as a spinous shape. Finally, the cell rounds up again to divide.

This cell attachment process provides a useful tool for measuring changes in cell attachment ability after pulse. We tested the cell attachment process of the pulsed and unpulsed cells by photographing them at 6, 12, 18, and 24 h.

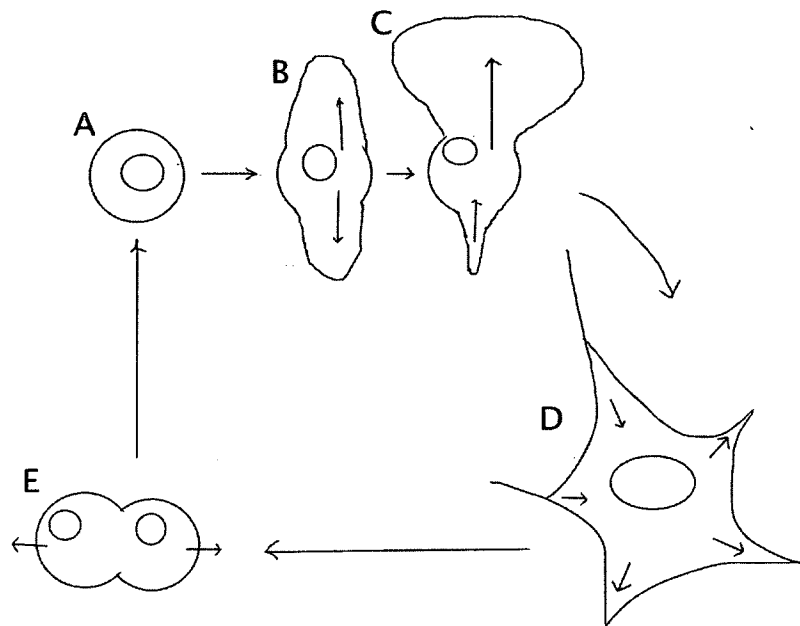


Figure 2. Cell Attachment Process

- (A) The cell after division. The cell is round.
- (B) Cell contents move upward and downward. The cell becomes spindle shaped.
- (C) Cell contents move to one end. The cell forms an umbrella shape.
- (D) Cell grows and the cell contents spread out. The cell forms a star or polygonal shape. The cell contents move towards the cell center, leaving two spines. DNA synthesis and the preparation of cell division cause a large nucleus.
- (E) One cell divided into two daughter cells. The daughter cells are round.

1.9 METHOD FOR MEASURING MIA mRNA EXPRESSION LEVEL

Two methods are normally used to quantify mRNA expression level: northern blot analysis and RT-qPCR. Northern blot analysis has three basic steps. The first step is to separate the RNA sample through gel electrophoresis. The second step is hybridizing the separated RNA sample bands with radioactive or fluorescence-labeled RNA probes. The labeled RNA probe is specific, and only binds to the target sequence. The third step is measuring the radioactivity or fluorescent intensity of the probe-bound band in a gel image. However, northern blot analysis requires large quantities of the RNA target in the sample and it is not completely accurate.

RT-qPCR is the combination of reverse transcription (RT) and quantitative (real-time) PCR (qPCR). Reverse transcription creates a single-stranded complement DNA (cDNA) template from the mRNA. The cDNA template is then amplified using a normal PCR process; however, the amplification detection is special for qPCR.

Two types of dyes are used in qPCR. One is a fluorescent probe that specifically binds to the target sequence and fluoresces only when they bind to the target. The fluorescence intensity from the probes increases as the amplification progresses because the probe binds to more of the target sequences. The other type is an intercalating dye, such as SYBR Green, which only binds to double-stranded DNA, but not to single-stranded DNA. The double-stranded DNA-SYBR Green complex absorbs light at 497 nm and emits green light at 520 nm. The exact amount of cDNA is determined in terms of green fluorescence.

Both types of dye can theoretically detect a single copy of the target cDNA. The advantage of the probe method is its high specificity; however, it is very expensive. The SYBR Green method is less expensive; however, it is less specific because double-stranded DNA also fluoresces. However, if the PCR reaction is very specific, i.e., it produces only the expected PCR product, the SYBR Green method can also be highly specific.

For this study, we used SYBR Green RT-qPCR to measure MIA mRNA expression levels. The single PCR product and its size were tested to ensure PCR specificity.

Quantitative real-time PCR uses internal control, such as β -actin, to

normalize the target mRNA expression level. β -actin forms cytoskeleton and is involved in structure and motility of a cell. β -actin is highly conserved and generally represented in all most every tissue. β -actin is formed by 375 amino acids. The molecular weight of β -actin is 42 kDa. Because of the stable expression of β -actin, it is well accepted to be the internal control of real-time PCR.

1.10 METHOD FOR MEASURING PCR EFFICIENCY

The amplified sequence is called an amplicon. PCR efficiency is the doubling of the amount of amplicon at each cycle. The theoretical PCR efficiency is 2, which indicates the amount of amplicon doubles at each cycle. PCR efficiencies ranging from 190 % to 210 % are satisfactory.

qPCR efficiency can be measured using two methods: the dilution or standard curve method and the amplification curve method.

The dilution or standard curve method uses a dilution series of templates to perform amplification. The quantity and Ct values of these amplifications are plotted on a graph, which is called the standard curve. The linear regression slope of the curve is used to calculate the PCR efficiency (Equation 1). Normally, tenfold dilutions are much better than twofold dilutions because the regression slope is confined to a smaller range (more accurate). The data for the standard curve should be repeated at least three times. The ideal slope is -3.32, which correlates to the PCR amplification efficiency of 2 (some researchers use 100%).

$$\text{Efficiency} = 10^{\left(-\frac{1}{\text{Slope}}\right)} \quad (1)$$

The standard curve method is simple and is traditionally used, but it needs a large amount of the template to perform at least six tenfold dilutions (1, 10, 100, 1000, 10000, 100000). This requirement is impossible for our study because we only have small amounts of the MIA cDNA template. After only three dilutions, the Cq values would be out of 40 cycles.

The amplification curve method uses computer software to calculate PCR efficiency for every individual qPCR. Software such as LinRegPCR and qpcR are freely available to the public and accepted by journals. Both programs calculate efficiency from the log linear phase of the qPCR fluorescence curve. LinRegPCR is very easy to use in Windows system. It allows the manual adjustment of the

upper and lower limits of the calculating range (Figure 31 on Page 77). The PCR efficiency results can be exported to an Excel sheet, which is very easy to analyze further. qpcR is a software package for R programming program that can be used in Windows, Mac, and Linux systems. In qpcR, we must first choose the best model to fit the raw fluorescence curve. We type in commands to calculate the PCR efficiency (Page 79).

The advantage of both LinRegPCR and qpcR is that they need smaller amounts of the template (theoretically one copy of template). LinRegPCR can be partially adjust manually, but it can only be used in Windows. By contrast, qpcR can be used on Windows, Mac, and Linux systems, but it cannot be manually adjusted, and it can only be adjusted through commands.

The amplification curve method was used in this study because the amount of MIA cDNA template was too low for the standard curve method. Both LinRegPCR and qpcR were used to determine qPCR efficiency.

1.11 STATISTICAL METHOD FOR ANALYZING THE RESULTS

Different group means can be compared using a t-test and an analysis of variance (ANOVA).

In the t-test, also called Student's t-test, the test statistics follows a Student's t distribution if the null hypothesis is supported. T-tests are normally used to compare two sets of data to determine whether they are significantly different from each other. If the scale parameter is large enough, the t-test can also be used for a normal distribution.

In ANOVA, the observed variance is partitioned into the components attributed to different sources of variation. An ANOVA is used to determine whether the means of at least two groups are equal or not. The different treatments or experimental procedures are called factors. For example, the treatment (pulse) and time points are two factors. ANOVA can be classified as fixed, random, or mixed. For fixed ANOVA, the dependent factors are assigned to the subjects. For random ANOVA, the dependent factors are randomly applied by the subjects. Mixed ANOVA is a combination of fixed and random ANOVA.

Using multiple t-test to compare means of multiple groups increases the chance of type I error, wherein the null hypothesis is true but is rejected. Thus, an ANOVA is used to compare two or more groups means. Follow-up tests such as

Tukey's test are used to compare two sets of data within the groups.

In this study, a two-factor fixed ANOVA and Tukey's follow-up test were used to compare the differences between the experimental group (pulsed group) means and the control group (unpulsed group) means, as well as among the means of four time points.

1.12 SIGNIFICANCE

High-voltage nsEPs are very useful for treating the melanoma in situ; however, curable treatment of metastatic melanoma remains limited. Evidence related to the effect of nsEPs on malignant melanomas is still inconclusive. Furthermore, the subsequent influence of nsEPs on melanoma metastasis is largely unknown. This study evaluates the effect of nsEP treatment (exposure) on the malignancy and metastatic marker MIA in murine B16-F10 melanoma cells. The results will enhance our understanding of the relationship of nsEP treatment and its positive and negative effects on melanoma malignancy or metastasis. Such information is critical for establishing proper nsEP treatments that can inhibit melanoma metastasis, reduce melanoma malignancy in humans, and increase patient with tumor survival.

Finding the relationship of nsEP treatment with melanoma malignancy and with inhibiting metastasis may inspire research on a new field of melanoma treatment.

1.13 INNOVATION

Our research is the first to study changes in MIA expression after applying high-voltage nsEPs. This dissertation evaluates nsEPs from a fresh point of view, which may yield a potential tool for treating melanoma metastasis. This research will increase knowledge in applying nsEPs in cancer research. Considering longer-term outcomes, this research may serve as a reference for future studies on nsEPs pulsing conditions. The effective treatment of malignant melanoma will significantly benefit public health. The next logical stage of research beyond this current application is to establish several guidelines for studying the mechanism of melanoma metastasis. The long-term goal of our laboratory is to develop and apply a new treatment for controlling melanoma metastasis and reducing melanoma malignancy. Completion of this research will allow us to obtain a better

understanding of the nsEPs effect on melanoma malignancy and metastasis. In the long run, understanding the interaction of nsEPs and melanoma during the regulation of melanoma metastasis will (1) lead to the development of new therapeutic modalities that activate melanoma responses and limit metastasis, (2) identify novel metastasis regulators that could be exploited as anticancer drug targets, and (3) identify melanoma responses that similarly control the development of other medically important obligate pathogens.

CHAPTER 2

MATERIALS AND METHODS

2.1 EXPERIMENTAL DESIGN

The design of this study was represented as shown in Figure 3.

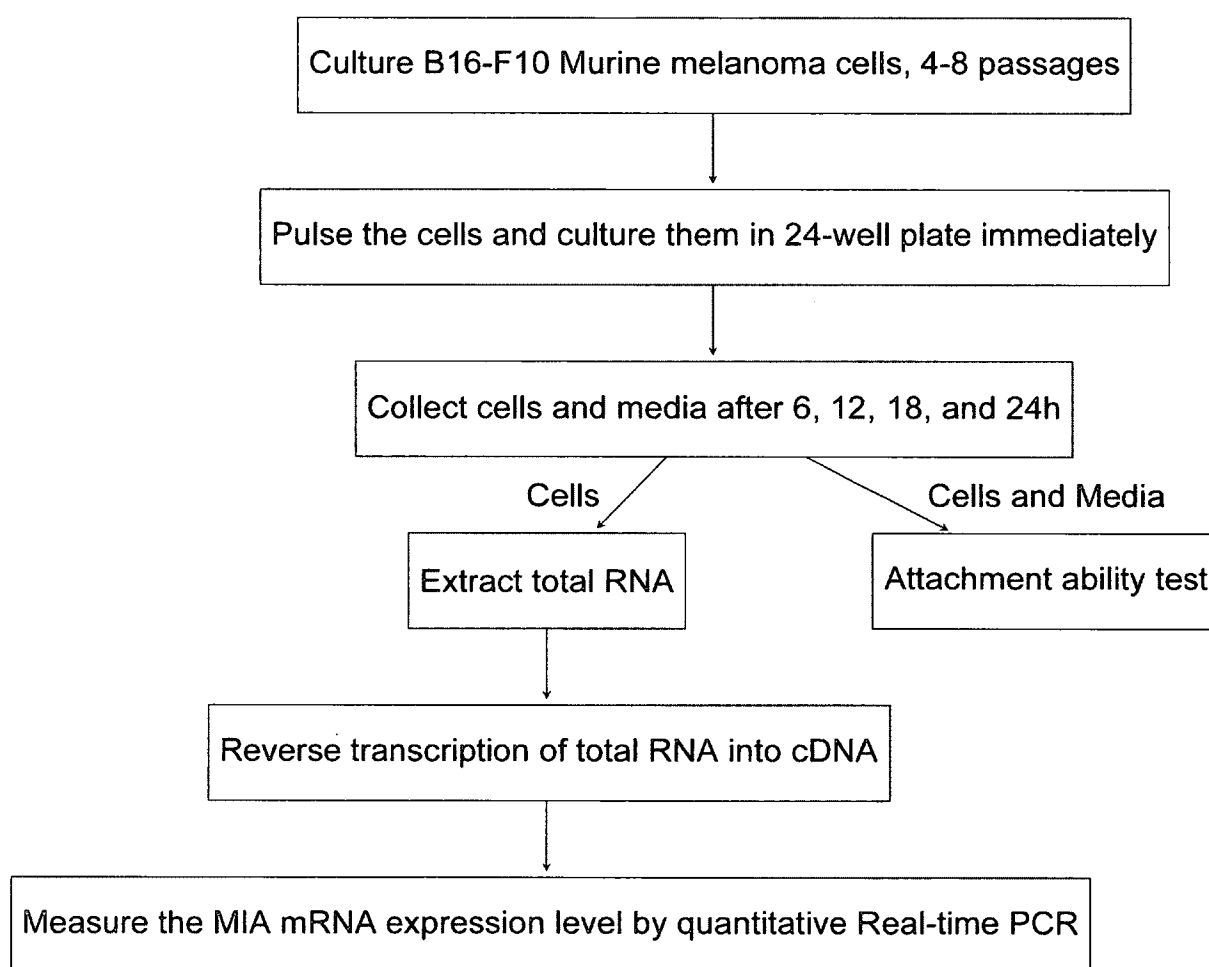


Figure 3. Experimental Design Flow Chart

2.2 CELL CULTURE

Frozen B16-F10 cells (ATCC® CRL-6475™) were kept in liquid nitrogen vapor phase until it thawed to maintain their viability. The composition of the complete growth medium is modified according to *Product Information Sheet for ATCC® CRL-6475™* (Table 1).

Table 1. Composition of Complete Growth Medium (500 mL) Receipt

Gradients (Abbrev., Source)	Catalog No.	Final Concentration (Final %)	Volume (mL)
ATCC-formulated Dulbecco's modified Eagle's medium (DMEM, ATCC)	30-2002	Base medium	430
Fetal bovine serum (FBS, GIBCO)	16141-061	10%	50
200 mM L-Glutamine (Mediatech, Inc.)(Nuccitelli et al., 2009a)	25-005-CI	4 mM (2%)	10
5000 IU/mL Penicillin-5000 µg/mL Streptomycin solution (Mediatech, Inc.)	30-001-CI	100 I.U./mL/100 µg/mL (2%)	10

2.2.1 RECOVERY OF CRYOPRESERVED CELLS PROCEDURE

Recovery procedures were modified according to *Product Information Sheet for ATCC® CRL-6475™*. Approximately, 20 mL of fresh complete growth medium was warmed in an incubator for at least 30 minutes to 1) warm up the medium to prevent chilling the cells and 2) reach normal pH (7.0 to 7.6) to prevent killing the cells under excessive alkalinity. The cap of the tube was loosened during the warming in the incubator. The 37°C water bath was turned on at the same time. When the water bath was ready, the frozen vial containing melanoma cells was removed from the liquid nitrogen. The cells were then thawed through gentle agitation in the 37°C water bath for approximately 2 minutes or until all the

contents were thawed by holding the cap with forceps and maintaining the o-ring of the vial was above the water level. The vial was removed from the water bath and sprayed with 70% ethanol to prevent contamination.

In a culture hood, the vial content was transferred into a sterile 15 mL centrifuge tube containing 9.0 mL of complete growth medium. The 15 mL centrifuge tube (Corning, Catalog No. 430766) was spun at $125 \times g$ ($R=16$ cm, 836 rpm, calculated via Equation 4) for 5 minutes on a low-speed centrifuge machine. Approximately, 4.5 mL of complete growth medium was added into 25 cm² culture flasks (LUX Scientific Corp., Catalog No. 5325). The supernatant was then removed and discarded. The cell pellet was resuspended with 3 mL of complete growth medium, and then dispensed into a 25 cm² flask to obtain a total volume of 7.5 mL. The flask was incubated at 37°C under a 100% humidified 5% CO₂ atmosphere in a water-jacketed cell culture incubator (NUAIR, model# NU-4750). The cells were checked daily. The complete growth medium was renewed every 2 to 3 days.

2.2.2 SUBCULTURE PROCEDURE

The subculture procedures were modified according to *Product Information Sheet for ATCC® CRL-6475™*. Approximately 36 mL of complete growth medium was warmed in a 50 mL centrifuge tube (Corning, Catalog No. 430921) in an incubator for at least 15 minutes. The cap of the tube was loosened during the incubation. About 5 mL of Trypsin-EDTA (0.25% Porcine Trypsin in HBSS, with 0.02% EDTA-2Na and without Ca and Mg, SAFC Biosciences, Catalog No. 59428C) was warmed for at least 15 minutes in a 15 mL centrifuge tube in an incubator. The old culture medium was then removed and discarded.

To remove all traces of serum, which contains trypsin inhibitor, the cell layer was rinsed with 2 mL of prewarmed Trypsin-EDTA. About 3 mL of prewarmed Trypsin-EDTA solution was added to the flask, and the cells were observed under a Nikon inverted microscope for 5 to 10 min until the cells were rounded and dispersed. To avoid clumping, the cells were not be disturbed, such as hitting or shaking, during detachment. Approximately 7 mL of prewarmed complete growth medium was added to a total of 10 mL, and the cells were aspirated by gently pipetting to prevent bubble formation and cell damage. About 29 mL of prewarmed complete growth medium was added into a new 75 cm² flask. About

1 mL of cell suspension was added into the new flask, to a total of 30 mL. The subculture ratio is 1:10. The new flask was then incubated at 37°C in a 100 % humidified 5% CO₂ atmosphere. The cells were subcultured every 3 days to 4 days or once the cells reached 90% confluence.

2.2.3 CRYOPRESERVATION PROCEDURE

The cryopreservation procedures were modified according to *ATCC® Animal Cell Culture Guide*. The cell culture was checked for contamination with bacteria, mycoplasma, fungi, and viruses immediately before cryopreservation. The cryoprotectant medium consisted of complete growth medium with 5% (v/v) DMSO (Mediatech Inc., Catalog No. 25-950-CQC). The cells were collected via Trypsin-EDTA treatment and gently centrifuged (5 minutes at 125× g). Afterward, the cells were resuspended in the cryoprotectant medium.

The cell concentration was adjusted from 1×10^6 to 5×10^6 viable cells/mL using a hemocytometer. CryoTube vials (Thermo Scientific, Catalog No. 375353) were labeled with 'Mouse Melanoma', passage number, date, and contributor. Then, 1 mL of cell suspension was added into each of the vials and the cap was closed. The cells were then allowed to equilibrate in the cryoprotectant medium at room temperature for at least 15 minutes, but no longer than 40 minutes. Approximately, 91 % of isopropyl alcohol was added to the fill line on the Nalgene® Mr. Frosty® Cryo 1°C Freezing Container (Thermo Scientific, Catalog No. 5100-0001). The tube holder was carefully replaced onto the container. CryoTube vials containing cells were placed into the holes in the tube holder. The freezing container was placed at the bottom of a –80°C freezer, and left undisturbed for 24 h. The frozen vials were then quickly transferred from the frozen container into the vapor-phase of liquid nitrogen tank for long time storage.

2.3 CELL COUNTING/VIABILITY ASSAY

Cell counting and viability assay were carried out using a hemocytometer (AO Scientific Instruments, Bright-line®). The procedures were modified according to *ATCC® Animal Cell Culture Guide*. The media of the pulsed and unpulsed cells were collected at 6, 12, 18, and 24 h after nsEPs. Cell viability was measured via the following procedures. Exactly 50 µL of cell suspension was mixed (1:1) with 50 µL of 0.4% (w/v) trypan blue solution in normal saline (Mediatech Inc., Catalog

No. 25-900-CI). The mixture was then incubated for 2 min to 5 min. The hemocytometer was cleaned, dried, and assembled with the cover slip. Exactly 100 μL of cell mixture was loaded onto the edge of each of the two counting chambers. The cell mixture was drawn automatically into the counting chamber through capillary action.

The hemocytometer was placed under a Nikon inverted microscope and the cells were viewed at 100 \times magnification. Nonviable cells were stained blue and viable cells remained unstained (transparent or clear). The number of viable and nonviable cells in the squares in the four corners and the square in the center were counted and recorded. The number of cells was the average of these five areas. The average number in the top section and the bottom section were added and multiplied by 10^4 cells/mL. Cell viability was calculated using Equation 2:

$$\text{Cell viability (\%)} = \frac{\text{Number of viable cells}}{\text{Total number of cells}} \times 100\% \quad (2)$$

2.4 PULSE GENERATORS

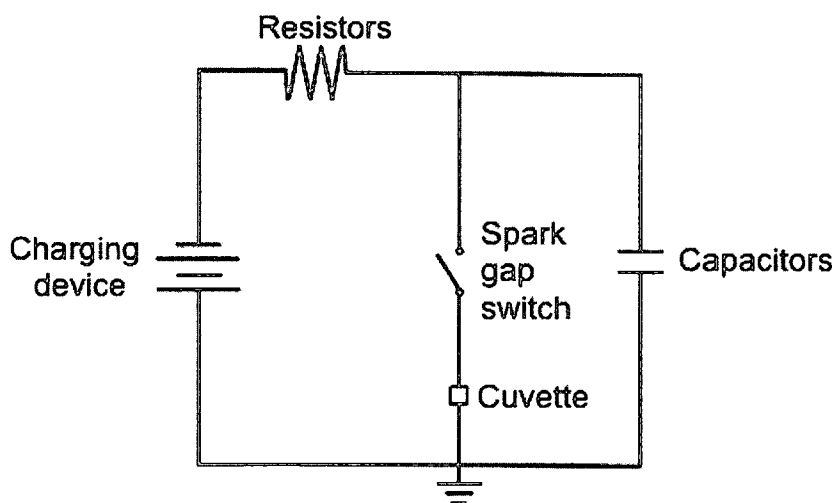


Figure 4. Pulse Forming Network

Pulse forming network is formed by two parallel circuits. One circuit includes the charging device, resistors, and capacitors. The other circuit includes the same capacitors, the biological sample in the cuvette, and a switch. The figure has been modified (Beebe et al., 2010).

Pulse generators are electronic equipments used for generating pulses. In this study, two 300-nanosecond pulse generators were used. One pulse generator based on the pulse forming network (Beebe et al., 2010) was designed in the Frank Reidy Research Center for Bioelectrics, and the assembly was modified by Dr. Yeong-Jer (Jack) Chen. This pulse generator for single pulse consists of charging device, resistors, inductors, high-voltage capacitors, and switch arranged in a pulse forming network configuration (Figure 4). Seven pairs of high-voltage capacitors (Figure 5A) were charged through five resistors to 4 kV. The capacitors were then discharged by a spark gap switch into a 0.1 cm electrode gap cuvette (Figure 5B) to generate a single 300 ns 40 kV/cm pulse. The high voltage across the cells was tracked using a high-voltage probe (Tektronix, P6015A), and the voltage (Figure 5C) was monitored using a digitizing oscilloscope (Tektronix, TDS3052). The pulse wave shown in this study has a sharp peak caused by the low resistance of the resistors around the cuvette. This peak in electric current also went through the cells.

To modify the pulse wave into a more square shape without peaks, another 300 ns pulse generator for multiple pulses was designed in the Frank Reidy Research Center for Bioelectrics, and the assembly was modified by Dr. Shu Xiao. This pulse generator employs a transmission line architecture. The transmission line included five parallel cables, each with an impedance of 50 Ω . The total impedance of the five parallel cables was 10 Ω . The pulse duration was proportional to the length of the cable. The longer the cable is, the higher the capacitance it has, thereby prolonging the pulse it delivers. The charges were stored in the cables and released once they were connected to the cuvette by a high-voltage switch. The high voltage across the cuvette was monitored and recorded with a digitizing oscilloscope (Tektronix, TDS 380) (Figure 6). The pulse wave shown in this study was nearly a rectangular, which had few and much lower peaks. The frequency of the pulses generated from this pulser was about 17 Hz. This improvement significantly reduced the unnecessary electric current after the nsEPs and allowed the cells to be pulsed more accurately.

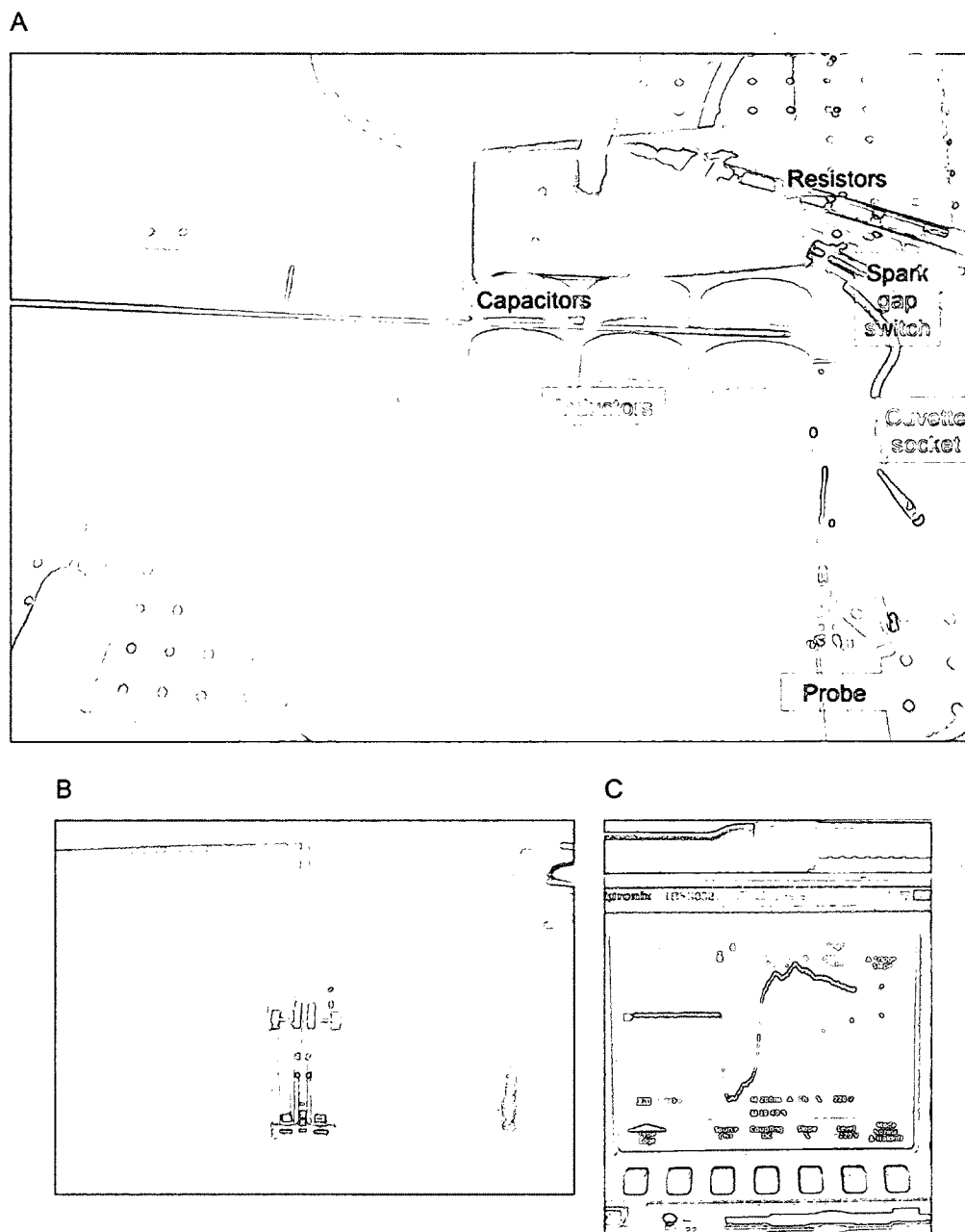


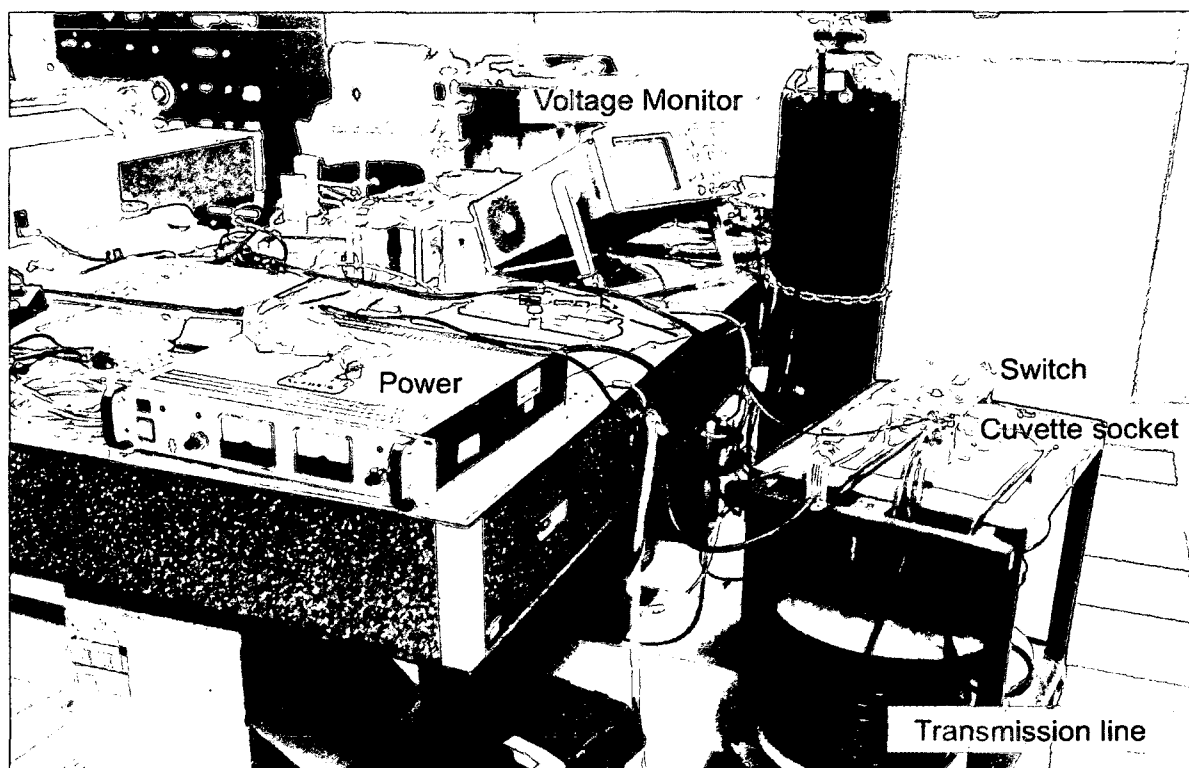
Figure 5. Single Pulse Generator

(A) Experimental setup. The charging device (not shown), resistors, and capacitors with inductors were connected in a circuit. The rod of the spark gap switch was manipulated by hand by obtaining the switch toward the capacitors. The electrical breakdown of the air will close the parallel circuit, which triggered the capacitors to charge the cells.

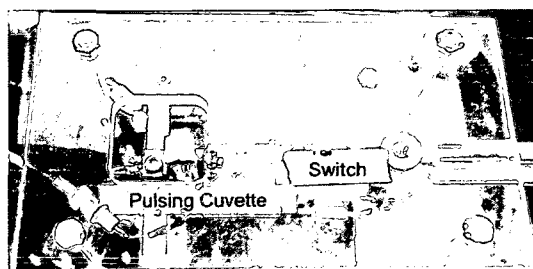
(B) Bio-Rad Gene Pulser® cuvette with 0.1 cm electrode gap, containing 90 μL of PBS ($1 \times 10^7/\text{mL}$ cell suspension was not shown in this picture).

(C) A single pulse wave (300 nanoseconds, 4 kV) was monitored using an oscilloscope.

A



B



C

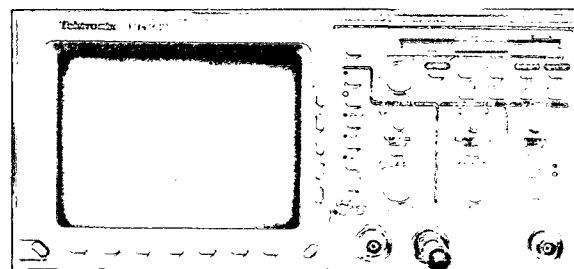


Figure 6. Multiple Pulses Generator

(A) Experimental setup. The charging device (power), transmission lines were connected in a circuit. The switch was manipulated using the red button on the power panel board. The electrical breakdown of the air between the switch would close the parallel circuit, which triggered the transmission lines to charge the cells.

(B) Bio-Rad Gene Pulser® cuvette with 0.1 cm electrode gap was in the cuvette socket. The cuvette contained 120 μL of cell suspension ($1 \times 10^7/\text{mL}$).

(C) A single pulse wave (300 nanoseconds, 4 kV) was monitored using an oscilloscope.

2.5 NANOSECOND PULSED ELECTRIC FIELD TREATMENT

Cell suspension was prepared using Trypsin-EDTA treatment. Cells for each replication were from different cell culture flask. The cells were gently centrifuged at $125\times g$ for 5 minutes, and then resuspended in Dulbecco's PBS (Sigma, Catalog No. D8537). Cell concentration was adjusted to 1×10^7 using a hemocytometer. Exactly 90 μL (for single pulse) or 120 μL (for multiple pulses) of cell suspension was added into the Gene Pulser[®] cuvette (Bio-Rad, Catalog No. 165-2083).

The cuvettes in the single-pulse groups were pulsed once for 300 ns at 40 kV/cm using the single pulse generator. The cuvettes in the multiple pulses groups were pulsed twice, thrice, or four times for 300 ns at 40 kV/cm using the multiple pulses generator. Control groups were loaded into the cuvettes without pulsing. The cell suspension was then transferred into a 1.5 mL Snap Seal graduated microtube (GeneMate, Catalog No. C-3262-1). The cells were gently centrifuged at $125\times g$ for 5 minutes. The supernatant was removed and discarded. Afterward, the cells were resuspended in 1 mL of complete growth medium. The cell resuspension was transferred into a well of a 24-well cell culture plate (Corning Inc., Catalog No. 3524). Eight tubes of cell resuspension were transferred into each plate (Figure 7 and 8). The 24-well plate was incubated at 37°C under a 100 % humidified 5% CO₂ incubator. Individual 24-well plates were used. Each experiment was repeated three times (n=3). For safety concern, the power for the charger was turned off after each pulse. The voltage and ampere of the pulse generator were returned to zero after each experiment.

2.6 SAMPLE COLLECTION FOR RNA EXTRACTION

At 6, 12, 18, and 24 h after pulsing, the growth media were removed and kept for cell counting from the corresponding well (Figure 7) for single pulse treatment. Considering the cells harvested for subsequent experiments were collected 6 hours earlier, the cells harvested later were disturbed. To prevent this disturbance, another cell setups were used (Figure 8) for multiple pulses treatment, so that the cells harvested at different time points remained undisturbed. Exactly 300 μL of RNAprotect Cell Reagent was added to the cell layer. The cells detached after the addition of the RNAprotect Cell Reagent. No

PBS rinsing or Trypsin-EDTA treatment was necessary. The Attached cells were suspended through gentle pipetting. The mixture was then stored at -20°C . The mixture can be stored for years without significant RNA degradation. The mixture was used within 1 week.

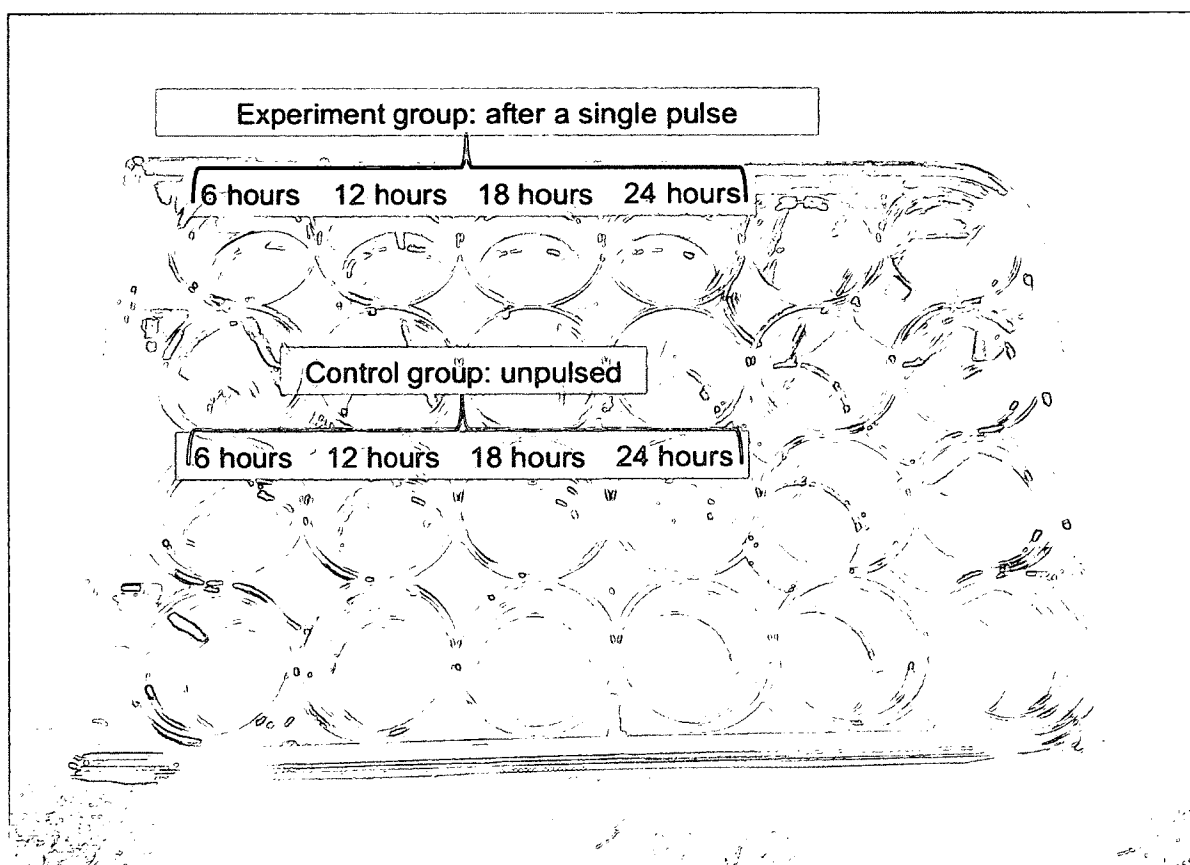


Figure 7. Samples arranged in a 24-well plate for single pulse

The cells were seeded immediately after a single pulse in four wells, as the single pulse group (upper row) and four wells were used as the control group (lower row). The wells were incubated for 6, 12, 18, and 24 h, respectively. A shortcoming of this arrangement was that the cells harvested at later hours were disturbed by the manipulation of the cells harvested at the earlier hours. The culture medium was complete growth medium.

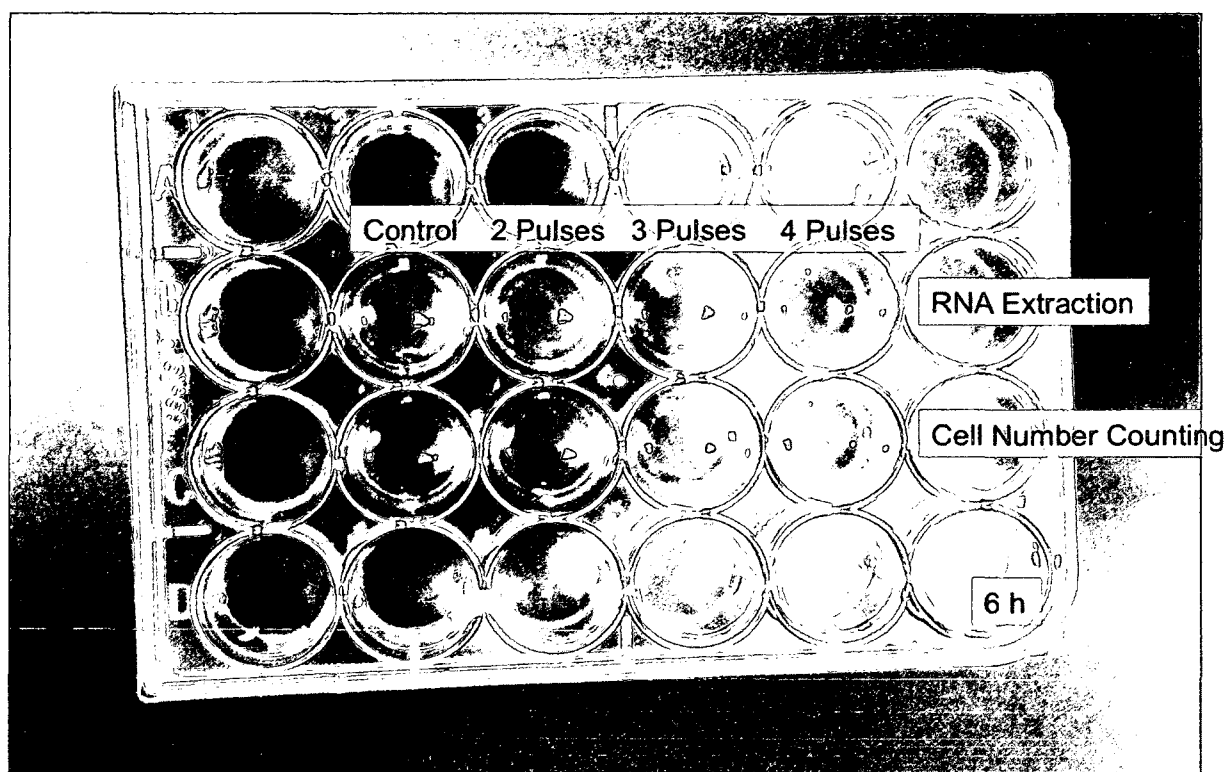


Figure 8. Samples arranged in a 24-well plate for multiple pulses

The cells were seeded immediately after multiple pulses and cultured until harvested at 6 h. The cells from the control, as well as the two-, three-, and four-pulse groups were seeded into the upper row for subsequent total RNA extraction and were seeded in the lower row for cell counting. The cells were arranged at 12, 18, and 24 h, similar to that for 6 h, using separate 24-well plates. This arrangement prevents disturbance of the cells during subsequent harvesting. The culture medium was complete growth medium.

2.7 LONG-TERM CELL VIABILITY TEST

About 1.2×10^6 cells were pulsed two, three, or four times for 300 ns at 40 kV/cm. After pulsing, the cell suspension was immediately transferred into 24-well plate for culture, as previously described. After 6, 12, 18, 24 h, the attached cells were harvested using trypsin-EDTA treatment, whereas the floating cells were counted under trypan blue staining. The cells were mixed 1:1 with 0.4% trypan blue. The attached cells and floating cells were counted, and the percentage of viable cells was calculated, as previously described. This experiment was repeated three times ($n=3$).

2.8 TOTAL RNA EXTRACTION AND DNA ELIMINATION

Total RNA extraction and DNA elimination were carried out using an RNeasy Protect Cell Mini Kit (Qiagen, Catalog No. 74624). The tips and tubes were Nuclease-free. RNaseZap™ (Sigma, Catalog No. R2020-250mL) was sprayed in the working area to remove RNase contamination. The procedures were referenced from *RNeasy® Plus Mini Handbook*. The mixture of the cells and RNaProtect Cell Reagent was centrifuged for 5 minutes at $5000 \times g$ ($R=6$ cm, 8634 rpm) in a 1.5 mL centrifuge tube using a Spectrafuge machine. The growth media were removed completely by pipetting. The cell pellet was loosened by flicking the tube. Then, 350 μ L of Buffer RLT Plus was added to the cell pellet. The cell pellet was dissolved completely by vortexing and then subjected immediately to the next step. The lysate was pipetted directly into a QIAshredder spin column placed in a 2 mL collection tube, and then centrifuged for 2 minutes at full speed ($R=6$ cm, 10000 rpm).

The homogenized lysate was transferred into a gDNA Eliminator spin column placed in a 2 mL collection tube. The spin column was then centrifuged for 30 seconds at $\geq 8000 \times g$ (≥ 10000 rpm). Afterward, the column was discarded, and the flow-through was saved. One volume of 70% ethanol was added to the flow-through, and mixed well by pipetting, without centrifugation. Up to 700 μ L of the mixture, including any precipitate that formed, was transferred to an RNeasy spin column placed in a 2 mL collection tube. The lid was closed gently, and the spin column was centrifuged for 15 seconds at $\geq 8000 \times g$ (≥ 10000 rpm). The flow-through was then discarded.

Up to 700 μL of Buffer RW1 was added to the RNeasy spin column. The lid was closed gently, and the spin column was centrifuged for 15 seconds at $\geq 8000 \times g$ (≥ 10000 rpm) to wash the spin column membrane. The flow-through was discarded. Approximately, 500 μL of Buffer RPE was added to the RNeasy spin column. The lid was closed gently, and the spin column was centrifuged for 15 seconds at $\geq 8000 \times g$ (≥ 10000 rpm) to wash the spin column membrane. The flow-through was discarded. Then, 500 μL of Buffer RPE was added to the RNeasy spin column. The lid was closed gently, and the spin column was centrifuged for 2 minutes at $\geq 8000 \times g$ (≥ 10000 rpm) to wash the spin column membrane. The RNeasy spin column was placed in a new 2 collection tube, and the old collection tube with the flow-through was discarded. The spin column was centrifuged at full speed (≥ 10000 rpm) for 1 minute. The RNeasy spin column was placed in a new 1.5 mL collection tube. Then, 30 μL of RNase-free water was added directly to the spin column membrane. The lid was closed gently, and the spin column was centrifuged for 1 minute at $\geq 8000 \times g$ (≥ 10000 rpm) to elute the RNA. The last step was repeated using the eluate from the last step. The collection tube was reused from the last step.

2.9 PURITY AND QUANTIFICATION OF RNA

The purity and quantification of the extracted total RNA were carried out using NanoDrop 2000 spectrophotometer (Thermo Scientific, Catalog No. ND 2000) in Dr. David Gauthier's laboratory. For total RNA extraction sample, a 260/280 ratio of 2.0 is generally accepted as "pure". A_{260}/A_{280} ratios ranging from 1.8 to 2.1 were considered "pure" RNA in this study. The readings were valid if $A_{260} > 0.15$ at a neutral pH. Nuclease-free water, which was used to dilute the RNA, was used to calibrate the spectrophotometer. The RNA concentration was determined by measuring the absorbance at 260 nm (A_{260}) and determined using the spectrophotometer. The procedures were modified according to *Thermo Scientific NanoDrop Spectrophotometers Nucleic Acid handbook*.

NanoDrop 2000 software for Windows was used to quantify RNA. One microliter of Nuclease-free water was loaded onto the lower measurement pedestal and the sampling arm was lowered. The "Blank" button in the software was used to measure the nuclease-free water and the references spectrum was stored into an external hard drive. The "Measure" button of the software was

used to perform the detection. After the measurement, a dry Kim wipe (Kimberly-Clark, Catalog No. 34155) was used to remove the liquid from both the top and bottom measurement surfaces. The blank result should be a straight line below 0.04 Abs from the baseline at 260 nm. If not, this step must be repeated. After the blank measurement was completed, the sample name was entered in the Sample ID box, and the sample type was set to RNA. One microliter of the total RNA extraction sample was pipetted onto the lower measurement pedestal, the sampling arm was lowered, and the "Measure" button was clicked. After the measurement, a dry Kim wipe was used to remove the sample from both the top and bottom measurement surfaces. The pipette tips were changed for the next measurement. Calibration between samples was unnecessary.

2.10 TOTAL RNA INTEGRITY TEST

The integrity of the total RNA was checked via natural agarose gel electrophoresis. Because 28S and 18S rRNA are highly conserved RNAs, we chose them as a marker to evaluate RNA integrity. If the total RNA was intact, the ratio of the light intensity of the 28S rRNA band to that of the 18S rRNA band should be approximately 2:1. About 0.5 g of agarose was mixed with 50 mL 1×Tris/Borate/EDTA (TBE) in a 250 mL Erlenmeyer flask. The mixture was microwaved for 30 seconds or until the liquid was clear, which indicates complete dissolution of the agarose. The mixture was cooled for 1 min, and 5 μ L of SYBR® Safe DNA gel stain was added to the mixture. The contents of the flask were then swirled and the flask was cooled under tap water until it could be handled safely. The bottom of the gel cassette was adjusted to make it level and allow the gels to have a uniform thickness. The gel mixture was then poured into the gel cassette and a comb was placed to form eight 10 μ L wells in the gel.

The gel was cooled at room temperature for 45 min and the comb was removed carefully without break the wells. The gel was then placed in a Mini-Sub Cell GT System (Bio-Rad, Catalog No. 170-4466) powered by PowerPac™ Basic Power Supply (Bio-Rad, Catalog No. 164-5050). and the gel was covered with 1×TBE. Then, 1 μ L of Blue Gel Loading Dye (6×) was mixed with 5 μ L of the DNA or RNA samples. Afterward, 6 μ L of the mixture was loaded into the well, and 5 μ L of 1kb DNA ladder (BioPioneer, Catalog No. MDL-1000) was loaded into the first well as a DNA size marker. The lid was then placed back on the

electrophoresis apparatus. The gel was run at 120 V for 30 minutes. DNA size and RNA integrity were then examined in the gel under UV light. The gel was photographed using a Bio-Rad Gel Doc 2000 Imaging System.

2.11 RNA REVERSE TRANSCRIPTION

RNA reverse transcription was carried out by QuantiTect® Reverse Transcription Kit (Qiagen, Catalog No. 205310) using Bio-Rad iCycler™ Thermal Cycler in Dr. Wayne L. Hynes' lab. The kit was store at –20°C, and the tips and tubes were Nuclease-free. RNase-Zap was sprayed on working area to eliminate RNase contamination. All reactions were set up on ice to minimize the risk of RNA degradation. The procedures were referenced from the *QuantiTect® Reverse Transcription Handbook*.

NRT control reaction contains all components including template RNA except for the Quantiscript Reverse Transcriptase. Reverse transcription therefore cannot take place, and the only template available is the contaminating genomic or environmental DNA. If the NRT control is not amplified in the downstream quantitative real-time PCR, it indirectly indicates that the total RNA was not contaminated with genomic or environmental DNA, i.e., no DNA contaminant would interfere with the downstream quantitative real-time PCR.

When set up more than one reaction, a master mix of reagents was prepared with a volume at least 10% greater than that required for the total number of reactions to be performed, allowing enough volume for each reaction. The extra volume is used to compensate for the volume loss during transfers.

The extracted total RNA (template) was thawed on ice. Quantiscript® Reverse Transcriptase, gDNA Wipeout Buffer, Quantiscript RT Buffer, RT Primer Mix, and RNase-free water were thawed at room temperature. Each solution was mixed by flicking the tubes. The residual liquid from the sides of the tubes was collected by brief centrifugation and kept on ice. The genomic DNA elimination reaction was prepared on ice (Table 2). The amount of RNA templates for single pulse experiments was 200 ng, whereas that for multiple pulses experiments was 100 ng. The genomic DNA elimination reaction mix was incubate for 2 minutes at 42°C, and then placed immediately on ice. RT Primer Mix was mixed with 5x Quantiscript RT Buffer at a 1:4 ratio. The reverse transcription reaction was prepared on ice (Table 3). The template RNA was added last. The reaction was

Table 2. Genomic DNA Elimination Reaction Components

Component	Volume/reaction
gDNA Wipeout Buffer, 7x	2 uL
Template RNA	Variable
RNase-free water	Variable
Total reaction volume	14 uL

Table 3. Reverse Transcription Reaction Components

Component	Volume/reaction
Quantiscript Reverse Transcriptase	1 uL
Mixture of Quantiscript RT Buffer 5x and RT Primer Mix	5 uL
Template: entire genomic DNA elimination reaction	14 uL
Total reaction volume	20 uL

mixed and then stored on ice. The reaction was incubated for 15 minutes at 42°C and immediately incubated for 3 minutes at 95°C to inactivate the Quantiscript Reverse Transcriptase. The products of the reverse transcription reactions (cDNAs) were stored at –20°C and used as template for the quantitative real-time PCR.

2.12 QUANTITATIVE REAL-TIME PCR

quantitative real-time PCR was carried out using iQ™ SYBR® Green Supermix Kit (Bio-Rad, Catalog No. 170-8880) in Dr. Wayne L. Hynes' laboratory. The kit was stored at –20°C, and the tips and tubes were nuclease-free. The working area was cleaned to eliminate RNase contamination. The procedures were extracted from the *iQ™ SYBR® Green Supermix Instructions*. MIA primers (Qiagen, Catalog No. QT01058673) and β -actin primers (Qiagen, Catalog No. QT00095242) were used. The MIA amplicon length was 103 bp, whereas the β -actin amplicon length was 149 bp.

The no template control (NTC) reaction contains all the components of the PCR reaction except for the cDNA template, thereby enabling the detection of carryover contamination from previous experiments, DNA contaminant, and primer dimer. If the NTC reaction has amplification in the quantitative real-time PCR, it represents carryover contamination from previous experiments, a DNA contaminant during PCR preparation, or the formation of a primer dimer.

About 1.1 mL of TE, pH 8.0, provided by Dr. David Gauthier, was added to the QuantiTect Primer Assay tubes. The tubes were vortexed for four to six times. The obtained reverse transcription reaction and primers were thawed on ice. Up to 2 μ L of template was derived directly from the obtained reverse transcription reaction (20 ng of template for single pulse, 10 ng of template for multiple pulses). The iQTM SYBR[®] Green Supermix was thawed to room temperature. The Supermix was mixed thoroughly, centrifuged briefly to collect solution at the bottom of tubes, and then stored on ice protected from light. The master mix for all reactions was prepared by adding all required components, except for the cDNA template (Table 4). The master mix was mixed thoroughly to ensure

Table 4. Quantitative Real-Time PCR Reaction Components

Component	Volume/reaction	Final Concentration
iQ TM SYBR [®] Green Supermix (2x)	10 μ L	1×
10×QuantiTect Primer Assay	2 μ L	1×
cDNA template	2 μ L	20 ng or 10 ng
Nuclease-free water	6 μ L	—
Total reaction volume	20 μ L	—

homogeneity and aliquoted equally into the wells of an unskirted low-profile 48-well clear qPCR plate (Bio-Rad, Catalog No. mLL4801). The cDNA template was added to the wells containing the master mix and the wells were sealed with flat caps. The 48-well plate was spun at 4000 rpm for 5 minutes to remove any air bubbles and collect the reaction mixture in the vessel bottom.

The thermal cycling protocol was programmed on the MiniOpticon™ Real-Time PCR Detection System (Bio-Rad, Catalog No. CFB-3120), in standard mode (Table 5). Afterward, the PCR plate was loaded onto the MiniOpticon™ PCR instrument and the PCR run was started.

Table 5. Thermal Cycling Protocol

Process	Temperature	Time
Polymerase Activation and DNA Denaturation	95°C	3 minutes
Amplification (40 cycles)		
Denaturation	95°C	10 seconds
Annealing/Extension+Plate Read	60°C	30 seconds
Melt Curve Analysis	Use default setting	

2.13 STATISTICS

Data were analyzed in a two-way fixed ANOVA using the SPSS 20.0.0 program. Transformations were calculated as follows: 'Transform' → 'Compute Variable' with logarithmic, square root, reciprocal, and power of e. Residues were generated by 'Analyze' → 'General Linear Model' → 'Univariate' → 'Save' → check 'Unstandardized Residuals'. Normality were checked by 'Analyze' → 'Descriptive Statistics' → 'Explore' → check 'Normality plots with tests'. In the same window, in the 'Spread vs Level WITH LEVENE Test' box, check 'Untransformed' for homogeneity of variance checking.

Significance (p-value) was calculated as follows: 'Analyze' → 'General Linear Model' → 'Univariate' → put data in the 'Dependent Variable' box, input treatment and time in the 'Fixed Factor(s)' box. Interaction graph was generated by same procedure above, 'Plots...' → put treatment in the 'Separate Lines:' box, put time in the 'Horizontal Axis:' box → click 'Add' → 'Continue'. Tukey follow-up test was generated by the same procedure above, 'Post Hoc...' → input time in the 'Post

Hoc Tests for:' box → check 'Tukey'. Observed power was generated by the same procedure above, 'Options' → check 'Observed power' in the 'Display' box → 'Continue'.

CHAPTER 3

RESULTS

3.1 CELL ATTACHMENT ABILITY TEST AFTER A SINGLE PULSE

To test the cell attachment ability after a single 300 ns 40 kV/cm pulse, the live and dead cells that did not attach after decanted the medium were counted in the floating medium at 6, 12, 18, and 24 h post-pulsing. This test is based on the inability of cells to adhere, leaving them to float in the growth medium and remain unattached to the bottom of the well. The live and strongly attaching cells would adhere onto the plate. The number of dead and live cells in the growth medium indicates how many cells detached and the viability of the cells in the floating medium of both the experimental group and the control groups.

The cells after a single 300 ns 40 kV/cm pulse were cultured for 6, 12, 18, and 24 h after pulsing. The dead and live cells in the growth media from each well of the 24-well plate were counted on a hemocytometer using trypan blue. The number of dead, live, total cells in the floating media, and the viability of the floating cells were recorded (Table 6) and analyzed using the two-factor fixed model ANOVA.

Table 6. Number of Floating Cells and Cell Viability in the Growth Media

Time	Trial	Treatment	Live ($\times 10^4$ cells)	Dead ($\times 10^4$ cells)	Total ($\times 10^4$ cells)	Viability (%)
6 hours	1	One Pulse	0.2	0	0.2	100
6 hours	2	One Pulse	0	0.4	0.4	0
6 hours	3	One Pulse	0.2	0.4	0.6	33.3
6 hours	1	Control	0	0.2	0.2	0
6 hours	2	Control	0.2	0	0.2	100
6 hours	3	Control	1	0	1	100
12 hours	1	One Pulse	0.2	0.2	0.4	50
12 hours	2	One Pulse	0.6	0	0.6	100
12 hours	3	One Pulse	0	0	0	-
12 hours	1	Control	0	0	0	-
12 hours	2	Control	0.2	0.2	0.4	50
12 hours	3	Control	0.4	0.2	0.6	66.7
18 hours	1	One Pulse	0	0	0	-
18 hours	2	One Pulse	0	0	0	-
18 hours	3	One Pulse	0.2	0	0.2	0
18 hours	1	Control	0.6	0	0.6	100
18 hours	2	Control	0	0	0	-
18 hours	3	Control	0	0	0	-
24 hours	1	One Pulse	0	0	0	-
24 hours	2	One Pulse	0	0.4	0.4	0
24 hours	3	One Pulse	0	0	0	-
24 hours	1	Control	0	0	0	-
24 hours	2	Control	0.2	0.2	0.4	50
24 hours	3	Control	0	0	0	-

Statistic parameters: IBM® SPSS® Statistics Version 20.0.0 was used to conduct the two-factor fixed model ANOVA. A Tukey follow-up test was carried out for multiple comparisons and to compare the time points factors. The independent factors include Factor A (the treatments) included two levels, a single pulse group and a control group, and factor B (is the time points) including four levels: 6, 12, 18, and 24 h. The dependent variables include number of live, dead, and total cells in the growth medium in each well. The sample number and replicates in this study are three wells per treatment per time point ($n=3$); two treatments per time point, four time points per treatment; 24 wells (samples) in total.

Statistical hypotheses (only showing live cells as an example):

H_O : The number of live cells in the growth media does not significantly differ between the experimental group and the control group excluding the time points

H_A : The number of live cells in the growth media significantly differs between the experimental group and the control group excluding the time points

H'_O : The number of live cells in the growth media does not significantly differ among the different time points excluding the treatment

H'_A : The number of live cells in the growth media significantly differs among the different time points excluding the treatment

H''_O : The treatments do not significantly interact with the time points in terms of the number of live cells in the growth media

H''_A : The treatments significantly interact with the time points in terms of the number of live cells in the growth media

Assumption checking and data transformations: Errors are independent and identically distributed because the cells in each well were pulsed in individual pulsing cuvette. Thus, treatments are applied independent of the replicates. The cells in each well did not affect the cells in the other wells. No autocorrelation was observed. The assumption of independent errors was met. The identically distributed assumption will be checked in next step. The data were checked for normality and homogeneity, and subjected to data transformation. Assumptions checking of residuals suggests that neither the original data nor the subsequent transformations (natural log, square root, reciprocal, exponential) sufficiently fulfilled the assumptions. Therefore, the rank values obtained from the original

data were analyzed.

Results based on rank data: The results of the two-way ANOVA (2×4 , pure model I) analysis indicate that the null hypotheses (H_0 , H'_0 , H''_0) should be accepted instead of the alternative hypothesis, i.e., the number of live, dead, and total cells did not differ significantly among the different time points, as well as between the two treatment groups (Table 7, 8, 9). No significant interaction was observed between the time points and the treatments in terms of the number of live, dead, and the total number of cells in the medium (Figure 9, 11, 13).

The results of this study indicate no significant interaction between the treatments and the time points in terms of the number of live cells in the growth media ($F=0.073$; $df=3, 16$; $P=0.974$) (Figure 9). The observed power in SPSS was 0.060. The number of live cells in the growth media did not significantly differ between the treatments ($F=0.452$; $df=1, 16$; $P=0.511$) (Figure 10). The observed power in SPSS was 0.097. The number of live cells did not significantly differ among the different time point ($F=1.280$; $df=3, 16$; $P=0.315$). The observed power in SPSS was 0.277.

No significant interaction was observed between the treatments and time points in terms of the number of dead cells in the growth media ($F=0.630$; $df=3, 16$; $P=0.974$) (Figure 11). The observed power in SPSS was 0.153. The number of dead cells in the growth media did not significantly differ between the treatments ($F=0.118$; $df=1, 16$; $P=0.736$) (Figure 12). The observed power in SPSS was 0.062. The number of live cells did not significantly differ among the different time points ($F=1.346$; $df=3, 16$; $P=0.295$). The observed power in SPSS was 0.290.

No significant interaction were observed between the treatments and the time points in terms of the total number of cells in the growth media ($F=0.049$; $df=3, 16$; $P=0.985$) (Figure 13). The observed power in SPSS was 0.057. No significant difference was observed in the number of dead cells in the growth media between the treatments ($F=0.049$; $df=1, 16$; $P=0.828$) (Figure 14). The observed power in SPSS was 0.055. No significant difference was observed in the number of live cells in the growth media among different time groups ($F=1.967$; $df=3, 16$; $P=0.160$). The observed power in SPSS was 0.412.

The observed powers in SPSS were all low, less than 0.7, thereby increasing the risk of a type II errors (false negatives). Large sample sizes may help

minimize this error in future studies.

All the aforementioned results suggest that a single 300 ns 40 kV/cm pulse does not change the number of floating cells compared with the control group. Therefore, a single 300 ns 40 kV/cm pulse does not affect cell attachment ability within 24 h of pulsing.

Table 7. Rank of the Number of Live Cells in the Growth Media after a Single Pulse, Two-Way Fixed ANOVA Table

Source	df	Mean Square	F	Significance	Observed Power
Treatment	1	37.500	0.452	0.511	0.097
Time	3	106.333	1.280	0.315	0.277
Treatment×Time	3	6.056	0.073	0.974	0.060
Error	16	83.042			
Total	24				
Corrected Total	23				

Table 8. Rank of the Number of Dead Cells in the Growth Media after a Single Pulse, Two-Way Fixed ANOVA Table

Source	df	Mean Square	F	Significance	Observed Power
Treatment	1	9.375	0.118	0.736	0.062
Time	3	106.931	1.346	0.295	0.290
Treatment×Times	3	50.042	0.630	0.974	0.153
Error	16	79.417			
Total	24				
Corrected Total	23				

Table 9. Rank of the Total Number of Cells in the Growth Media after a Single Pulse, Two-Way Fixed ANOVA Table

Source	df	Mean Square	F	Significance	Observed Power
Treatment	1	3.375	0.049	0.828	0.055
Time	3	136.486	1.967	0.160	0.412
Treatment×Times	3	3.375	0.049	0.985	0.057
Error	16	69.375			
Total	24				
Corrected Total	23				

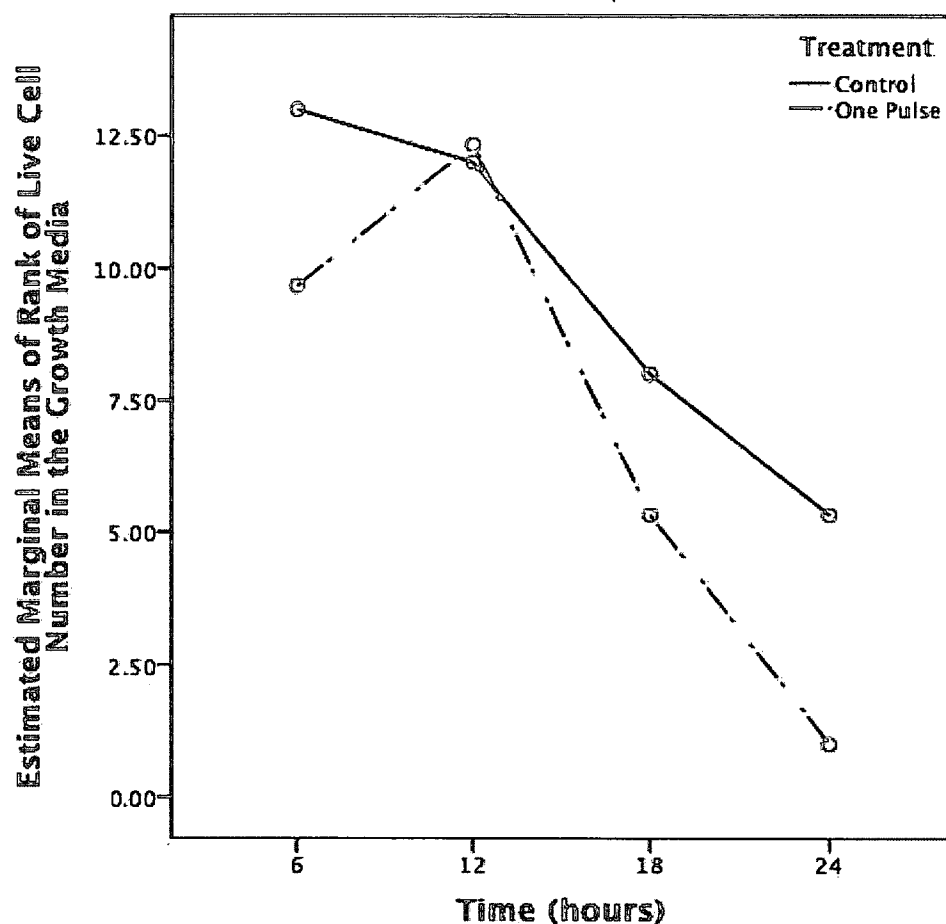


Figure 9. Interaction Plot of the Number of Live Cells between Treatments and Time Points after a Single Pulse

The live cells in the growth media after a single 300 ns 40 kV/cm pulse, as well as in the unpulsed group were counted using trypan blue after 6, 12, 18, and 24 h of culture. The live cells remain clear. The solid line (control group) and the dashed line (one pulse group) are almost parallel. No significant interaction was observed between the time points and the treatment in terms of the number of live cells in the growth media ($F=0.073$; $df=3, 16$; $P=0.974$), $n=3$.

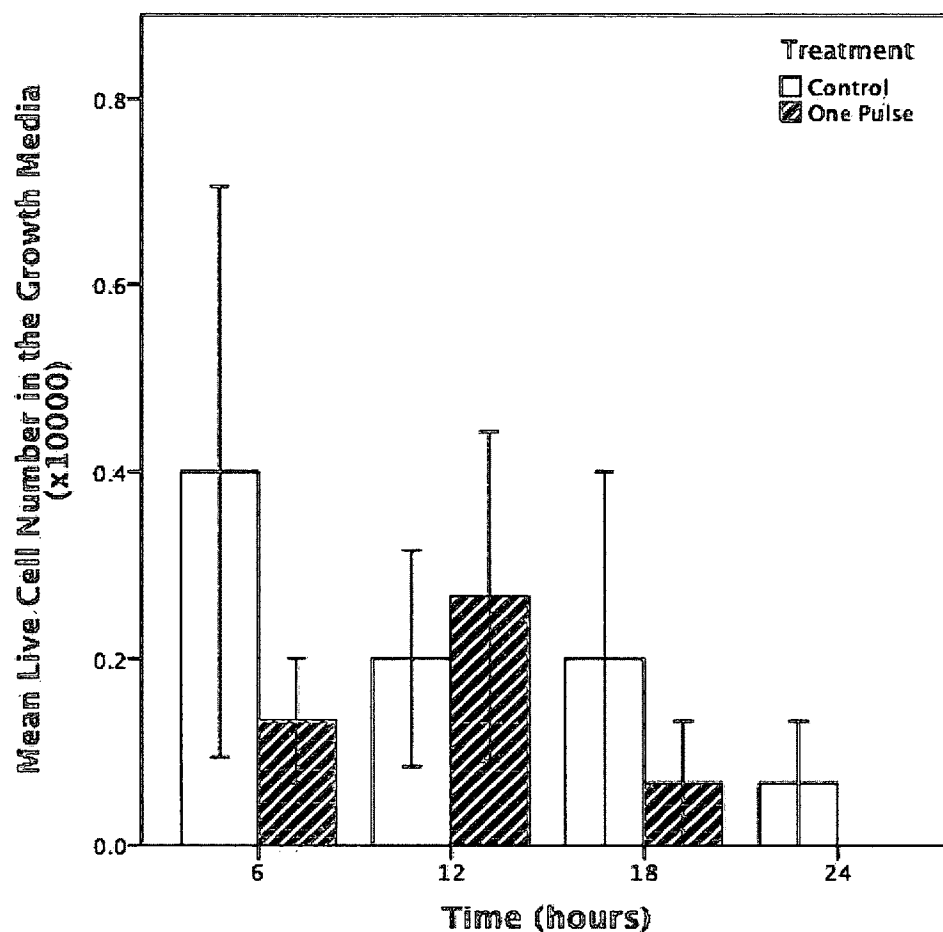


Figure 10. Number of Floating Live Cells after a Single Pulse

The floating live cells in the growth media after a single 300 ns 40 kV/cm pulse, as well as in the unpulsed group were counted using trypan blue after 6, 12, 18, and 24 h of culture. The clear staining cells are live cells. The number of floating live cells did not significantly differ between the single pulse group and the control group ($F=0.452$; $df=1, 16$; $P=0.511$). The number of floating live cells did not significantly differ among the 6, 12, 18, and 24 h time points ($F=1.280$; $df=3, 16$; $P=0.315$). The data shown are means \pm SEM, $n=3$.

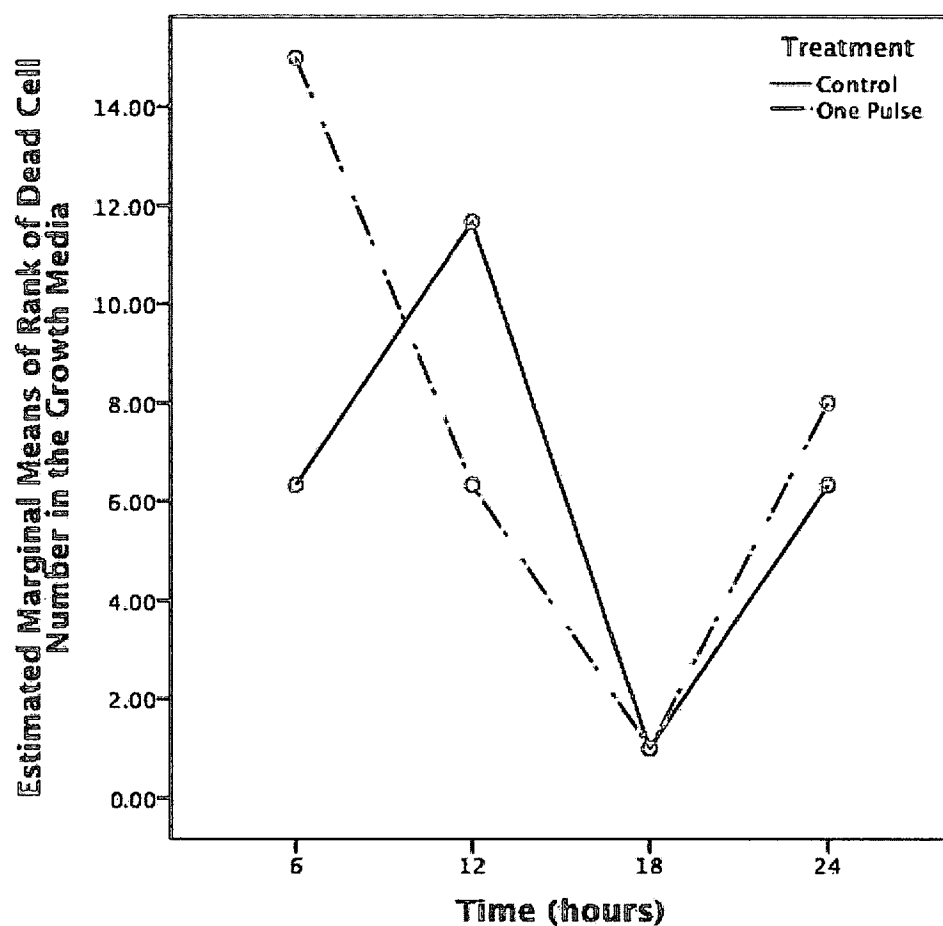


Figure 11. Interaction Plot of the Number of Dead Cells between the Treatments and the Time Points after a Single Pulse

The dead cells in the growth media after a single 300 ns 40 kV/cm pulse, as well as in the unpulsed group were counted using trypan blue after 6, 12, 18, and 24 h of culture. The dead cells were stained blue. The solid line (control group) and the dashed line (one pulse group) are almost parallel. No significant interaction was observed between the time points and the treatments in terms of the number of dead cells in the growth media ($F=0.630$; $df=3, 16$; $P=0.974$), $n=3$.

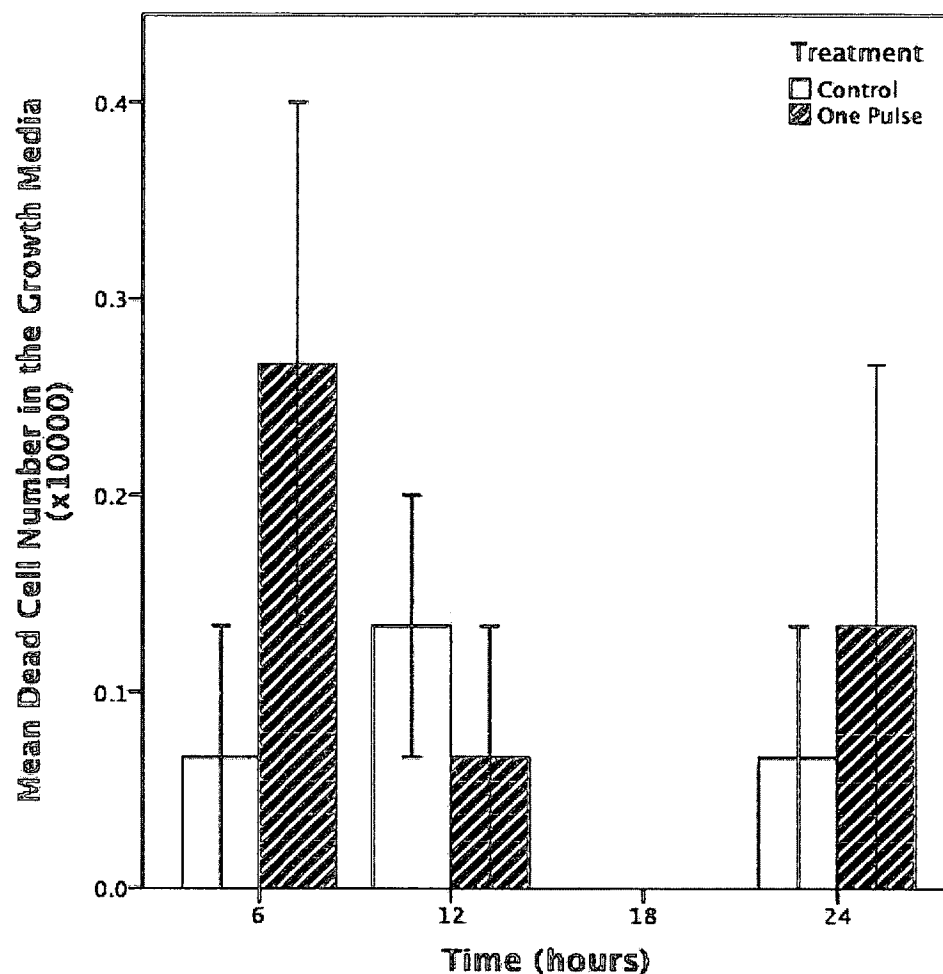


Figure 12. Number of Floating Dead Cells after a Single Pulse

The number of floating dead cells in the growth media after a single 300 ns 40 kV/cm pulse, as well as in the unpulsed group were counted using trypan blue after 6, 12, 18, and 24 h of culture. The dead cells were stained blue. The number of dead cells did not significantly differ between the single pulse group and the control group ($F=0.118$; $df=1, 16$; $P=0.736$). The number of dead cells in the growth media did not significantly differ among the 6, 12, 18, and 24 h time points ($F=1.346$; $df=3, 16$; $P=0.295$). The data shown are means \pm SEM, $n=3$.

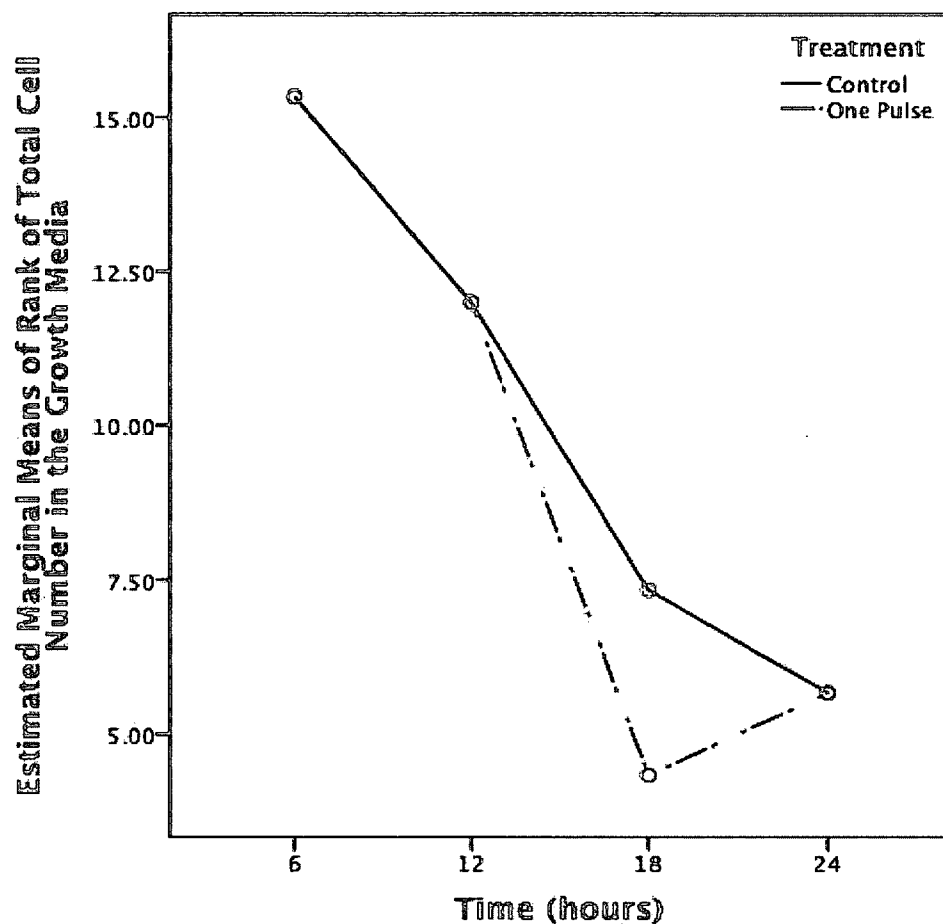


Figure 13. Interaction Plot of the Number of Dead Cells between the Treatment and the Time Points after a Single Pulse

The total number of cells in the growth media after a single 300 ns 40 kV/cm pulse, as well as in the unpulsed group were counted using trypan blue after 6, 12, 18, and 24 h of culture. The total number of cells was equal to the number of live cells plus the number of dead cells. The solid line (control group) and the dashed line (one pulse group) are almost parallel. No significant interaction was observed between the time points and the treatment in terms of the total number of cells in the growth media ($F=0.049$; $df=3, 16$; $P=0.985$), $n=3$.

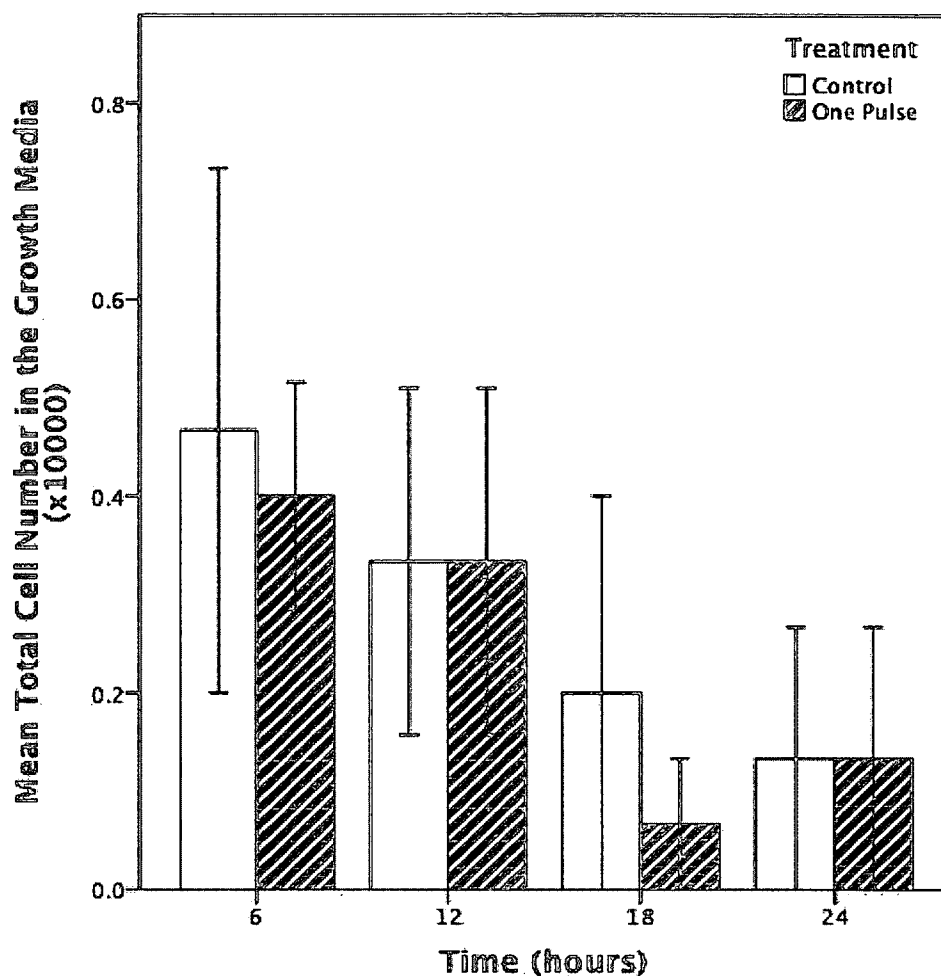


Figure 14. Total Number of the Floating Cells after a Single Pulse

The floating live and dead cells in the growth media after a single 300 ns 40 kV/cm pulse, as well as in the unpulsed group were counted using trypan blue after 6, 12, 18, and 24 h of culture. The total number of cells was equal to the number of live cell plus the number of dead cells. The total number of cells in the growth media did not significantly differ between the single pulse group and the control group ($F=0.049$; $df=1, 16$; $P=0.828$). The total number of cells did not significantly differ among the 6, 12, 18, and 24 h time points ($F=1.967$; $df=3, 16$; $P=0.160$). The data shown are means \pm SEM, $n=3$.

3.2 CELL MORPHOLOGY AFTER A SINGLE PULSE

To examine the changes in cell morphology after a single 300 ns 40 kV/cm pulse, single pulsed cells and unpulsed cells (control) were seeded immediately after pulsing and cultured in the incubator. The cells were observed and photographed under a Nikon inverted microscope at 200 \times magnification at 6, 12, 18, and 24 h after pulsing (Figure 15).

Cell shape was defined as the contour or outline of the cell attaching area on the 24-well plate surface, which is determined by the cell adhesion ability. Larger attachment areas indicate stronger adhesion ability. The shape of the attachment area changed with time. The cells that have just attached onto the 24-well plate surface were round. The cells then spread out on two ends, forming a spindle shape. The cell contents then move from one end to the other end, forming an umbrella shape. The cells then grow spines and form polygonal shapes. However, the biological procedure during these shape changes is still unclear. Thus, analyzing these changes in shape provides an opportunity to examine the changes in attachment ability.

Almost all the cells from both control and single pulse groups adhered to the 24-well plate surface at 6 h (Figure 15A, 15B). Most of the cells were spindle-shaped, with one end spreading out like umbrella. At 12 h, some cells rounded up to divide due to weak adhesion (Figure 15C, 15D). Some cells spread out further and became polygonal or stellate at 18 h (Figure 15E, 15F). At 24 h, Some cells spread out even further (Figure 15G, 15H). Some cells produce dendrite-like or axon-shape spines, overlapping each other at 18 and 24 h. No obvious difference in cell shape and spreading area were observed between the control group and the single pulse group under direct visualization.

All the results above show that the single pulse group and the control group cells did not significantly differ in cell shape and spread area at 6, 12, 18, and 24 h after 300 ns 40 kV/cm pulsing. Thus, a single 300 ns 40 kV/cm pulse does not change the attach ability, which supports the previous floating cell number test.

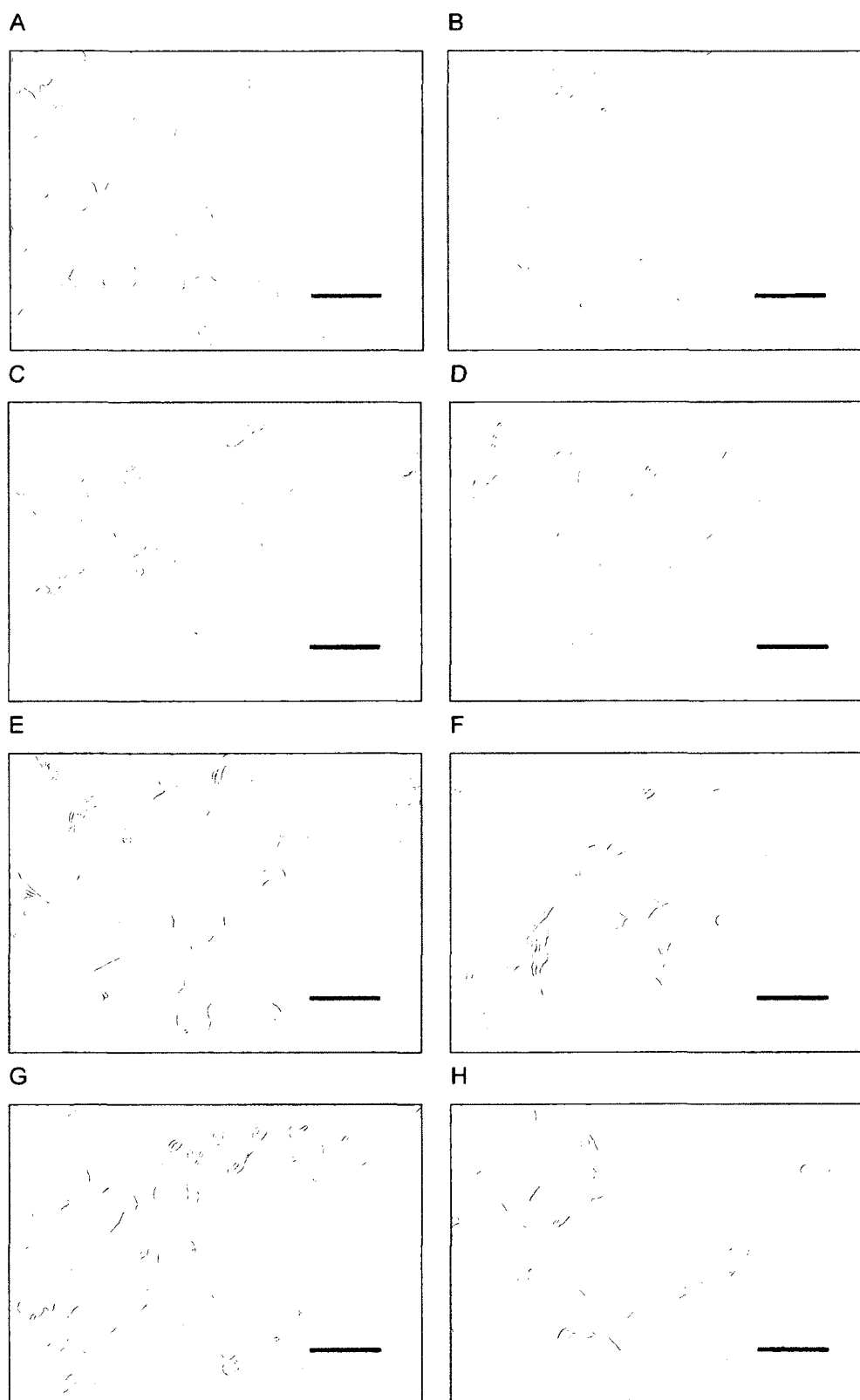


Figure 15. Cell Morphology after a Single Pulse

(A, C, E, G) Cells were seeded and cultured without pulsing at 6, 12, 18, and 24 h, respectively.
(B, D, F, H) Cells were seeded and cultured until 6, 12, 18, and 24 h after a single 300 ns 40 kV/cm pulse, respectively. Scale bar=100 μm .

Two methods can be used to examine the difference in the number of cells that attached onto the 24-well surface between the pulsed and unpulsed cells. One is to harvest the cells using EDTA-trypsin treatment, and then counting the cell number using a hemocytometer. The other way is to estimate the number of attached cells in terms of the cell density in micrographs.

Considering the number of floating cells did not significant differ between the single pulse group and control group at 6, 12, 18, and 24 h and that the number of cells in the cuvettes in the single pulse group were the same as those in the control group, the number of attached cells should have no significant differences. Thus, the cell densities in micrographs were used to estimate the number of attached cells under direct visualization. However, for later multiple pulses, the attached cells were harvested using EDTA-trypsin and counted using a hemocytometer.

The cell density examination averages the cell density in at least two sets of photographs to cancel out the random error. Thus, another set of photographs are shown. The cell densities of the single pulse group seemed less in one set of photographs (Figure 15), but seemed more in the other set of photographs (Figure 16). The average cell density in the two photographs did not significantly differ between the single pulse group and control group at 6, 12, 18, and 24 h. These results indicates that single pulse does not change the number of attached cells, which is consistent with the finding that single pulse does not change the attachment ability in the floating cell assay.

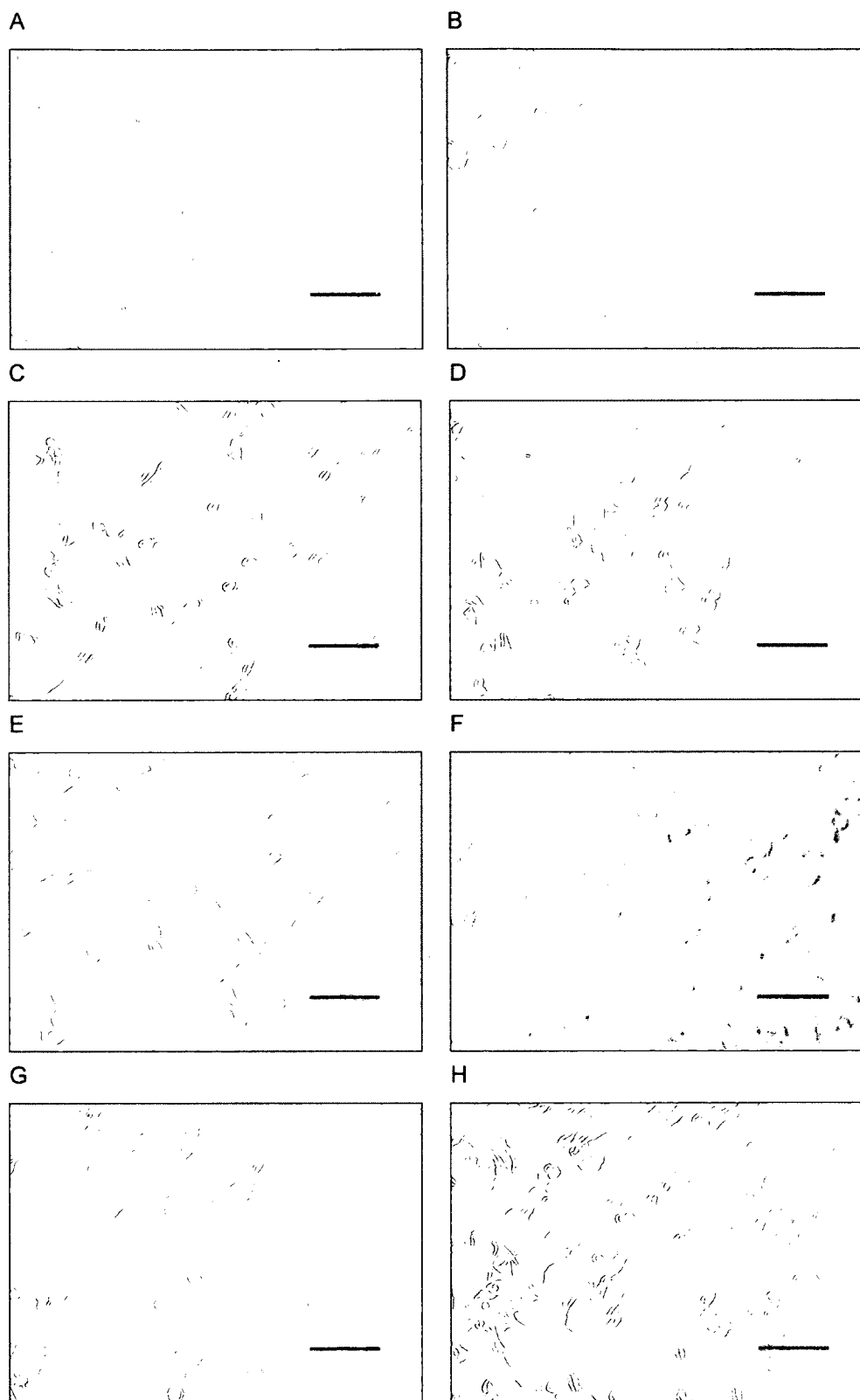


Figure 16. A Second Set of Cell Morphology Photographs

(A, C, E, G) Cells were seeded and cultured without pulsing at 6, 12, 18, and 24 h, respectively.
(B, D, F, H) Cells were seeded and cultured until 6, 12, 18, and 24 h after a single 300 ns 40 kV/cm pulse, respectively. Scale bar=100 μm.)

3.3 LONG-TERM VIABILITY TEST AFTER MULTIPLE PULSES

3.3.1 TOTAL CELL VIABILITY TEST AFTER MULTIPLE PULSES

The number of attached and floating cells in each well were counted at 6, 12, 18, and 24 h after pulsing and incubation using the trypan blue viability test to determine the long-term cell viability and cell growth ability after multiple 300 ns, 40 kV/cm pulses. The total number of live cells is the sum of the number of attached live cells and the number of floating live cells. The total number of dead cells is the sum of the number of attached dead cells and the number of floating dead cells. The viability values were then calculated (Equation 2).

The nature log, square root, reciprocal, and exponential transformation did not meet the assumptions for normal distribution and homogeneity of variance. Therefore, the rank values of the raw viability values were used in the two-way fixed ANOVA. The hypotheses were similar to those previously described for the single 300 ns 40 kV/cm pulse treatment, except for the four levels (control group and two-, three-, and four-pulse groups) in the treatment factor. Three replicates were conducted.

The result of the two-way fixed ANOVA indicates that cell viability did not significantly differ among the 6, 12, 18, and 24 h time points ($F=1.434$; $df=3, 32$; $P=0.251$) (Table 10), but significantly differed among the different number of pulses ($F=2516.799$; $df=3, 32$; $P<0.0000005$). No significant interaction was observed between the time points and the pulse treatments ($F=22.113$; $df=9, 32$; $P=0.810$) (Figure 17). The Tukey's follow-up test shows that the cell viability of the control group differed significantly from the two-, three-, and four-pulse groups (all $P<0.0001$) (Figure 18). The cell viability of the two-pulse group was significantly different from those of three- pulse group and four-pulse group (all $P<0.0001$). However, that of the three-pulse group did not significantly differ from that of the four-pulse group.

Therefore, multiple 300 ns 40 kV/cm pulses significantly decrease total cell viability compared with that of the control group. The total cell viability after three or four pulses was significantly lower than that after two pulses. These results indicate that total cell viability decreases with the number of pulses. This finding provides a good opportunity to reduce the melanoma of melanoma cells in clinical treatment.

**Table 10. Rank of Long-term Total Cell Viability (%) after Multiple Pulses,
Two-Way Fixed ANOVA Table**

Source	df	Mean Square	F	Significance	Observed Power
Time	3	55.465	1.434	0.251	0.343
Pulses	3	2516.799	65.055	<0.0000005	1.000
Time×Pulses	9	22.113	0.572	0.810	0.228
Error	32	38.688			
Total	48				
Corrected Total	47				

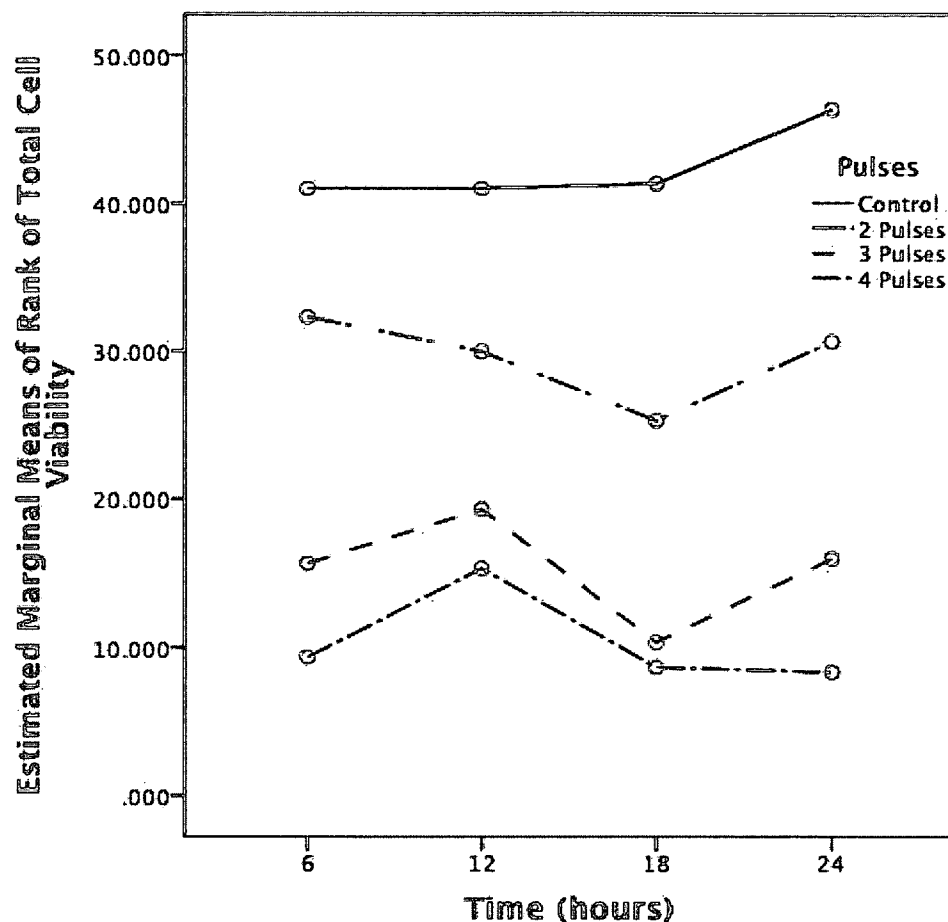


Figure 17. Long-term Total Cell Viability Interaction Graph after Multiple Pulses

The attached and floating cells after two, three, and four 300 ns 40 kV/cm pulses, as well as in the unpulsed group were counted using trypan blue after 6, 12, 18, and 24 h of culture. The total number of live cells is equal to the number of attached live cells plus the number of floating live cells. The total number of dead cells is equal to the number of attached dead cells plus the number of floating dead cells. Total cell viability was counted (Equation 2). The solid line (control group) and the three dashed lines (two-, three-, and four-pulse groups) were almost parallel. No significant interaction was observed between the time points and the pulse treatments in terms of total cell viability ($F=22.113$; $df=9, 32$; $P=0.810$), $n=3$.

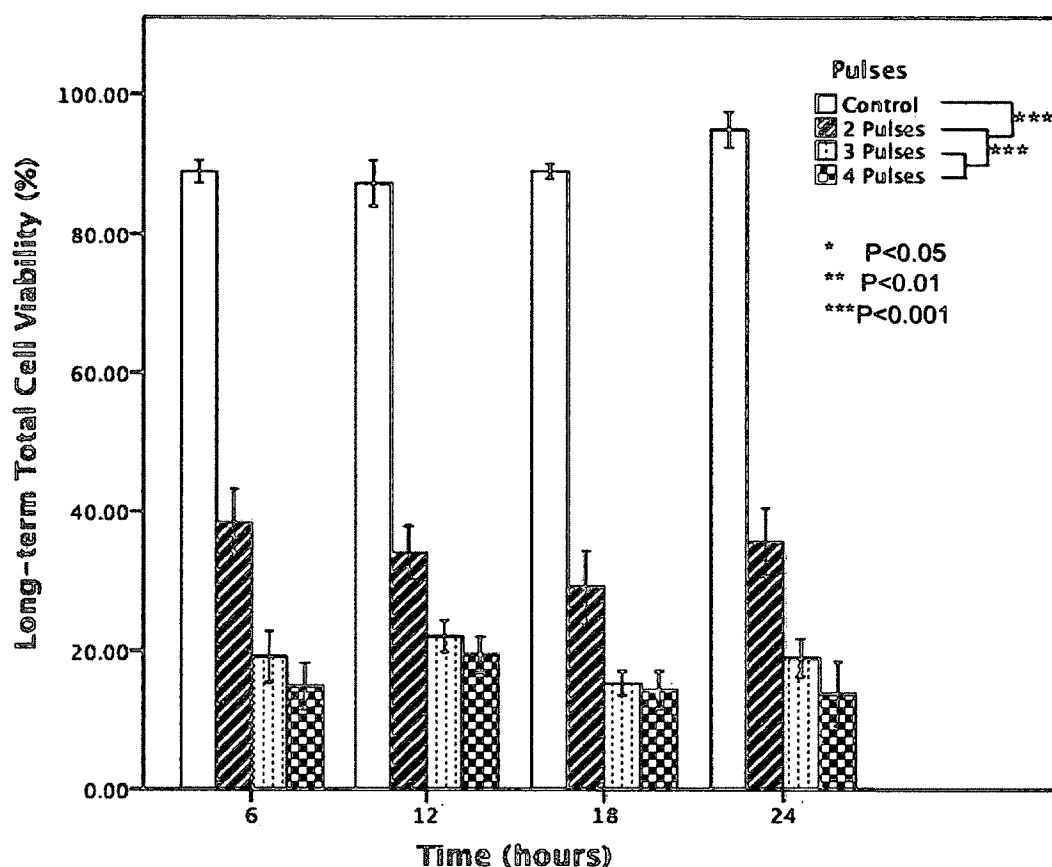


Figure 18. Long-term Total Cell Viability after Multiple Pulses

The attached and floating cells after two, three, and four 300 ns 40 kV/cm pulses, as well as in the unpulsed group were counted using trypan blue after 6, 12, 18, and 24 h of culture. The total number of live cells was equal to the number of attached live cells plus the number of floating live cells. The total number of dead cells was equal to the number of attached dead cells plus the number of floating dead cells. The total cell viability was counted (Equation 2). Total cell viability significantly differed among the different pulse treatments ($F=2516.799$; $df=3, 32$; $P<0.0000005$). The Tukey's follow-up test shows that the cell viability of the control group was significantly higher than those in the two-, three-, and four-pulse groups (all $P<0.0001$). The cell viability of two-pulse group was significantly higher than those of the three- and four-pulse groups (all $P<0.0001$), but it did not significantly differ between the three-pulse group and the four-pulse group. The data shown are the means \pm SEM, $n=3$.

3.3.2 TOTAL LIVE CELL NUMBER AFTER MULTIPLE PULSES

The attached and floating live cell were counted using a trypan blue test at 6, 12, 18, and 24 h after pulsing and incubation to determine how many live cells were left and the differences in cell growth among the multiple pulse treatments. The total number of live cells was equal to the number of attached live cells plus the number of floating live cells.

The natural log, square root, reciprocal, and exponential transformation did not exhibit a normal distribution and was non-homogenous. Therefore, the rank values of the total number of live cells were used to conduct two-way ANOVA. The hypotheses were similar to those previously described for the single pulse treatment, except for the four levels (control group and two-, three-, and four-pulse groups) in the treatment factor. Three replicates were conducted.

The two-way fixed ANOVA indicates that the total number of live cells significantly differed among the 6, 12, 18, 24 h time points ($F=221.861$; $df=3, 32$; $P=0.021$) (Table 11). The total number of live cells significantly differed among the multiple pulse treatments ($F=2301.806$; $df=3, 32$; $P<0.0000005$). No significant interaction was observed between the time points and the multiple pulse treatments ($F=30.028$; $df=9, 32$; $P=0.862$) (Figure 19). The Tukey's follow-up test of the time points showed significant differences in the total number of live cells between the 12 h and the 18 h time points ($P=0.011$) (Figure 20). The Tukey's follow-up test of the multiple pulse treatments showed that the total number of live cells in the control group significantly differed from those of the two-, three-, and four-pulse treatments (all $P<0.0001$). The total number of live cells in the two-pulse group was significantly different from those in the three- and four-pulse groups ($P=0.013$ and 0.000182 , respectively).

The aforementioned results indicate that two, three, and four 300 ns 40 kV/cm pulses significantly decreased the total number of live cells compare with the control group. Increasing the number of pulses also increased cell death. These results are very promising for reducing melanoma size and cell number in future melanoma treatments.

Table 11. Rank of Total Number of Live Cells after Multiple Pulses, Two-Way Fixed ANOVA Table

Source	df	Mean Square	F	Significance	Observed Power
Time	3	221.861	3.712	0.021	0.754
Pulses	3	2301.806	38.511	<0.0000005	1.000
Time×Pulses	9	30.028	0.502	0.862	0.202
Error	32	59.771			
Total	48				
Corrected Total	47				

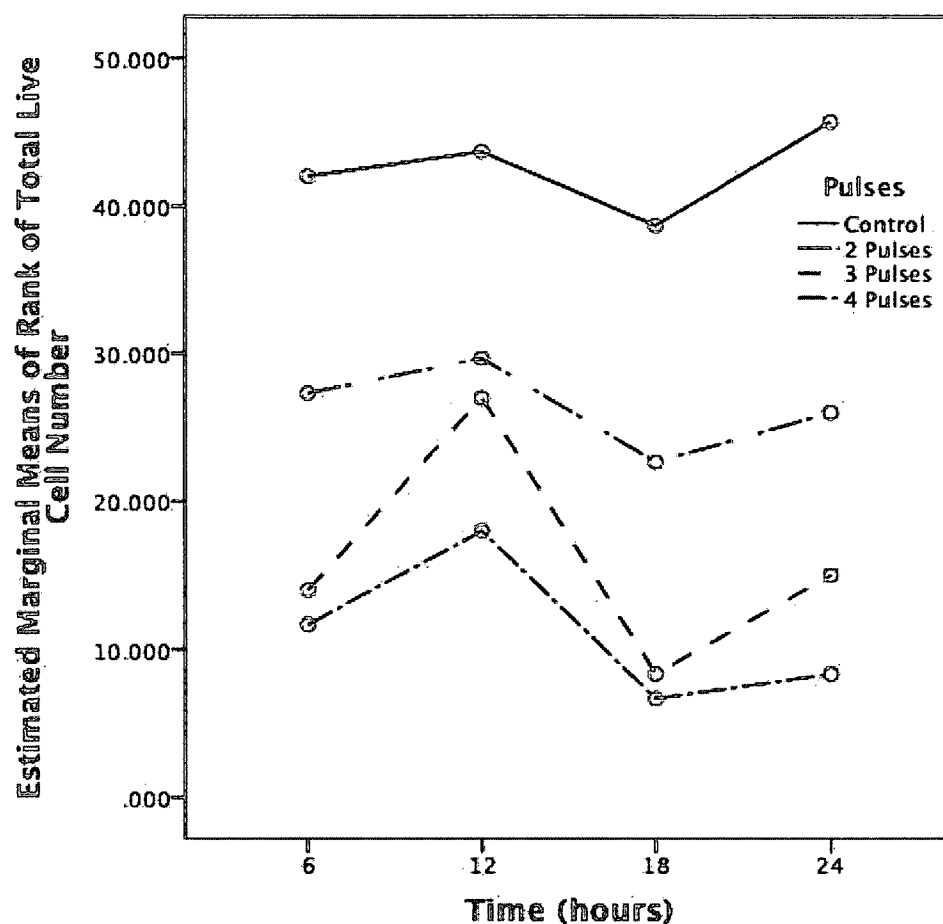


Figure 19. Long-Term Total Number of Live Cells after Multiple Pulses

The attached and floating cells after two, three, and four 300 ns 40 kV/cm pulses, as well as in the unpulsed group were counted using trypan blue after 6, 12, 18, and 24 h of culture. The total number of live cells was equal to the number of attached live cells plus the number of floating live cells. The solid line (control group) and the three dashed lines (two-, three-, and four-pulse groups) were almost parallel. No significant interaction was observed between the time points and the multiple pulse treatments in terms of the total number of live cells ($F=30.028$; $df=9, 32$; $P=0.862$), $n=3$.

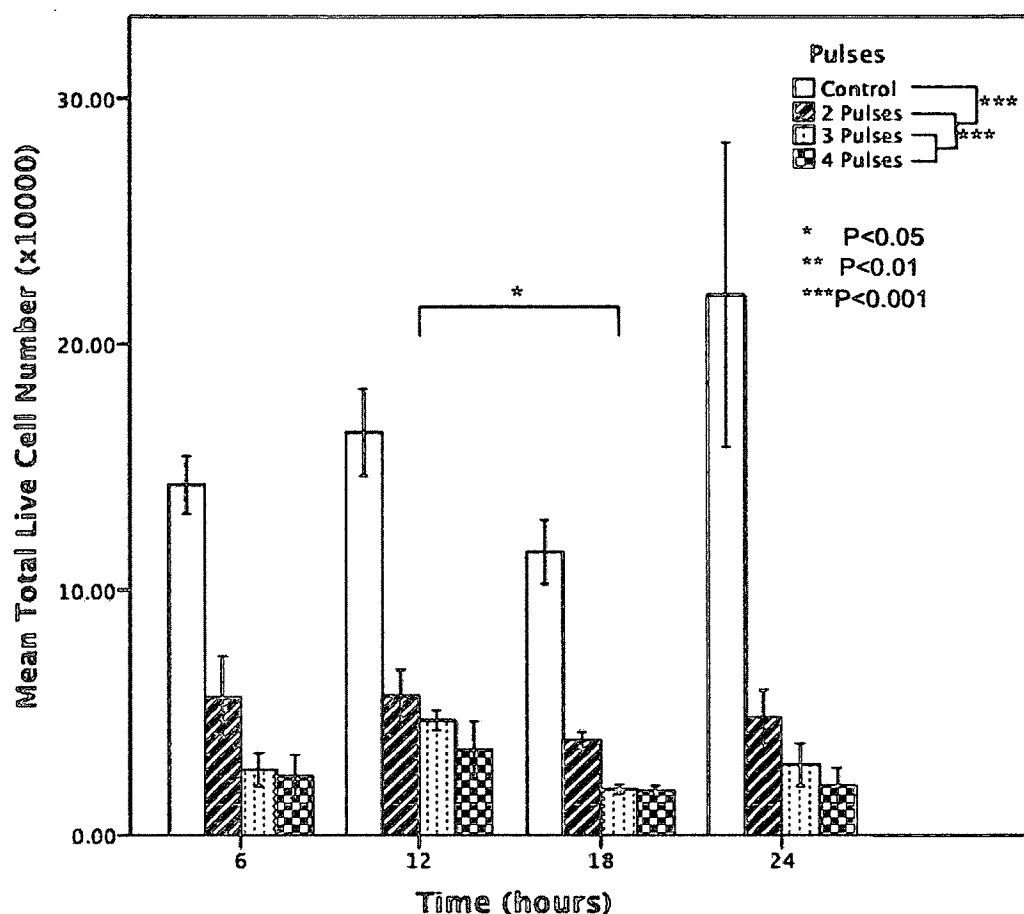


Figure 20. Long-Term Total Number of Live Cells after Multiple Pulses

The attached and floating cells after two, three, and four 300 ns 40 kV/cm pulses, as well as in the unpulsed group were counted using trypan blue after 6, 12, 18, and 24 h of culture. The total number of live cells was equal to the number of attached live cells plus the number of floating live cells. The total number of live cells significantly differed among the 6, 12, 18, and 24 h time points ($F=221.861$; $df=3, 32$; $P=0.021$). The Tukey's follow-up test of the time points showed a significant difference in the total number of live cells between the 12 h and the 18 h time points ($P=0.011$). The total number of live cells significantly differed among the multiple pulse treatments ($F=2301.806$; $df=3, 32$; $P<0.0000005$). The Tukey's follow-up test of the multiple pulse treatments showed that the total number of live cells in the control group was significantly higher than those in the two-, three-, and four-pulse treatments (all $P<0.0001$). The total number of live cells in the two-pulse group was significantly higher than those in the three-pulse group ($P=0.013$) and four-pulse group ($P=0.000182$). The data shown were means \pm SEM, $n=3$.

3.3.3 TOTAL NUMBER OF DEAD CELLS AFTER MULTIPLE PULSES

The total number of dead cells were counted using trypan blue at 6, 12, 18, and 24 h after pulsing and incubation. The total number of dead cells was equal to the number of attached dead cell plus the number of floating dead cells.

The natural log plus 1 transformation best exhibited a normal distribution and homogeneity. Therefore, the natural log transformation was used to conduct a two-way fixed ANOVA. The hypotheses were similar to those previously described for the total number of live cells. Three replicates were conducted.

The two-way fixed ANOVA indicated no significant interaction between the time points and the multiple pulse treatments ($F=0.809$; $df=9, 32$; $P=0.611$) (Table 12, graph not shown). The total number of dead cells significantly differed among the 6, 12, 18, and 24 h time points ($F=3.499$; $df=3, 32$; $P=0.027$) (Figure 21). The total number of dead cells significantly differed among the two-, three-, and four-pulse groups and the control group ($F=124.378$; $df=3, 32$; $P<0.0000005$). The Tukey's follow-up test of the time points comparisons revealed that the total number of dead cells at 12 h was significantly different from that at 24 h ($P=0.021$). The Tukey's follow-up test of the pulse treatment comparisons show that the total number of dead cells in the control group was significantly different from those in the two-, three-, and four-pulse groups (all $P<0.0000005$).

These results indicate that multiple pulses cause significant cell death, which is consistent with the decrease in total cell viability and in the number of total live cells.

Table 12. Natural Log Transformation of the Total Number of Dead Cells after Multiple Pulses, Two-Way Fixed ANOVA Table

Source	df	Mean Square	F	Significance	Observed Power
Time	3	0.218	3.499	0.027	0.726
Pulses	3	7.746	124.378	<0.0000005	1.000
Time×Pulses	9	0.050	0.809	0.611	0.323
Error	32	0.062			
Total	48				
Corrected Total	47				

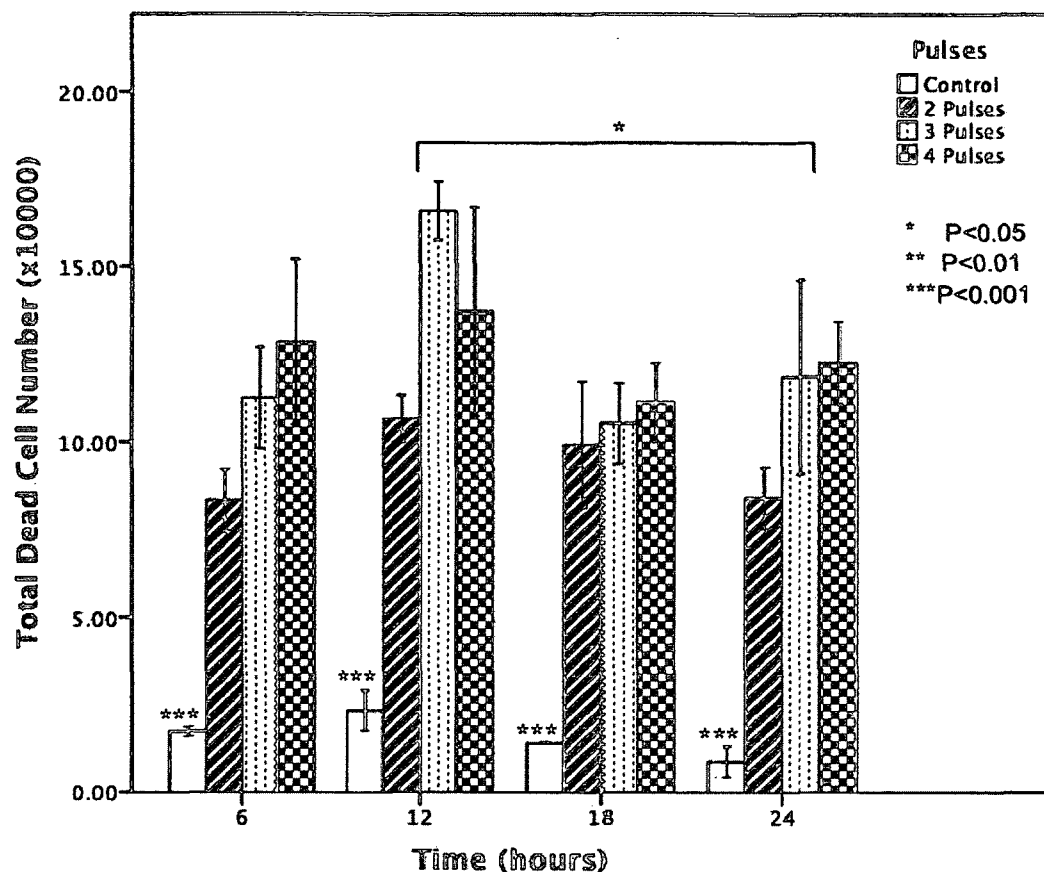


Figure 21. Long-Term Total Number of Dead Cells after Multiple Pulses

The attached and floating cells after two, three, and four 300 ns 40 kV/cm pulses, as well as in the unpulsed group, were counted using trypan bus after 6, 12, 18, and 24 h of culturing. The total number of dead cells was equal to the number of attached dead cells plus the number of floating dead cells. No significant interaction was observed between the time points and the multiple pulse treatments ($F=0.809$; $df=9, 32$; $P=0.611$). The total number of dead cells significantly differed among the 6, 12, 18, and 24 h time points ($F=3.499$; $df=3, 32$; $P=0.027$). The Tukey's follow-up test of time point comparisons showed that the total number of dead cells at 12 h was significantly higher than that at 24 h ($P=0.021$). The total number of dead cells significantly differed among the two-, three-, and four-pulse groups and control group ($F=124.378$; $df=3, 32$; $P<0.0000005$). The Tukey's follow-up test of the pulse treatment comparisons showed that the total number of dead cells in the control group was significantly lower than those in the two-, three-, and four-pulse groups (all $P<0.0000005$). The data shown were means \pm SEM, $n=3$.

3.4 CELL ATTACH ABILITY AFTER MULTIPLE PULSES

The attached and floating cells were counted using trypan blue to determine the changes in cell attachment ability at 6, 12, 18, and 24 h after multiple 300 ns 40 kV/cm pulses. The cell attachment ability can be represented in two ways. One way is as the percentage of the attached live cells of the total number of live cells. The total number of live cells is equal to the number of attached live cells plus the number of floating live cells. The other way is by comparing the number of live, dead, and the total cells in the floating growth medium with those of the attached live, dead, and total cells attached to the plate surface. Interpreting the comparison between the number of floating cells and number of attached cells is difficult and complex because multiple pulses cause cell death. Therefore, we only tested the cell attach ability using the percentage of attached live cells among the total live cells.

The attached and floating cells were counted at 6, 12, 18, and 24 h after two, three, and four 300 ns 40 kV/cm pulses and incubation. Cell attachment ability is represented as the percentage of the attached live cells among the total live cells. Three replicates were conducted.

The data transformed using natural log, square root, reciprocal, and exponential transformation did not meet the assumptions for normal distribution and homogeneity of variance. Thus, the rank values of the percentage of attached live cells were used to conduct a two-way fixed ANOVA. The hypotheses were similar to those for single pulse attachment ability, except for the four levels of the treatment factor (control group and two-, three-, and four-pulse groups).

The two-way fixed ANOVA indicated no significant interaction between the time points and the pulse treatments ($F=2.037$; $df=3, 32$; $P=0.067$) (Table 13, graph not shown). The percentage of attached cells significantly differed among the 6, 12, 18, and 24 h time points ($F=6.353$; $df=3, 32$; $P=0.002$). The percentage of attached cells significantly differed among the two-, three-, and four-pulse groups and the control group ($F=10.724$; $df=3, 32$; $P<0.00005$) (Figure 22). The Tukey's follow-up test of the time point comparisons revealed that the percentage of attached cells at 24 h was significantly different from those at 6, 12, and 18 h (all $P<0.05$). The Tukey's follow-up test of the pulse treatments show that the percentage of attached cells in the control group was significantly different from those in the two-pulse group ($P=0.014$), the three-pulse group ($P=0.004$), and the

four-pulse group ($P=0.00002$).

These results indicate that two, three, and four 300 ns 40 kV/cm pulses significantly decrease the cell attach ability, with more pulses decreasing the cell attachment ability further.

Table 13. Rank of the Percentage of Attached Cells after Multiple Pulses, Two-Way Fixed ANOVA Table

Source	df	Mean Square	F	Significance	Observed Power
Time	3	586.694	6.353	0.002	0.946
Pulses	3	990.361	10.724	<0.00005	0.997
Time×Pulses	9	188.083	2.037	0.067	0.755
Error	32	92.354			
Total	48				
Corrected Total	47				

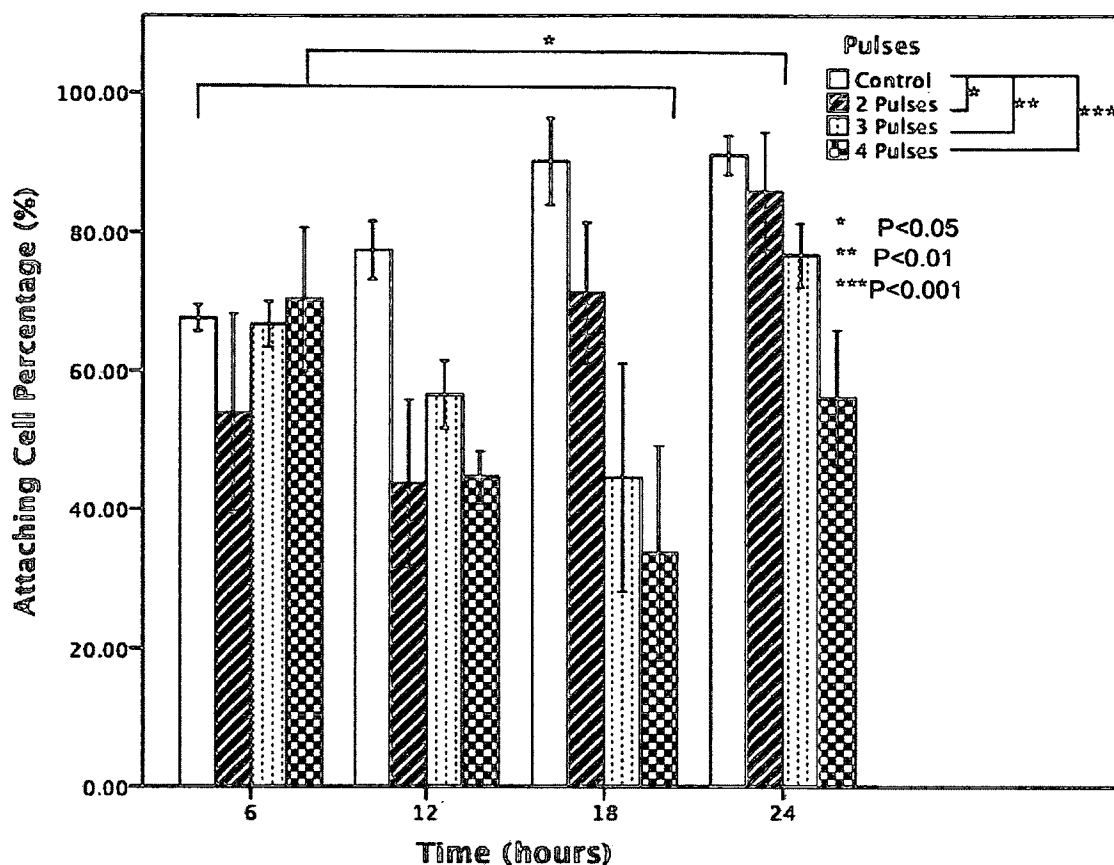


Figure 22. Percentage of Attached Cells after Multiple Pulses

The floating and attached live cells after two, three, four 300 ns 40 kV/cm pulses, as well as in the unpulsed group were counted using trypan blue after 6, 12, 18, and 24 h of pushing and incubation. The total number of live cells was equal to the number of floating live cells plus the number of attached live cells. Attachment ability was the percentage of attached live cell divided by the total number of live cells. No significant interaction was observed between the time points and the pulse treatments ($F=2.037$; $df=3, 32$; $P=0.067$). The percentage of attached cells significantly differed among the 6, 12, 18, and 24 h time points ($F=6.353$; $df=3, 32$; $P=0.002$). The Tukey's follow-up test of time point comparisons show that the percentage of attached cells at 24 h was significantly higher than those at 6, 12, and 18 h time points (all $P<0.05$). The percentage of attached cells significantly differed among the two-, three-, and four-pulse groups and the control group ($F=10.724$; $df=3, 32$; $P<0.00005$). The Tukey's follow-up test of the pulse treatments showed that the percentage of attached cells in the control group was significantly higher than those in the two-pulse group ($P=0.014$), the three-pulse group ($P=0.004$), and the four-pulse group ($P=0.00002$). The data shown were means \pm SEM, $n=3$.

3.5 CELL MORPHOLOGY AFTER MULTIPLE PULSES

The pulsed cells and the unpulsed cells (control) were immediately seeded after pulsing and were cultured in an incubator to determine the changes in cell morphology after multiple 300 ns 40 kV/cm pulses. The cells were observed and photographed using an inverted microscope at 200 \times magnification at 6, 12, 18, and 24 h after pulsing. Cell shape was described in the section on cell morphology after a single pulse.

At 6 h after pulsing, the number of attached cells and the spread area in the two-, three-, and four-pulse groups were significantly lower than in the control group (Figure 23). The cells were less spread out with more pulses. The cells subjected to four pulses exhibited the least spread area.

At 12 h after pulsing, the nuclei of the cells in the control group started to divide (Figure 24). Some control group cells rounded up to divide, which is caused by weak attachment of the cells onto the culturing plate. The cells after two, three, and four pulses spread out and showed less nuclear division.

At 18 h after pulsing, the control group reached 90% confluence (Figure 25). The cells in the control group had long spines and became multipolar or stellate. The function of the long spines is unknown but could be traces after cell division or traces after cell migration. The cells in all multiple pulse groups spread out. The cells in the two-, three-, and four-pulse groups exhibited less nuclear division and cell division than those in the control group.

At 24 h after pulsing, the nuclei of the cells in the control group were dividing and some cells rounded up for division (Figure 26). Some of the cell nuclei divided after two pulses to three pulses and formed long spines. Spines also formed after four pulses, but fewer cells exhibited nuclear division and cell division.

Therefore, multiple 300 ns 40 kV/cm pulses significantly decrease the cell attachment area, nuclear division, and cell proliferation and slow down cell attachment compared with the control group.

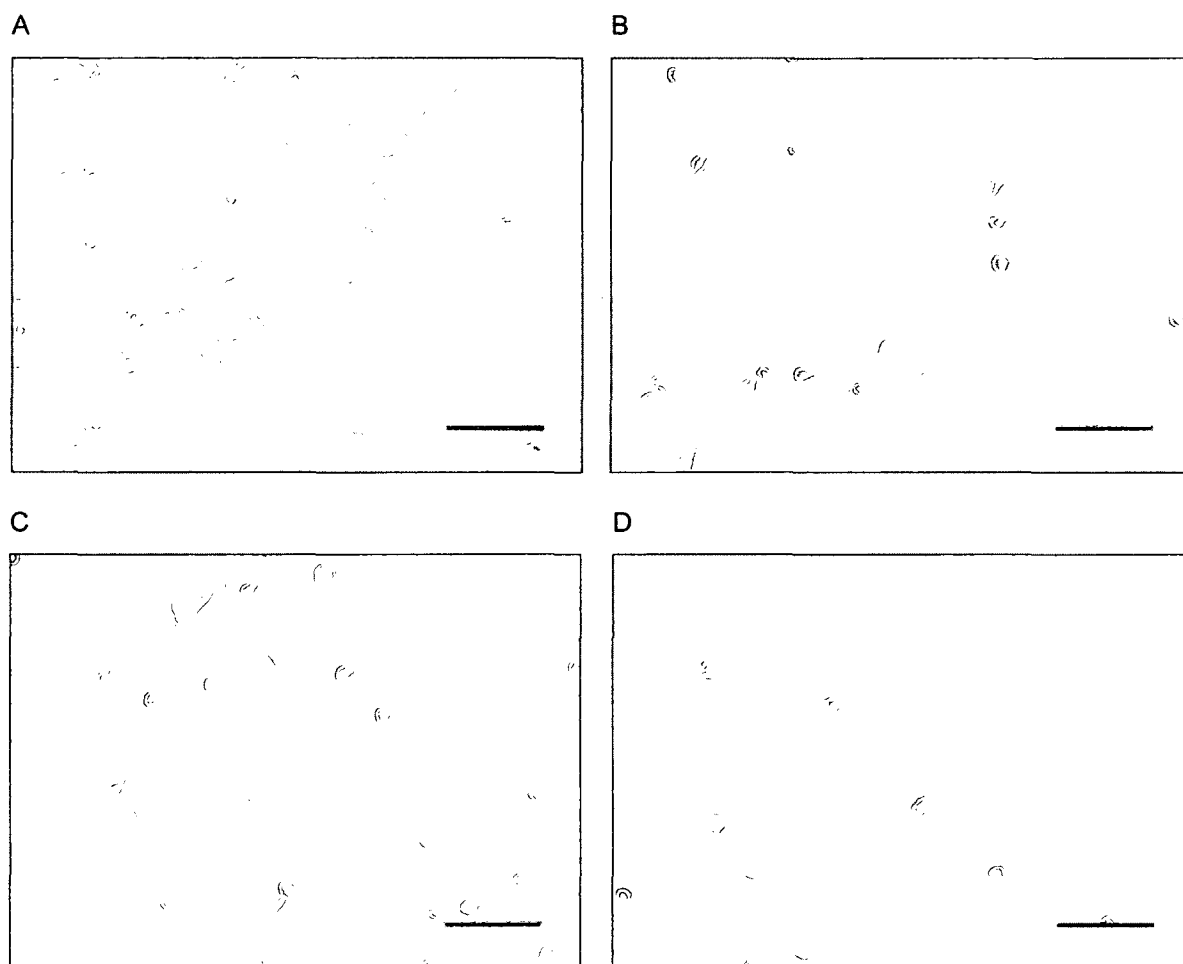


Figure 23. Cell Morphology at 6 h after Multiple Pulses

(A) Unpulsed control cells.

(B) Cells after two 300 ns 40 kV/cm pulses.

(C) Cells after three pulses.

(D) Cells after four pulses. Scale bar=100 μm . Cells were less spread out after multiple pulses. The cells after four pulses were the least spread out among the pulse treatments.

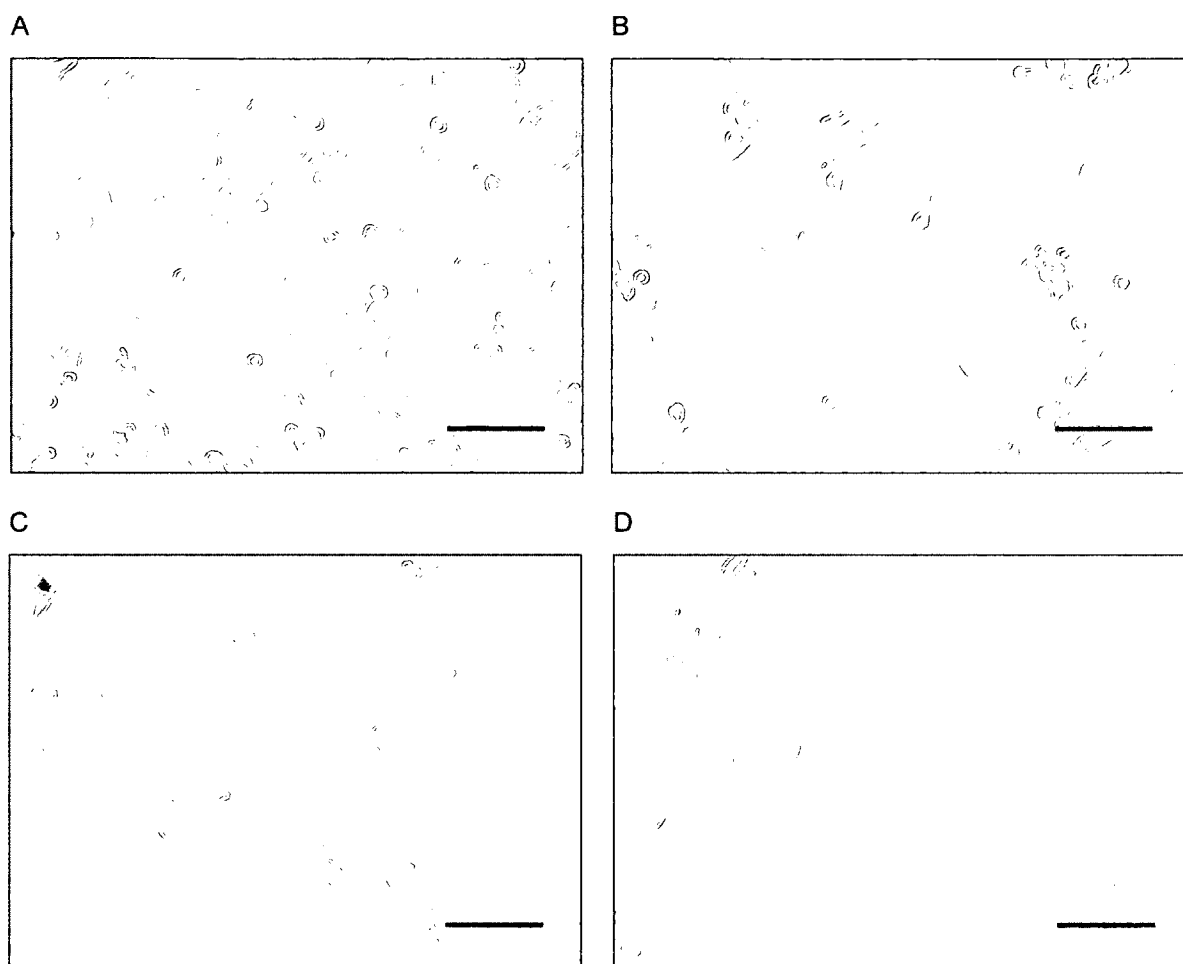


Figure 24. Cell Morphology at 12 h after Multiple Pulses

(A) Unpulsed control group.

(B) Two 300 ns 40 kV/cm pulse group.

(C) Three-pulse group.

(D) Four-pulse group. Scale bar=100 μ m. The nuclei of the control group began to divide. Some control group cells rounded up. The cells were spread out and exhibited less nuclear division after multiple pulses.

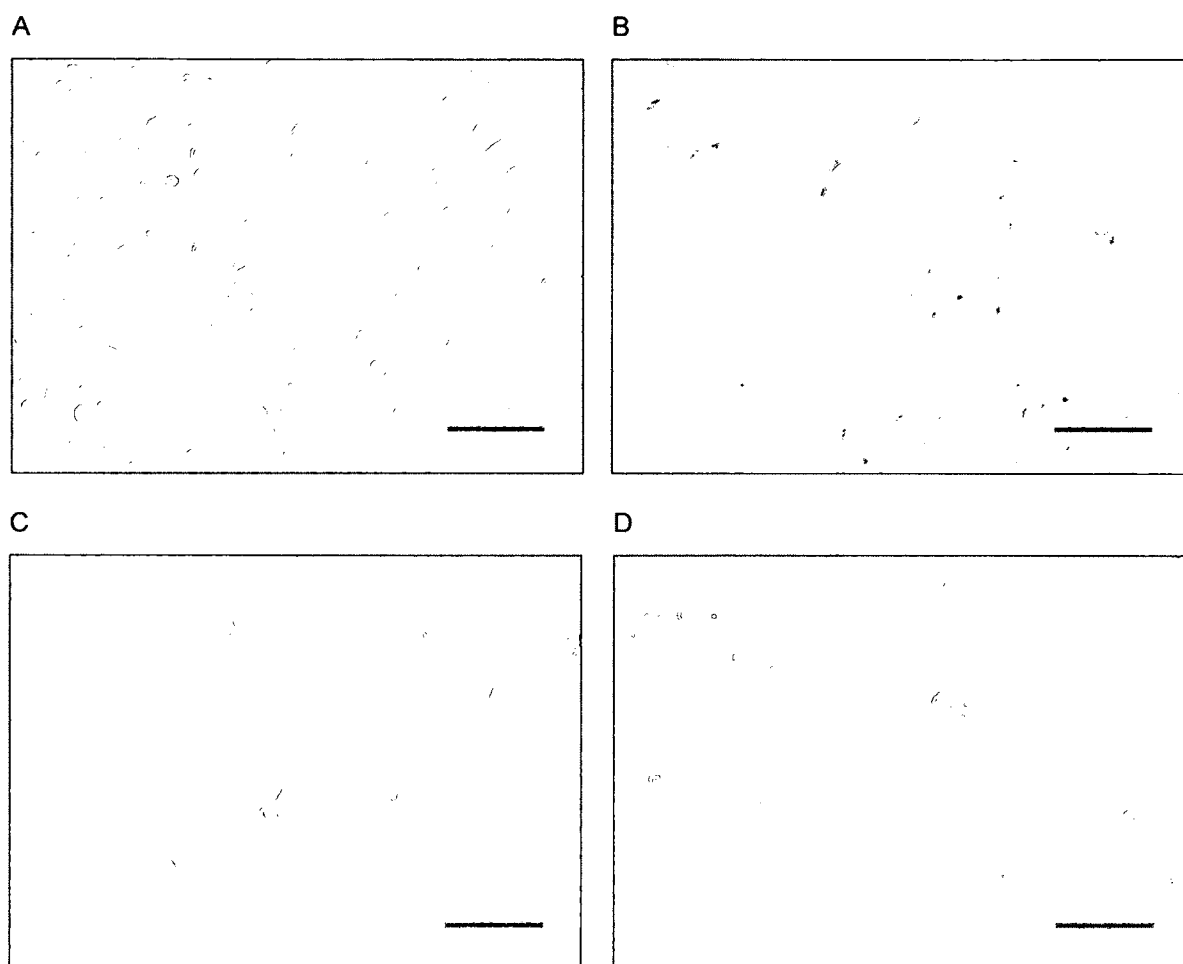


Figure 25. Cell Morphology at 18 h after Multiple Pulses

(A) Unpulsed control group.

(B) Two 300 ns 40 kV/cm pulse group.

(C) Three-pulse group.

(D) Four-pulse group. Scale bar=100 μ m. The control group reached 90% confluence. The cells in the control group formed long spines and were multipolar or stellate. The cells after two, three, and four pulses were spread out and they exhibited less nuclear division and cell division.

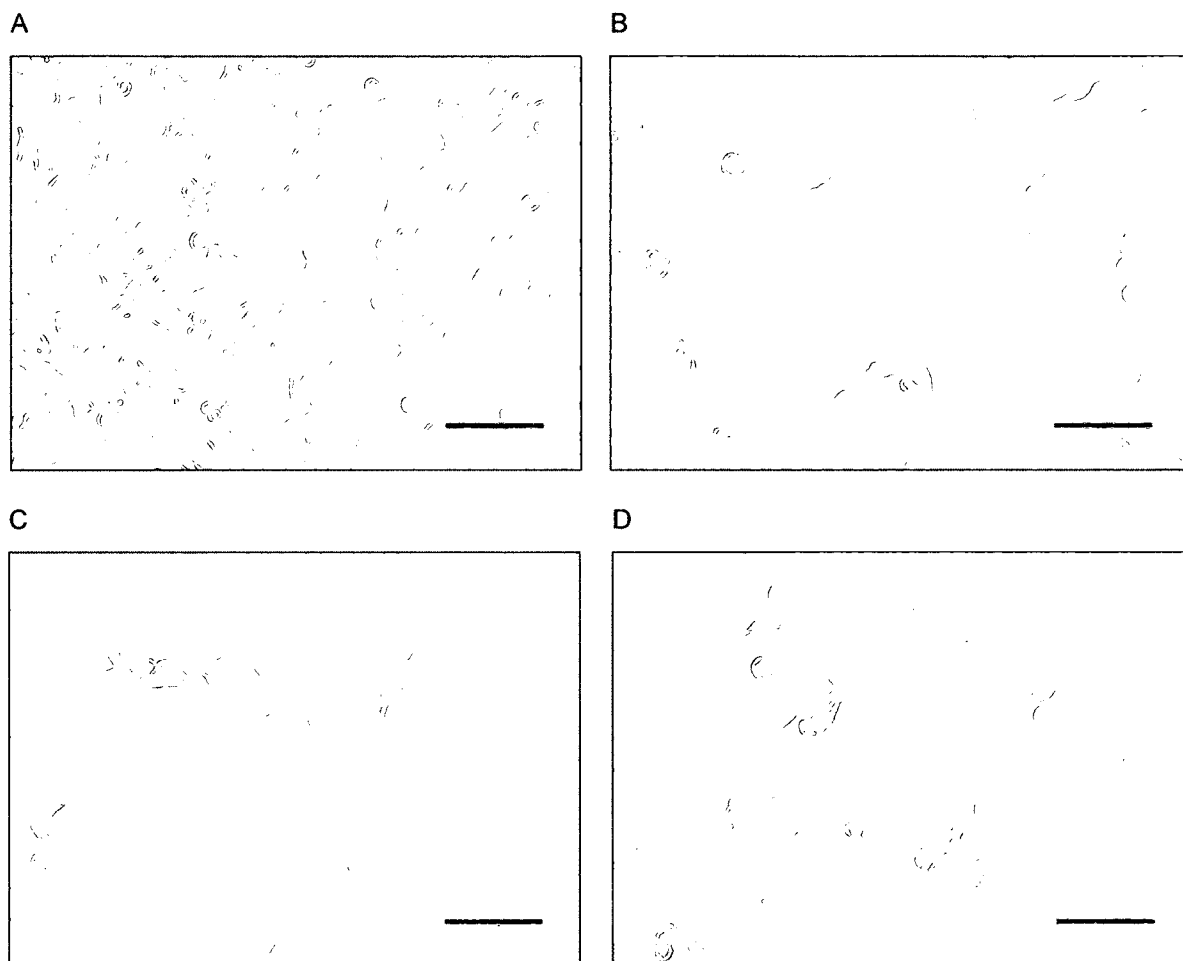


Figure 26. Cell Morphology at 24 h after Multiple Pulses

(A) Unpulsed control group.

(B) Two 300 ns 40 kV/cm pulse group.

(C) Three-pulse group.

(D) Four-pulse group. Scale bar=100 μ m. The control group began to divide again. Long spines were shown in the control group and multiple pulses group. Some of the cells exhibited nuclear division after two pulses to three pulses. No obvious nuclear division occurred in the cells after four pulses.

3.6 RNA QUALITY CONTROL AND REAL-TIME PCR QUALITY CONTROL

The integrity and purity of the total RNA extracted from all cell samples were tested to maintain the quality of the total RNA.

3.6.1 TOTAL RNA INTEGRITY

Gel electrophoresis was used to test total RNA integrity. Mouse 28S rRNA was 4700 nt and 18S rRNA was 1900 nt. The theoretical 28S:18S ratio was 2.7:1. The clear 28S and 18S rRNA bands indicated the RNA was intact. A random RNA sample was subjected to gel electrophoresis. The 28S and 18S rRNA bands were clearly shown in lane 2 (Figure 27). The ladder is a DNA marker, which has double strands of nucleotides. rRNA is a single strand nucleotide. Therefore, the 4700 nt single strand of 28S rRNA was slightly smaller than the 3000 bp DNA ladder. The 1900 nt single strand of 18S rRNA was slightly smaller than the 1000 bp DNA ladder. The intensity of the 28S band and 18S band was more than 2:1. The two rRNA bands were sharp. Therefore, the total RNA samples extracted from the cell samples were intact.

3.6.2 TOTAL RNA PURITY AND CONCENTRATIONS

We took the data from the single pulse treatment as an example. The data after the multiple pulses were similar (data not shown). The volume of the RNA extracted from each sample was 30 μ L. One microliter of the extracted total RNA was analyzed for purity and concentration. The A_{260}/A_{280} ratio of all extracted total RNA were between 1.8 and 2.1 (Table 14), which indicates that all extracted total RNA can be considered pure RNA. The concentration of all the RNA samples were measured and recorded.

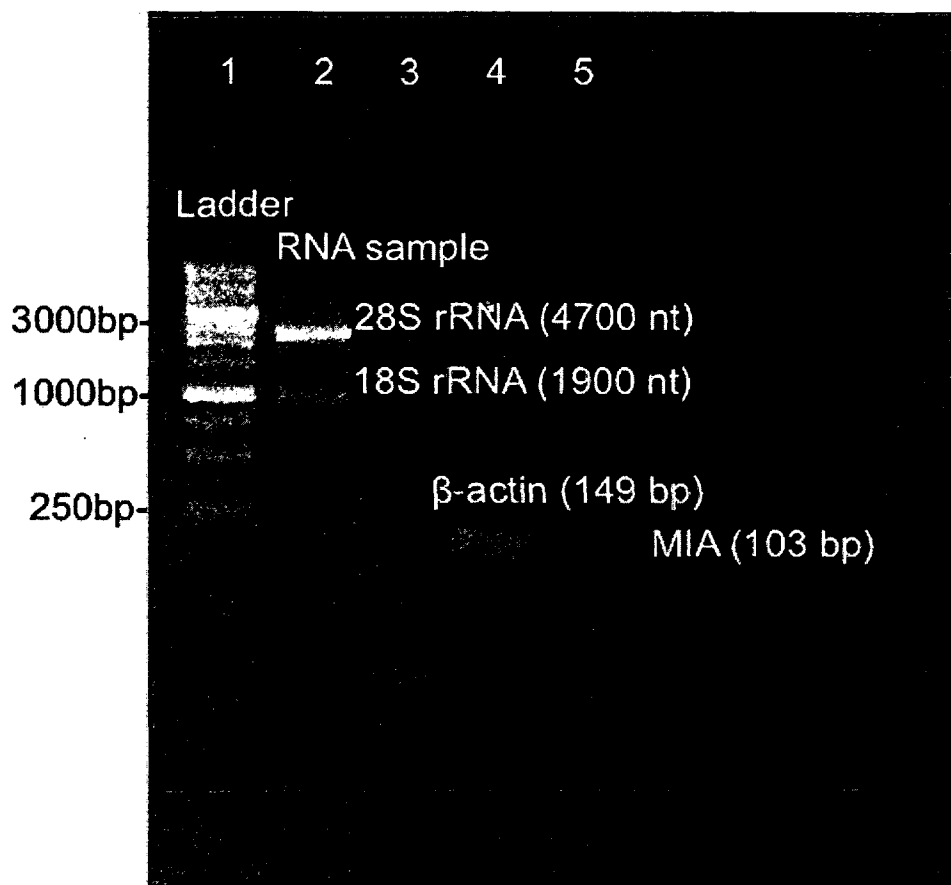


Figure 27. Gel Image of the RNA Sample and quantitative Real-time PCR product

The gel electrophoresis of total RNA sample extracted from a randomly chosen specimen and the quantitative real-time PCR product were conducted using 1% natural agarose gel at 120 V for 30 min.

(Lane 1) DNA ladder.

(Lane 2) The extracted total RNA sample was randomly chosen. A 28 S rRNA band (4700 nt) was observed at around 3000 bp and a 18S rRNA band (1900 nt) was observed at around 1000 bp. The intensity of the 28S/18S band exceeded 2:1. Therefore, the extracted total RNA sample was intact.

(Lane 4) The intense β -actin band of quantitative real-time PCR product (149 bp).

(Lane 5) Very faint band of MIA quantitative real-time PCR product (103 bp).

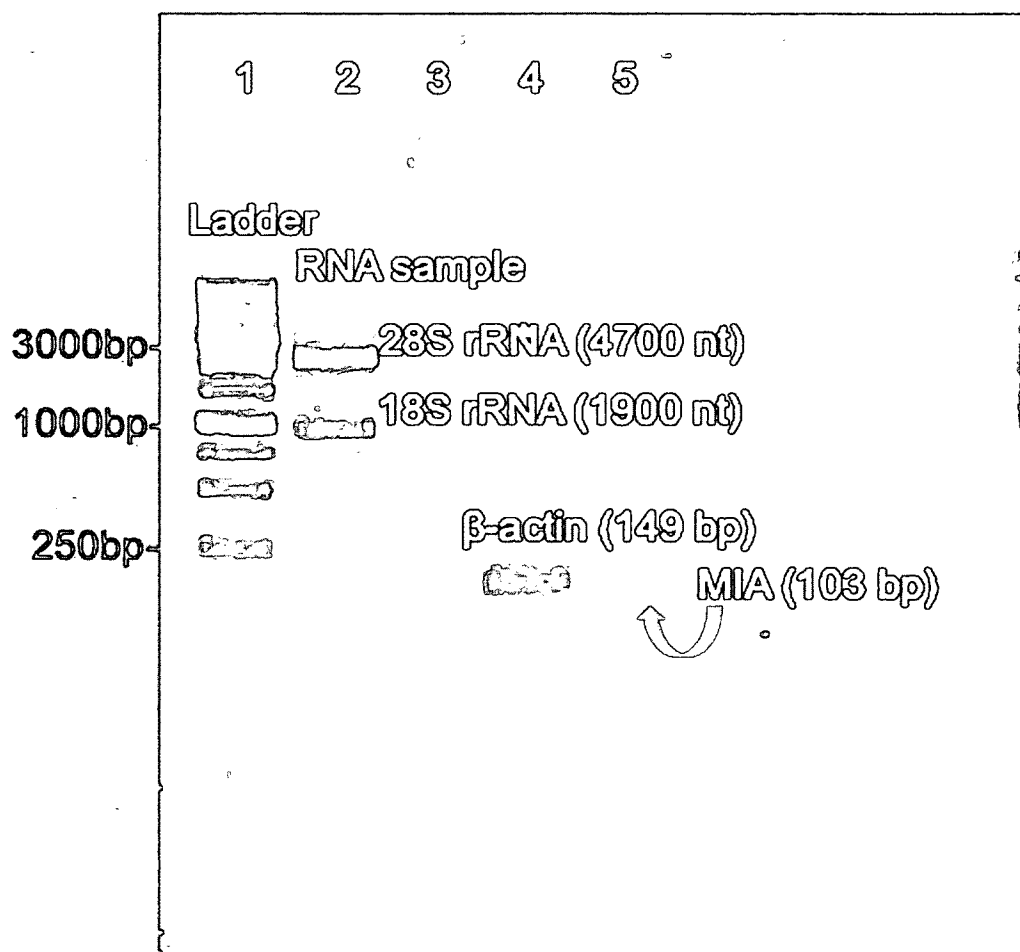


Figure 28. Adjusted Gel Image to Show MIA Band

This is an adjusted gel image from the original gel image in Figure 27. The arrow pointing to a very faint band in Lane 5 is MIA quantitative real-time PCR product. The MIA quantitative real-time PCR product was 103 bp.

Table 14. Purity and Concentrations of the Extracted Total RNA

Time	Trial	Treatment	A260	A280	A260 /A280	RNA con- centration (ng/uL)
6 hours	1	Experiment	0.657	0.341	1.93	26.3
6 hours	2	Experiment	1.206	0.607	1.99	48.3
6 hours	3	Experiment	0.944	0.463	2.04	37.7
6 hours	1	Control	1.899	0.975	1.95	76.0
6 hours	2	Control	1.884	1.049	1.80	75.4
6 hours	3	Control	1.542	0.795	1.94	61.7
12 hours	1	Experiment	1.704	0.870	1.96	68.2
12 hours	2	Experiment	2.262	1.223	1.85	90.5
12 hours	3	Experiment	1.461	0.736	1.98	58.4
12 hours	1	Control	0.554	0.306	1.81	22.2
12 hours	2	Control	1.966	1.013	1.94	78.6
12 hours	3	Control	1.503	0.779	1.93	60.1
18 hours	1	Experiment	1.926	0.968	1.99	77.0
18 hours	2	Experiment	2.278	1.149	1.98	91.1
18 hours	3	Experiment	2.032	1.016	2.00	81.3
18 hours	1	Control	2.089	1.047	2.00	83.6
18 hours	2	Control	2.510	1.250	2.01	100.4
18 hours	3	Control	2.806	1.391	2.02	112.2
24 hours	1	Experiment	3.507	1.723	2.04	140.3
24 hours	2	Experiment	2.171	1.070	2.03	86.8
24 hours	3	Experiment	2.476	1.220	2.03	99.0
24 hours	1	Control	4.058	1.989	2.04	162.3
24 hours	2	Control	3.855	1.895	2.03	154.2
24 hours	3	Control	2.919	1.439	2.03	116.8

3.6.3 REAL-TIME PCR QUALITY CONTROL

The NRT and NTC negative controls, melting curve analysis, and gel electrophoresis of the quantitative real-time PCR product were used to control the real-time PCR quality.

NRT and NTC negative controls

A no reverse transcriptase (NRT) negative control and a no template control (NTC) were used during reverse transcription to check for DNA contamination of the RNA sample. The NRT negative control and the NTC should not have any real-time PCR product. If the NRT negative control formed a PCR product, the total RNA sample was contaminated with genomic or environmental DNA.

The Taq DNA polymerase used in the real-time PCR acts as a reverse transcriptase (Martel et al., 2002), which generates cDNA from RNA during the real-time PCR step. The RNA sample was treated with 1 μ L of 1 mg/mL RNase A (Bioo Scientific, Catalog No. 344005) at 37°C for 30 min in the cell culture incubator before conducting a reverse transcription reaction to eliminate false positive NRT results.

The quantification cycle (Cq) value is the number of cycles required for the fluorescent signal to exceed the threshold. The Cq value is inversely proportional to the amount of target nucleic acid in the sample. The Cq value of the NRT negative control was between 38 cycles to 40 cycles (Figure 29), which indicates the occurrence of a very weak reaction and minimal amounts of the target nucleic acid, genomic, or environmental contamination. The Cq of the NRT negative control was 8 cycles more than the MIA amplified samples, which means that the DNA contamination in the RNA samples is less than 0.5% of the cDNA. Therefore, the RNA and cDNA samples were not significantly contaminated with DNA.

DNA-free/RNA-free water was used to replace the cDNA template during the real-time PCR procedure, which is called the NTC, to test for non-specific PCR products and DNA contamination. If the NTC negative control forms a PCR product, non-specific PCR or DNA contamination occurred during the real-time PCR.

The Cq value of one NTC ranged from 38 cycles to 40 cycles (Figure 29). The

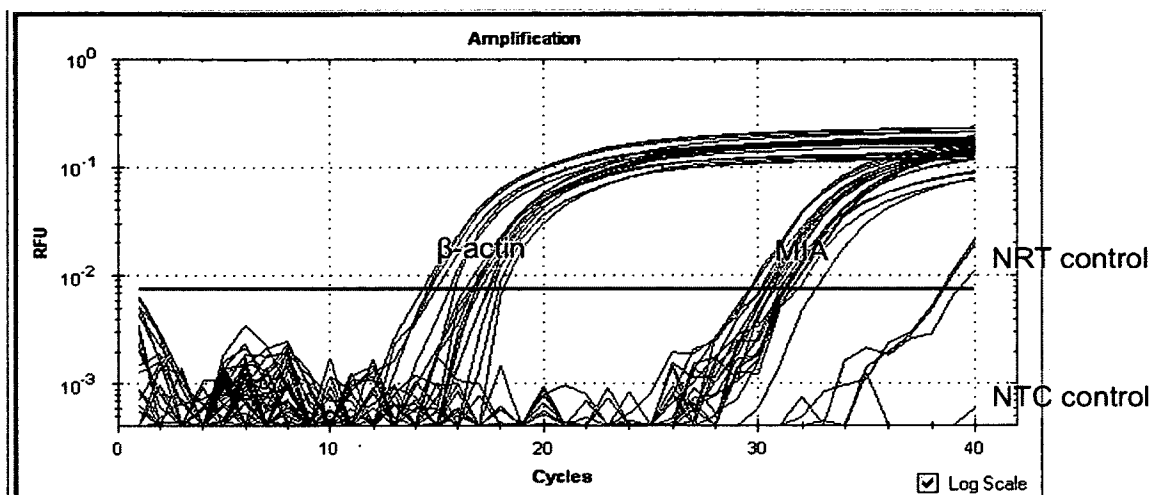


Figure 29. The NRT Negative Control and the NTC Negative Control

The Cq of the batch β -actin quantitative real-time PCR ranged from 14 cycles to 18 cycles. The Cq of the batch MIA reactions ranged from 29 cycles to 33 cycles. The Cq values of the two NRT negative control reactions ranged from 38 and 40 cycles. The Cq value of one NTC ranged from 38 cycles to 40 cycles. The Cq of another NTC was undetectable, which exceeded 40 cycles. The extracted total RNA sample and the quantitative real-time PCR product were free of genomic DNA contamination and environmental DNA contamination.

Cq of the other NTC was undetectable, which exceeded 40 cycles. These findings indicate minimum environmental DNA contamination, which is negligible. No PCR product was detected in the second NTC control, which indicates the absence of non-specific products or DNA contamination.

Thus, the extracted total RNA sample and the quantitative real-time PCR product were pure.

Melting curve analysis

A melting curve analysis was conducted to determine the presence of single real-time PCR amplification or multiple PCR amplifications. Melting curve analyses measure the dissociation characteristics of double-stranded DNA during heating.

The double-stranded DNA dissociates with increasing temperature, causing a decrease in absorbance. When the temperature was increased uniformly, the pure double-stranded DNA PCR product would dissociate into single-stranded

DNA. The resulting sharp decrease in fluorescence is caused by the dissociation of SYBR Green to exhibit a single melting peak. Different double-stranded DNA PCR product would exhibit multiple melting peaks.

The melting peak analysis of MIA and β -actin real-time PCR product was performed at the end of PCR. The MIA melting peaks of all samples were aggregated at 83°C and the β -actin melting peaks of all samples were aggregated at 89°C (Figure 30). The four off-peak curves are from NTC and NRT negative control.

Thus, a single double-stranded DNA PCR product was observed for MIA and for β -actin.

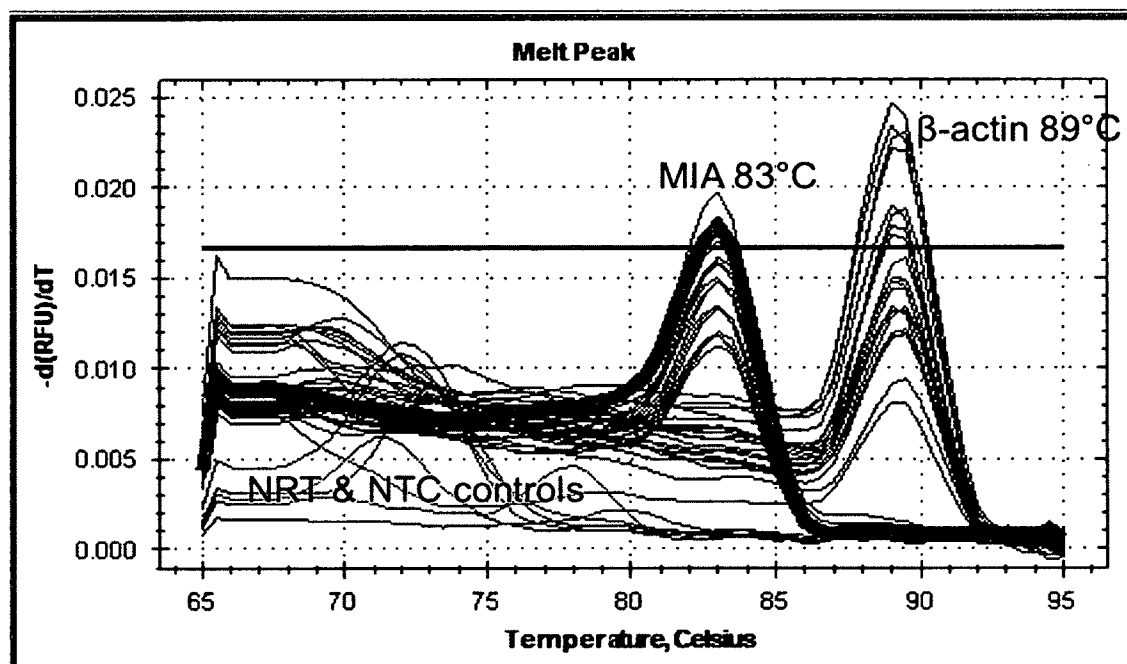


Figure 30. Melting Curve Analysis

Melting curve analysis was performed at the end of quantitative real-time PCR retains. The MIA melting peaks of all the samples were aggregated at 83°C and the β -actin melting peaks of all the samples were aggregated at 89°C. The four off-peak curves were obtained from the NTC and NRT negative control.

Gel electrophoresis of the PCR product

The size of the real-time PCR product was examined through gel electrophoresis to test the specificity of the real-time PCR reaction. The MIA amplicon should be 104 bp, whereas the β -actin amplicon should be 149 bp. A clear β -actin band was observed below 250 bp (Figure 27), and a very faint MIA band was found below and to the right of the β -actin band in the gel image (Figure 28). These band sizes match their corresponding theoretical specific PCR amplicon size. Therefore, the real-time PCR reactions have highly specific amplifications.

The intensity of the 3 kb and the 1 kb bands in the ladder indicates that the amount of the DNA was 92 ng. The intensity of the 250 bp ladder indicates that the amount of DNA was 45 ng. Therefore, the amount of the β -actin amplicon was less than 92 ng and that of the MIA amplicon was much less than 45 ng. The amounts of these PCR products are consistent with their Cq values, which shows that β -actin is expressed much more than MIA.

3.7 DETERMINING REAL-TIME PCR AMPLIFICATION EFFICIENCY

The amplification efficiencies of the real-time PCR were calculated via single real-time PCR (Ramakers et al., 2003) using LinRegPCR (2012.0), a Windows program for analyzing real-time PCR (Ruijter et al., 2009). The efficiencies were compared with those using qpcR, an R package for real-time PCR analysis (Ritz and Spiess, 2008).

The amplification efficiencies from all the real-time PCR reactions from the single 300 ns 40 kV/cm pulse experiments were calculated using LinRegPCR and qpcR, from the raw fluorescence data. The means of the amplification efficiencies of β -actin and MIA in both programs should be close to 2 to use the $2^{-\Delta Cq}$ method; otherwise, individual efficiency must be employed in the calculation (Equation 3).

3.7.1 LinRegPCR:

The amplification efficiency of each real-time PCR was derived from the slope of the regression line in the log-linear phase (Figure 31). The percentage efficiency is shown in box plot (Figure 32). The amplification efficiency of the

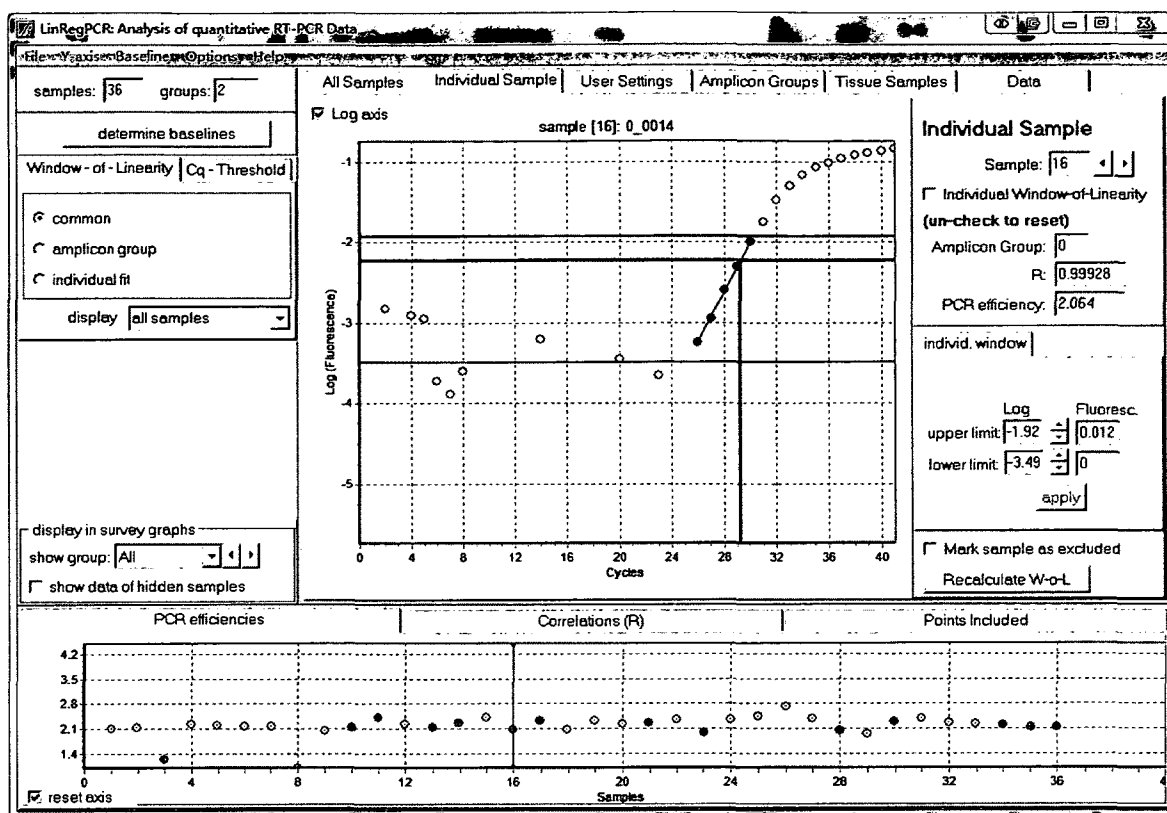


Figure 31. Determination of Individual Amplification Efficiency Using LinRegPCR

PCR efficiency was calculated using LinRegPCR from the slope of the regression line in the log-linear phase (5 red dots). The PCR efficiency of sample 16 was 2.064, as shown in the graph.

β -actin reactions was 2.21 ± 0.27 (mean \pm SD, $n=71$), and the efficiency of the MIA reactions was 2.04 ± 0.15 (mean \pm SD, $n=67$). The amplification efficiencies for both primers were close to 2. Therefore, 2 can be substituted for the amplification efficiency. The MIA and β -actin mRNA expression were calculated (Equation 3).

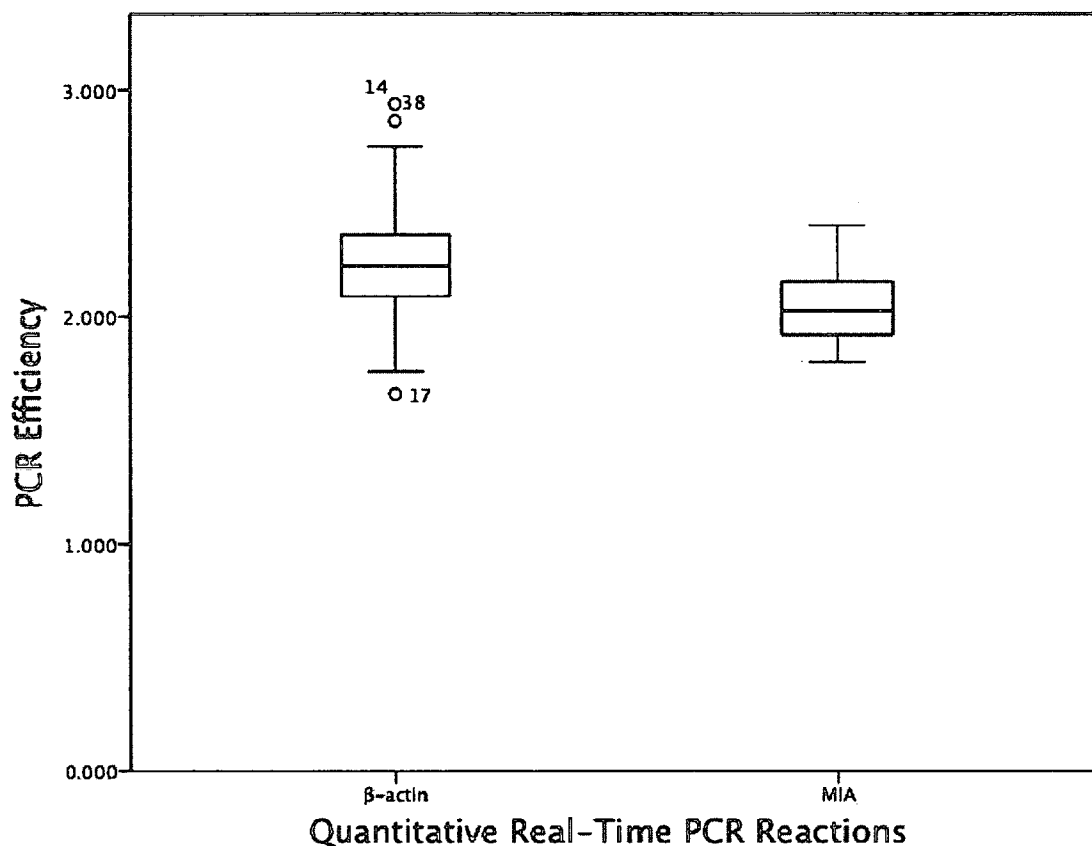


Figure 32. Box Plot of Amplification Efficiencies, Determined by LinRegPCR

The quantitative real-time PCR amplification efficiencies obtained using LinRegPCR were plotted. The bottom and top of the box are the 1st and 3rd quartiles (Q1 and Q3). The band inside the box is the 2nd quartile (Q2) or the median. The interquartile range (IQR) is $Q3 - Q1$. The top end of the whisker is $Q1 + 1.5 \times IQR$. The bottom end of the whisker is $Q3 - 1.5 \times IQR$. The data points beyond the whiskers are outliers. Sample 14, 17, and 38 were outliers of the β -actin PCR efficiencies. The β -actin and MIA PCR efficiencies were around 2, and were not significantly different.

3.7.2 qpcR:

Both the β -actin and MIA individual amplification efficiencies were analyzed using the qpcR package of the R program. The qpcR package of the R program was installed and loaded before typing in the following steps (the β -actin reaction efficiencies are shown as an example), which were modified from Package 'qpcR' Document as follows:

```
# import fluorescence raw data of all actin reactions to 'pcr'
> pcr=read.csv(file="Efficiency_actin.csv", header=TRUE)

# fit all reactions into b7 model, the best fit model
> mL1=modlist(pcr, model=b7)

# calculated efficiencies of each reaction and put into 'res'
> res=sapply(mL1, function(x) efficiency(x)$eff)

# draw a bar plot to show all actin reaction efficiencies
> barplot(as.numeric(res), xlab="beta-actin Real-time PCR
Reactions", ylab="Real-time PCR Amplification Efficiencies")

# calculate the mean efficiencies of all reactions
> mean(as.numeric(res))

# calculate the standard deviation
> sd(as.numeric(res))
```

The efficiencies are derived from the peak of the second derivative curve (type="cpD2" by default, Figure 33). The bar plots for β -actin and MIA indicate that the PCR efficiency of β -actin were more than 2, whereas that for MIA was around 2 (Figure 34 and 35). The mean amplification efficiency of β -actin was 3.32 ± 1.01 (mean \pm SD). The mean amplification efficiency of MIA was 2.19 ± 0.11 (mean \pm SD). The β -actin and MIA amplification efficiencies were close to 2. Therefore, the PCR efficiencies of both β -actin and MIA was confirmed as 2.

The β -actin and MIA PCR efficiencies in both LinRegPCR and qpcR were around 2 or more than 2. The β -actin PCR efficiency was slightly higher than the

MIA PCR efficiency, possibly because the amount of β -actin in the samples was much greater than that of MIA and the Cq values of MIA was more than 10 cycles greater than that of β -actin. Therefore, the real-time PCR of MIA was less efficient after 10 more cycles than that of β -actin. However, the PCR efficiencies of both β -actin and MIA remained greater than or around 2. Therefore, the β -actin and MIA mRNA expression levels were calculated using 2 as the PCR efficiencies (Equation 3).

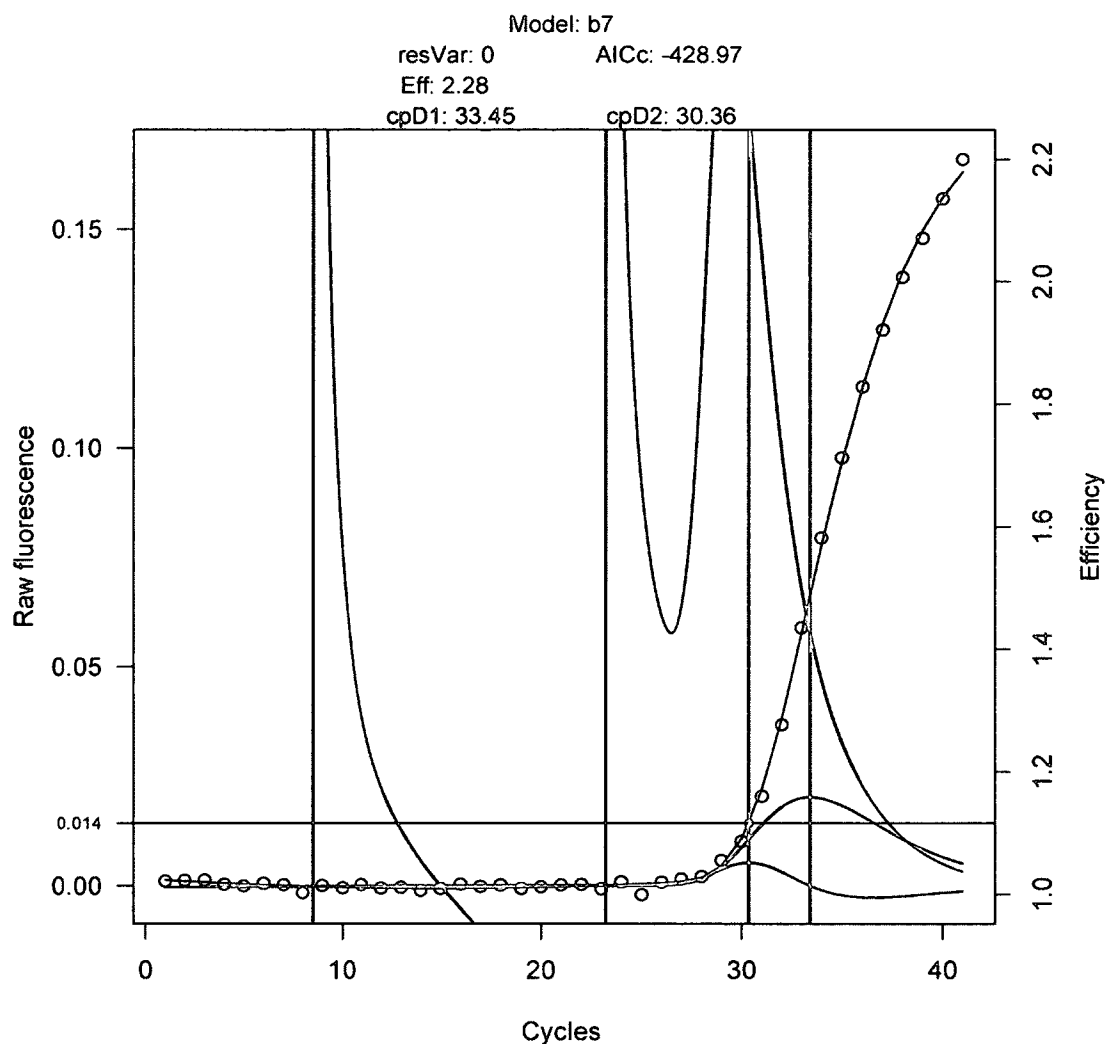


Figure 33. Real-time PCR Amplification Efficiency Determined by qpcR

The PCR efficiencies were calculated from the second derivative curve (cpD2) using the best fit b7 model. The PCR efficiency of this sample was 2.28, which was obtained from the intersection of the green line and the blue curve at right at 30.36 cycles.

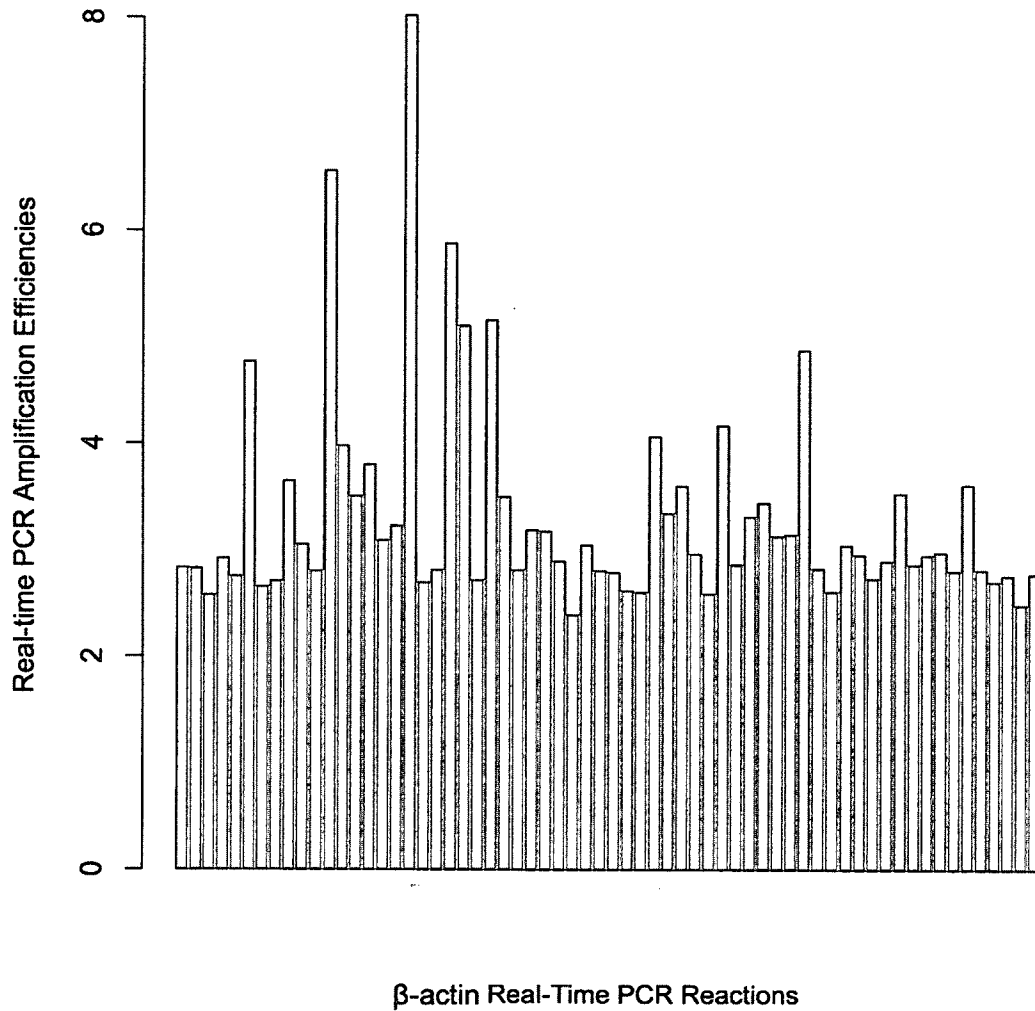


Figure 34. β -actin Real-Time PCR Amplification Efficiency

All the β -actin PCR efficiencies of the single pulse experiments were obtained from the qpcR program and were more than 2. A few outliers, which were more than 4, were observed. The β -actin PCR efficiency was 3.32 ± 1.01 (mean \pm SD).

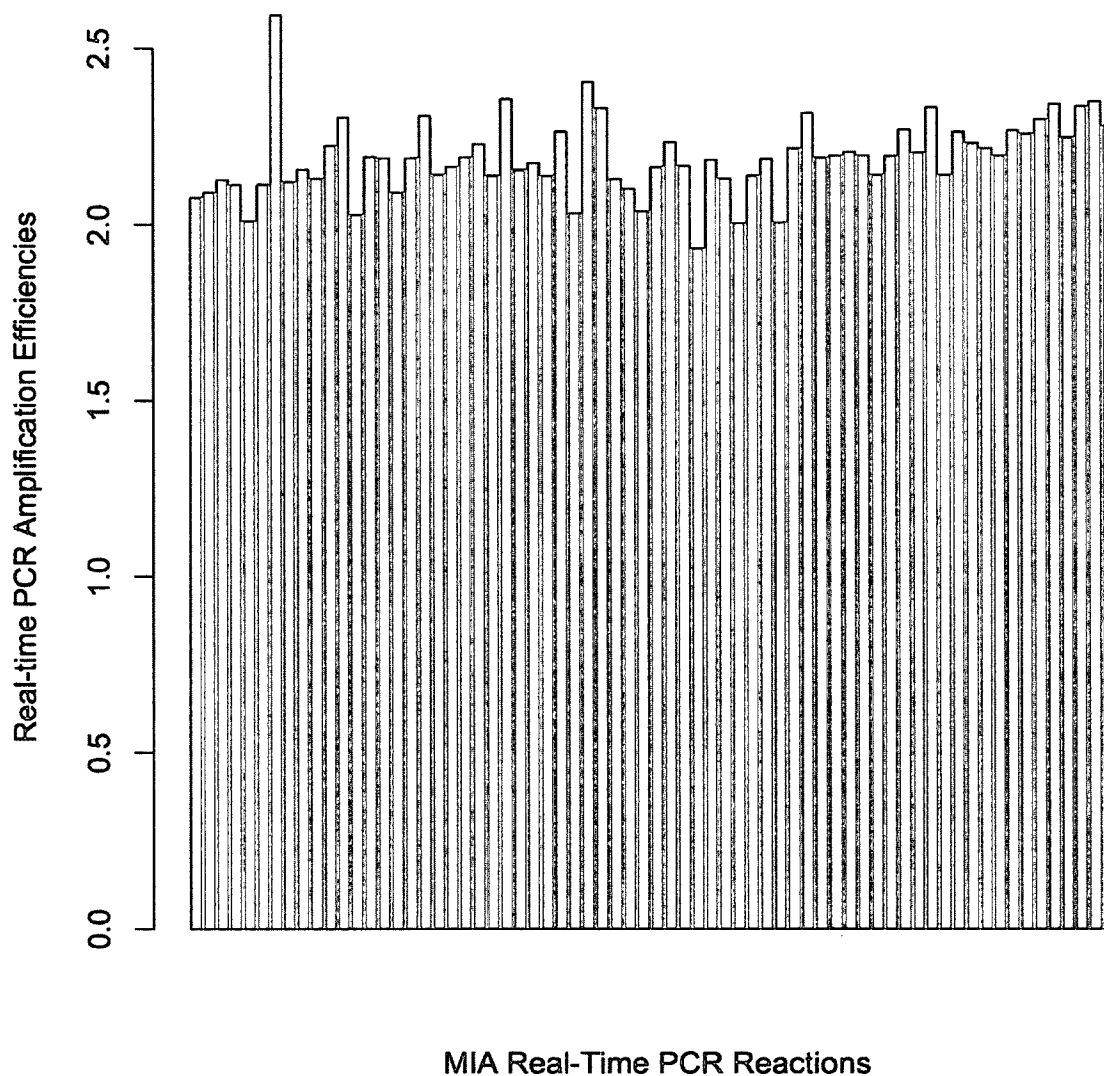


Figure 35. MIA Real-Time PCR Amplification Efficiency

All of the MIA PCR efficiencies of the single pulse experiments were obtained from the qpcR program and were around 2. Only one outlier was observed, which exceeded 2.5. The MIA PCR efficiency was 2.19 ± 0.11 (mean \pm SD).

3.8 MIA mRNA EXPRESSION LEVEL AFTER A SINGLE PULSE

The cells that were seeded and immediately incubated after a single 300 ns 40 kV/cm pulse were harvested at 6, 12, 18, and 24 h to measure their MIA mRNA expression levels. Three replicates were conducted. Total RNA was extracted from each cell sample. The cDNA templates were produced through reverse transcription. The reverse transcription templates for all samples were adjusted to the same amount (200 ng total RNA). The real-time PCR templates (cDNAs from reverse transcription) were applied at the same amount (2 μ L). Therefore, the C_q values within each group were close. Any value that deviated from other group members was checked as a suspect outlier.

Each cDNA sample had three real-time PCR replicates. The mean C_q values of the three replicates of each trial were calculated (Table 15). The β -actin and MIA cDNA level in the third trial of the control group at 6 h were omitted in the following statistical analysis because 32.70 was an obvious outlier and no real-time PCR raw curve was constructed for MIA. A problem may have occurred during the reverse transcription for this sample. Manipulating reverse transcription should be conducted more carefully in the future.

Table 15. Mean C_q Values of β -actin and MIA cDNA after a Single Pulse

Treatment	6 h		12 h		18 h		24 h	
	β -actin	MIA	β -actin	MIA	β -actin	MIA	β -actin	MIA
1 Pulse	13.61	27.64	13.59	29.32	13.67	29.62	14.22	30.02
	13.92	27.51	14.14	29.77	13.93	29.83	14.03	29.97
	13.60	27.40	13.42	29.17	13.88	29.92	13.99	29.73
Control	13.63	27.68	13.66	29.60	13.73	30.16	14.09	29.79
	14.28	28.58	14.09	29.54	13.95	29.69	14.21	29.97
	32.70	–	13.59	29.30	13.76	30.17	14.19	30.13

The MIA mRNA expression level was calibrated by the β -actin for each

sample (Equation 3, Table 16).

$$\text{Calibrated MIA mRNA Expression Level} = 2^{Cq_{\beta\text{-actin}} - Cq_{\text{MIA}}} = 2^{-\Delta Cq} \quad (3)$$

Table 16. Calibrated MIA mRNA Expression Level after a Single Pulse

Time	Trial	Treatment	$-\Delta Cq$	MIA mRNA Level ($\times 0.00001$)
6 hours	1	One Pulse	-14.03	5.99
6 hours	2	One Pulse	-13.59	8.09
6 hours	3	One Pulse	-13.80	7.01
6 hours	1	Control	-14.06	5.88
6 hours	2	Control	-14.30	4.95
12 hours	1	One Pulse	-15.73	1.84
12 hours	2	One Pulse	-15.64	1.96
12 hours	3	One Pulse	-15.75	1.81
12 hours	1	Control	-15.94	1.59
12 hours	2	Control	-15.45	2.23
12 hours	3	Control	-15.71	1.87
18 hours	1	One Pulse	-15.95	1.58
18 hours	2	One Pulse	-15.91	1.63
18 hours	3	One Pulse	-16.04	1.49
18 hours	1	Control	-16.43	1.13
18 hours	2	Control	-15.74	1.83
18 hours	3	Control	-16.41	1.15
24 hours	1	One Pulse	-15.80	1.76
24 hours	2	One Pulse	-15.93	1.60
24 hours	3	One Pulse	-15.75	1.82
24 hours	1	Control	-15.70	1.87
24 hours	2	Control	-15.76	1.81
24 hours	3	Control	-15.93	1.60

Statistical test Two-factor crossed ANOVA (2×4 , pure model I) with Tukey's follow-up test (multiple comparison and contrast for treatment). The independent factors are the treatments and the time points. The treatment has two levels: a single pulse group and control group. The time points have four levels: 6, 12, 18, and 24 h. The dependent variable is the MIA mRNA expression level (calibrated to β -actin) of each sample. Three wells were used per treatment at each time point (3 replicates). Two treatments were used per time point, with four time points per treatment. A total of 24 wells (samples) were used.

Statistical hypotheses:

H_O : The MIA mRNA expression level do not significantly differ between the single pulse group and the control group excluding the time points

H_A : The MIA mRNA expression level significantly differ between the single pulse group and the control group excluding the time points

H'_O : The MIA mRNA expression level do not significantly differ among the different time points excluding there treatments

H'_A : The MIA mRNA expression level significantly differ among the different time points excluding there treatments

H''_O : The treatments do not significantly interact with the time points in terms of the MIA mRNA expression levels in the cells

H''_A : The treatments significantly interact with the time points in terms of the MIA mRNA expression levels in the cells

Assumption checking and data transformations: The errors were independent, as discussed on Page 36. Checking the residuals suggest that the original data and the subsequent transformations (natural log, square root, reciprocal, and exponential) did not follow a normal distribution and were non-homogenous. Therefore, the rank values obtained from original data were analyzed.

The results of the two-factor ANOVA (2×4 , pure model I) analysis (Table 17) indicate that the null hypothesis H'_O should be rejected in favor of the alternative hypothesis. However, the null hypotheses (H_O and H''_O) should be accepted instead of the alternative hypotheses, which indicate significant differences in MIA mRNA expression levels among the different time points. The MIA mRNA expression levels did not significantly differ between the single pulse group and the control group. The treatments did not significantly interact with the time points

in terms of the MIA mRNA expression levels in the cells.

The results of this study (Figure 37) indicate that the treatments did not significantly interact with the time points (Figure 36) in terms of the MIA mRNA expression levels in the cells ($F=0.242$; $df=3, 15$; $P=0.8653$). The observed power in SPSS was 0.086. The MIA mRNA expression levels did not significantly differ between the single pulse group and the control group ($F=0.063$; $df=1, 15$; $P=0.8059$). The observed power was 0.056. Both observed powers were less than 0.7, which indicates a high chance of false negative results. Larger sample sizes may reduce this type of error in the future studies. The MIA mRNA expression levels significantly differed among the different time points ($F=12.053$; $df=3, 15$; $P=0.0003$). The Tukey's multiple comparison follow-up test (Table 18) indicated that the mean MIA mRNA expression level at 6 h was significant higher than those at 12 h ($P=0.0477$), 18 h ($P=0.001$), and 24 h ($P=0.036$). The mean MIA mRNA expression level at 12 h was significantly higher than that at 18 h ($P=0.0249$). Therefore, the MIA mRNA expression level at 6 h after pulsing was higher than those at 12, 18, and 24 h. The MIA mRNA expression levels at 12 h after pulsing was higher than those at 18 h. If the MIA mRNA expression level at 6 h was consider 100%, that at 12 h was reduced to 29.5%, that at 18 h was reduced to 23.0%, and that at 24 was slightly increased to 27.3%. However, the differences between 18 h and 24 h were not significant.

Table 17. Rank of MIA mRNA Expression Levels after a Single Pulse, Two-way Fixed ANOVA Table

Source	df	Mean Square	F	Significance	Observed Power
Treatment	1	1.186	0.063	0.8059	0.056
Time	3	228.599	12.053	0.0003	0.997
Treatment×Times	3	4.599	0.242	0.8653	0.086
Error	15	18.967			
Total	23				
Corrected Total	22				

Table 18. Multiple Comparisons (Tukey's) Test

(I) Time	(J) Time	Mean Difference (I-J)	Std. Error	Significance
6 hours	12 hours	7.6667	2.63713	0.0477
	18 hours	15.8333	2.63713	0.0001
	24 hours	11.1667	2.63713	0.0036
12 hours	6 hours	-7.6667	2.63713	0.0477
	18 hours	8.1667	2.51440	0.0249
	24 hours	3.5000	2.51440	0.5229
18 hours	6 hours	-15.8333	2.63713	0.0001
	12 hours	-8.1667	2.51440	0.0249
	24 hour	-4.6667	2.51440	0.2872
24 hours	6 hours	-11.1667	2.63713	0.0036
	12 hours	-3.5000	2.51440	0.5229
	18 hours	4.6667	2.51440	0.2872

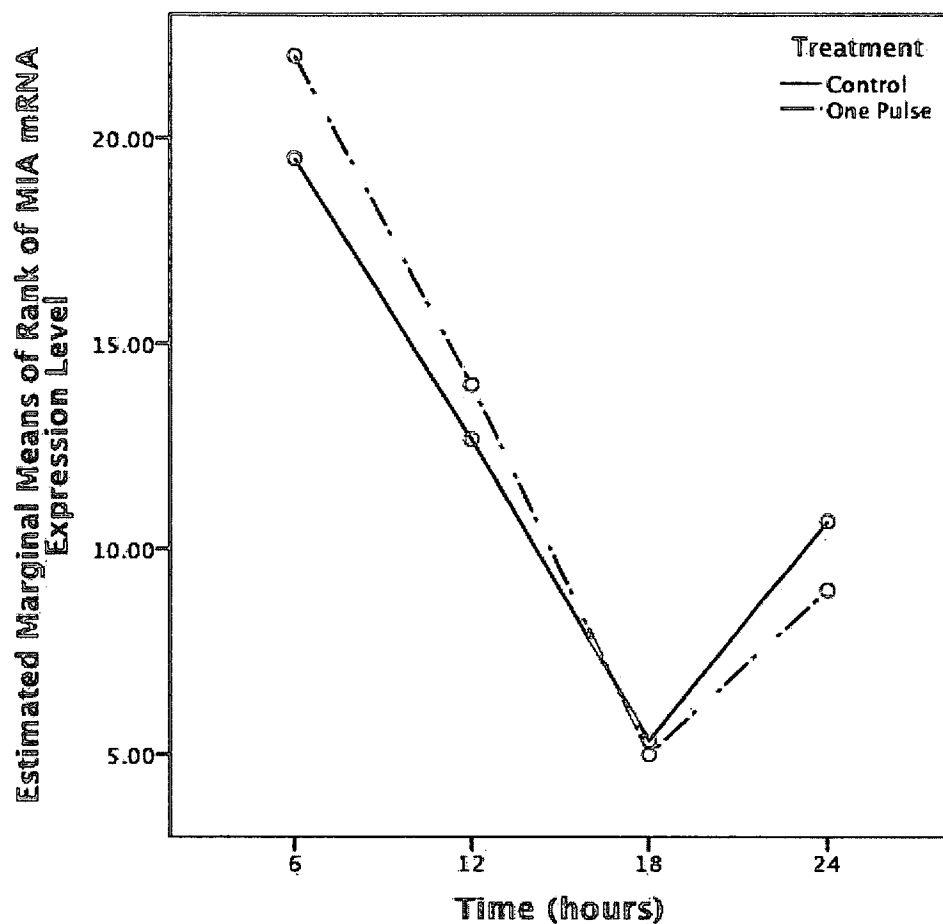


Figure 36. MIA mRNA Interaction Graph

The attached cells after a single 300 ns 40 kV/cm pulse and those in the unpulsed groups were harvested using trypsin-EDTA treatment after 6, 12, 18, and 24 h of culture. Total RNA were extracted from each cell sample. Three replicates were conducted. cDNA was produced from the total RNA using reverse transcription. Exactly 200 ng of cDNA template was employed in each real-time PCR. Each sample had a real-time PCR triplet. SYBR Green fluorescence was detected, and the Cq values of all reactions were calculated. The MIA mRNA expression levels were calibrated using β -actin as the internal control. Two-way fixed ANOVA indicated that the treatments did not significantly interact with the time points in terms of the mean MIA mRNA expression levels in the cells ($F=0.242$; $df=3, 15$; $P=0.8653$), $n=3$.

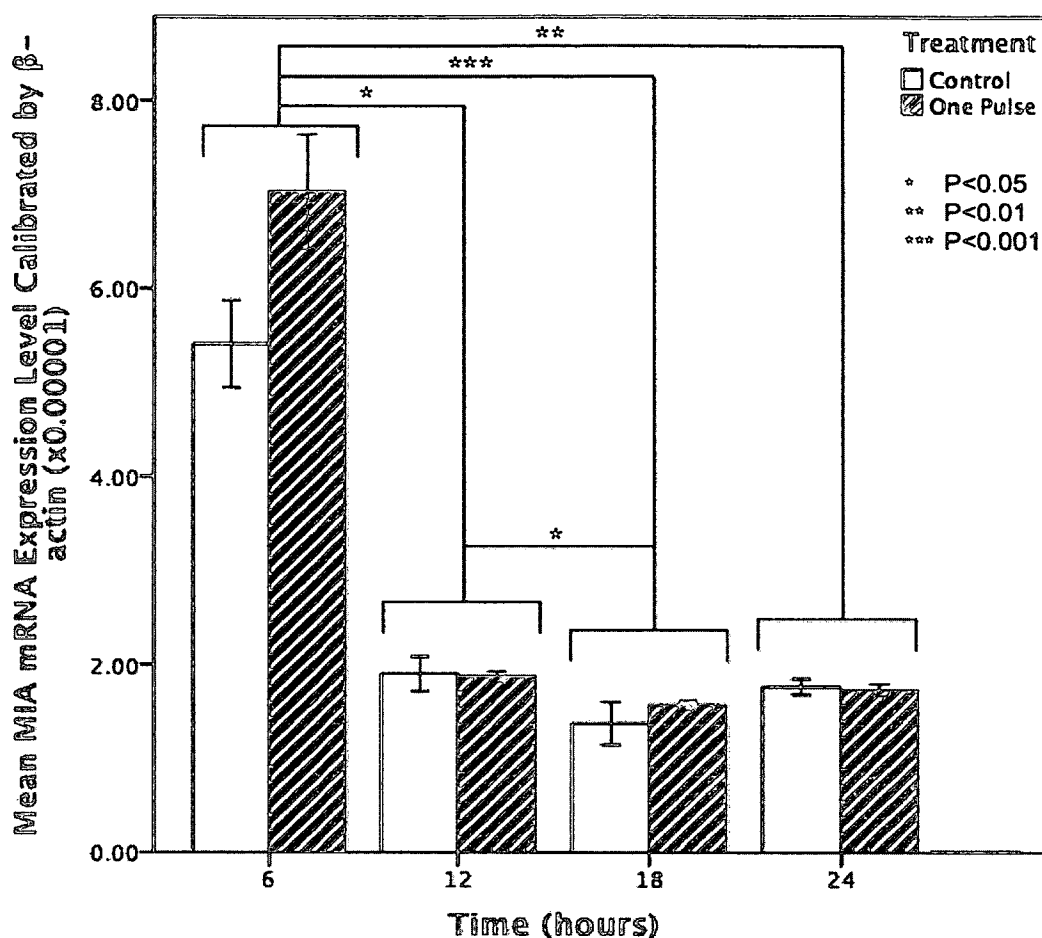


Figure 37. MIA mRNA expression levels (calibrated with β -actin) after a Single Pulse

The attached cells after a single 300 ns 40 kV/cm pulse and those in the unpulsed group were harvested using trypsin-EDTA treatment after 6, 12, 18, and 24 h of culture. Total RNA were extracted from each cell sample. Three replicates were conducted. cDNA was produced from the total RNA through reverse transcription. Exactly 200 ng of cDNA template was employed in each real-time PCR. Each sample had a real-time PCR triplet. SYBR Green fluorescence was detected, and the Cq values of all reactions were calculated. The MIA mRNA expression level were calibrated using β -actin as the internal control. The MIA mRNA expression levels did not significantly differ between the single pulse group and control group ($F=0.063$; $df=1, 15$; $P=0.8059$). The MIA mRNA expression levels significantly differed among the different time points ($F=12.053$; $df=3, 15$; $P=0.0003$). The Tukey's multiple comparison follow-up test indicated that the mean MIA mRNA expression levels at 6 h was significantly higher than those at 12 h ($P=0.0477$), 18 h ($P=0.001$), and 24 h ($P=0.036$). The mean MIA mRNA expression levels at 12 h was significantly higher than that at 18 h ($P=0.0249$). The data shown are means \pm SEM, $n=3$.

3.9 MIA MRNA EXPRESSION LEVEL AFTER MULTIPLE PULSES

The cells were immediately seeded and cultured after two, three, and four 300 ns 40 kV/cm pulses to measure the MIA mRNA expression levels. The cells were harvested using trypsin-EDTA treatment at 6, 12, 18, and 24 h. Three replicates were conducted. Total RNA were extracted from each cell sample. The cDNA templates were produced through reverse transcription. The reverse transcription templates for all samples were adjusted to the same amount (100 ng total RNA). The real-time PCR templates (cDNAs from reverse transcription) were applied at the same amount (2 μ L). Therefore, the C_q values within each group were close. Any value that deviated from the other group members was checked as a suspect outlier. Each cDNA sample had three real-time PCR replicates. The mean C_q values of the three replicates were then calculated (Table 19).

Table 19. Mean C_q Values of β -actin and MIA cDNA after Multiple Pulses

Treatment	6 h		12 h		18 h		24 h	
	β -actin	MIA	β -actin	MIA	β -actin	MIA	β -actin	MIA
Control	15.87	31.20	15.30	30.68	15.18	33.17	15.40	33.29
	14.93	30.24	14.57	30.92	15.30	33.10	14.88	34.14
	14.97	29.56	15.11	31.35	14.19	32.21	14.71	32.43
2 Pulses	17.88	31.41	16.09	31.80	15.17	32.21	15.92	33.41
	16.55	31.17	16.18	31.51	15.12	33.33	15.51	34.33
	16.62	30.50	15.86	31.02	15.61	33.32	15.26	32.63
3 Pulses	15.83	30.56	17.32	32.26	15.44	33.62	16.54	33.57
	16.57	30.99	14.54	30.23	15.34	31.95	16.37	34.37
	17.32	31.18	15.59	31.80	15.69	32.74	15.49	32.94
4 Pulses	17.40	31.96	16.17	32.05	16.14	32.52	16.43	34.01
	17.07	31.03	16.02	31.41	17.44	34.30	17.08	34.16
	17.34	30.72	16.87	31.41	15.53	32.59	16.55	33.88

The MIA mRNA expression levels were calibrated using β -actin (Table 20)

and 21), as previously described for the single pulse.

Table 20. Calibrated MIA mRNA Expression Level after Multiple Pulses (6 h and 12 h)

Time/Treatment	$-\Delta Cq$	MIA mRNA Level ($\times 0.00001$)
6 hours		
Control	-15.33	2.42
	-15.31	2.47
	-14.60	4.04
2 Pulses	-13.53	8.43
	-14.62	3.97
	-13.87	6.66
3 Pulses	-14.73	3.68
	-14.42	4.55
	-13.86	6.73
4 Pulses	-14.56	4.15
	-13.97	6.25
	-13.38	9.36
12 hours		
Control	-15.38	2.35
	-16.35	1.20
	-16.23	1.30
2 Pulses	-15.70	1.87
	-15.32	2.44
	-15.16	2.73
3 Pulses	-14.94	3.17
	-15.69	1.89
	-16.22	1.31
4 Pulses	-15.88	1.66
	-15.39	2.33
	-14.55	4.18

Table 21. Calibrated MIA mRNA Expression Level after Multiple Pulses (18 h and 24 h)

Time/Treatment	$-\Delta Cq$	MIA mRNA Level ($\times 0.00001$)
18 hours		
Control	-17.99	0.38
	-17.80	0.44
	-18.02	0.38
2 Pulses	-17.04	0.74
	-18.21	0.33
	-17.71	0.47
3 Pulses	-18.18	0.34
	-16.61	1.00
	-17.05	0.74
4 Pulses	-16.38	1.17
	-16.86	0.84
	-17.06	0.73
24 hours		
Control	-17.89	0.41
	-19.26	0.16
	-17.72	0.46
2 Pulses	-17.49	0.54
	-18.82	0.22
	-17.37	0.59
3 Pulses	-17.03	0.75
	-18.01	0.38
	-17.45	0.56
4 Pulses	-17.58	0.51
	-17.08	0.72
	-17.33	0.61

Statistical test: Two-factor crossed ANOVA (4×4 , pure model I) with Tukey's follow-up tests (multiple comparison and contrast for treatments and time points). The independent factors were the treatments and time points. The treatments have four levels: the two-, three-, and four-pulse groups and the control group. The time points have four levels: 6, 12, 18, and 24 h. The dependent variable was the MIA mRNA expression levels of each sample (calibrated with β -actin). Three wells per treatment were used per time point (3 replicates) with four treatments per time point and four time points per treatment. A total of 48 wells (samples).

Statistical hypotheses:

H_O : The MIA mRNA expression levels do not significantly differ among the control group and the two-, three-, and four-pulse groups excluding the time points

H_A : The MIA mRNA expression levels significantly differ among the control group and the two-, three-, and four-pulse groups excluding the time points

H'_O : The MIA mRNA expression levels do not significantly differ among the different time points excluding the treatments

H'_A : The MIA mRNA expression levels significantly differ among the different time points excluding the treatments

H''_O : The treatments do not significantly interact with the time points in terms of the mean MIA mRNA expression levels in the cells

H''_A : The treatments significantly interact with the time points in terms of the mean MIA mRNA expression levels in the cells

Assumption checking and data transformations: The errors were independent as previously discussed in the single pulse treatments. The raw data were normally distributed, but non-homogenous. Thus, the residues were tested again for normality and homogeneity using the raw $-\Delta Cq$ values, square root, reciprocal, and exponential transformations. Only the residues of raw $-\Delta Cq$ values were normally distributed and homogenous. Therefore, the raw $-\Delta Cq$ values were used for the two way ANOVA.

The results of the two way ANOVA (4×4 , pure model I) indicated that the null hypotheses (H_O and H'_O) should be rejected in favor of the alternative hypotheses (Table 22). However, the null hypothesis (H''_O) should be accepted instead of the alternative hypothesis, which indicates a significant difference in MIA mRNA expression levels among the treatments and among the different time

points, but the treatments did not significantly interact with the time points in terms of the mean MIA mRNA expression levels in the cells.

The ANOVA results of this experiment indicate that the treatments did not significantly interact with the time points in terms of the MIA mRNA expression levels in the cells ($F=0.413$; $df=9, 32$; $P=0.919$) (Figure 38). The observed power in SPSS was 0.169, which is less than 0.7 and indicates a high chance of false negative results. Larger sample sizes may reduce this type of error in future studies. The MIA mRNA expression levels significantly differed among the control group, the two-pulse group, three-pulse group, and the four-pulses group ($F=6.408$; $df=3, 32$; $P=0.001594$) (Figure 39). The observed power was 0.948. The MIA mRNA expression levels significantly differed among the different time points ($F=97.647$; $df=3, 32$; $P<0.0000005$). The observed power was 1.000.

The Tukey's multiple comparison follow-up for the different time points indicated that the mean MIA mRNA expression level at 6 h was significantly different from those at 12 h ($P=0.000044$), 18 h ($P<0.000001$), and 24 h ($P<0.000001$) (Table 23). The mean MIA mRNA expression level at 12 h was also significant different from that at 18 h ($P<0.000001$) and 24 h ($P<0.000001$). The mean MIA mRNA expression level at 18 hours was no significant different from that at 24 h ($P=0.447615$). Therefore, the MIA mRNA expression level at 6 h after pulsing was significantly higher than those at 12, 18, and 24 h. The MIA mRNA expression level at 12 h after pulsing was also significantly higher than those at 18 and 24 h.

The Tukey's multiple comparison follow-up test for the different time points (Table 24) indicated that the mean MIA mRNA expression level after two pulses did not significantly differ from those of the control group ($P=0.070$), the three-pulse group ($P=0.995$) and the four-pulse group ($P=0.312$). The mean MIA mRNA expression level after three pulses significantly differed from that of the control group ($P=0.041$), but had not from those of the two-pulse group ($P=0.995$) and the four-pulse group ($P=0.439$). The mean MIA mRNA expression level of the four-pulse group significantly differed from that of the control group ($P=0.001$), but not from those of the two-pulse group ($P=0.312$) and the three-pulse group ($P=0.439$). Therefore, the MIA mRNA expression levels of the three-pulse and four-pulse groups were significantly higher than that of the control group, but that of the two-pulse group was not significantly higher than

that of the control group.

Table 22. Raw $-\Delta Cq$ of MIA mRNA Expression Level after Multiple Pulses, Two-way Fixed ANOVA Table

Source	df	Mean Square	F	Significance	Observed Power
Time	3	30.724	97.647	<0.0000005	1.000
Pulses	3	2.016	6.408	0.001594	0.948
Time \times Pulses	9	0.130	0.413	0.918629	0.169
Error	32	0.315			
Total	48				
Corrected Total	47				

Table 23. Multiple Comparisons (Tukey's) Test for Different Time Points

(I) Time	(J) Time	Mean Difference (I-J)	Std. Error	Significance
6 hours	12 hours	1.219444	0.228998760	0.000044
	18 hours	3.060278	0.228998760	<0.000001
	24 hours	3.404444	0.228998760	<0.000001
12 hours	6 hours	-1.219444	0.228998760	0.000044
	18 hours	1.840833	0.228998760	<0.000001
	24 hours	2.185000	0.228998760	<0.000001
18 hours	6 hours	-3.060278	0.228998760	<0.000001
	12 hours	-1.840833	0.228998760	<0.000001
	24 hour	0.344167	0.228998760	0.447615
24 hours	6 hours	-3.404444	0.228998760	<0.000001
	12 hours	-2.185000	0.228998760	<0.000001
	18 hours	-0.344167	0.228998760	0.447615

Table 24. Multiple Comparisons (Tukey's) Test for Multiple Pulses

(I) Time	(J) Time	Mean Difference (I-J)	Std. Error	Significance
Control	2 Pulses	-0.5858333	0.228998760	0.070
	3 Pulses	-0.6405556	0.228998760	0.041
	4 Pulses	-0.9883333	0.228998760	0.001
2 Pulses	Control	0.5858333	0.228998760	0.070
	3 Pulses	-0.5472222	0.228998760	0.995
	4 Pulses	-0.4025000	0.228998760	0.312
3 Pulses	Control	0.6400556	0.228998760	0.041
	2 Pulses	0.0547222	0.228998760	0.995
	4 Pulses	-0.3477778	0.228998760	0.439
4 Pulses	Control	0.9883333	0.228998760	0.001
	2 Pulses	0.4025000	0.228998760	0.312
	3 Pulses	0.3477778	0.228998760	0.439

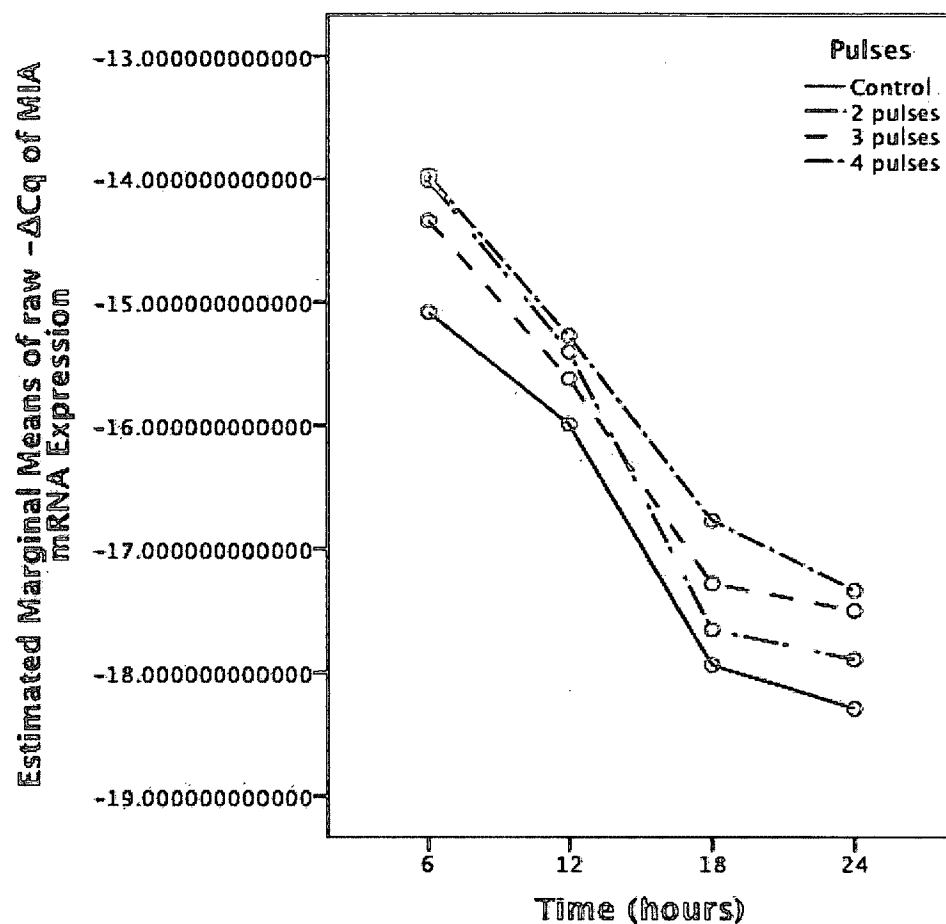


Figure 38. MIA mRNA Interaction Graph after Multiple Pulses

The attached cells after two, three, and four 300 ns 40 kV/cm pulses, as well as in the unpulsed group were harvested using trypsin-EDTA treatment after 6, 12, 18, and 24 h of culture. Total RNA were extracted from each cell sample. Three replicates were conducted. The cDNA was produced from the total RNA using reverse transcription. Exactly 200 ng of the cDNA template was employed in each real-time PCR. Each sample had a real-time PCR triplet. SYBR Green fluorescence was detected, and the Cq values of all the reactions were calculated. The MIA mRNA expression levels were calibrated using β -actin as the internal control. The treatments did not significantly interact with the time points in terms of the MIA mRNA expression levels in the cells ($F=0.413$; $df=9, 32$; $P=0.919$), $n=3$.

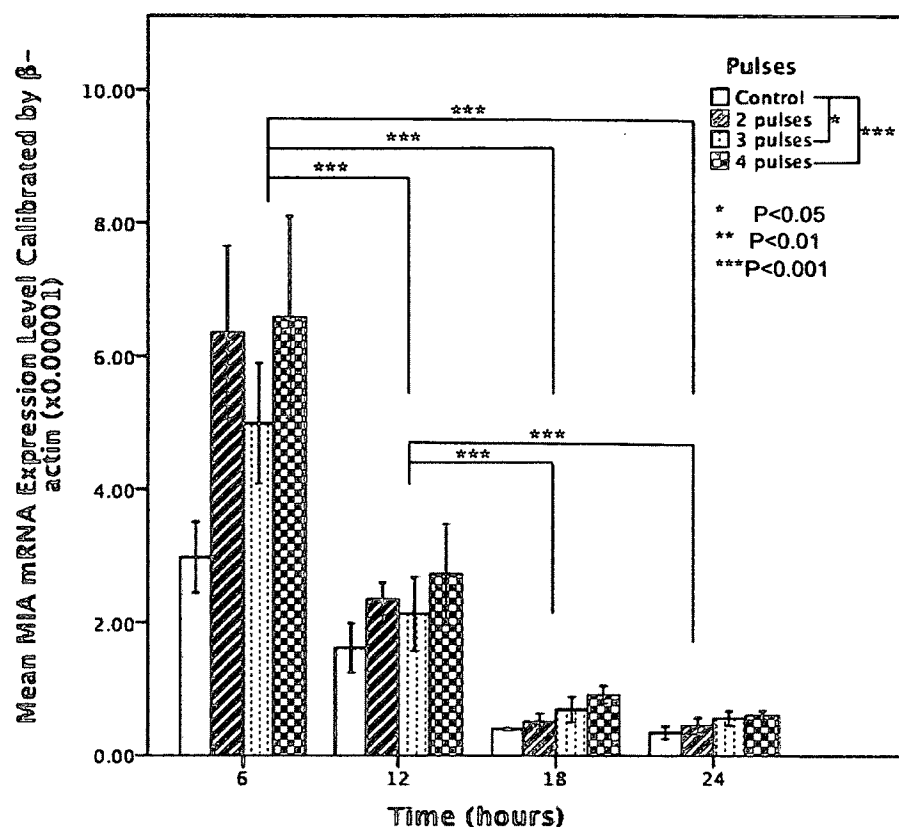


Figure 39. MIA mRNA Expression Level (calibrated to β -actin) after Multiple Pulses

The attached cells after two, three, and four 300 ns 40 kV/cm pulses, as well as in the unpulsed group were harvested using trypsin-EDTA treatment after 6, 12, 18, and 24 h of culture. Total RNA were extracted from each cell sample. Three replicates were conducted. The cDNA was produced from the total RNA using reverse transcription. Exactly 200 ng of the cDNA template was employed in each real-time PCR. Each sample had a real-time PCR triplet. SYBR Green fluorescence was detected, and the Cq values of all the reactions were calculated. The MIA mRNA expression levels were calibrated using β -actin as the internal control. The mean MIA mRNA expression levels at 6 h was significant higher than that at 12 h ($P=0.000044$), 18 h ($P<0.000001$), and 24 h ($P<0.000001$). The mean MIA mRNA expression level at 12 h was significantly higher than that at 18 h ($P<0.000001$) and 24 h ($P<0.000001$). The mean MIA mRNA expression level at 18 h was not significant different from that at 24 h ($P=0.447615$). The mean MIA mRNA expression level of the two-pulse group did not significantly differ from those of the control ($P=0.070$), the three-pulse group ($P=0.995$), and the four-pulse group ($P=0.312$). The mean MIA mRNA expression level of the three-pulse group was significantly higher than that of the control group ($P=0.041$), but not from that of the two-pulse group ($P=0.995$) and the four-pulse group ($P=0.439$). The mean MIA mRNA expression level of the four-pulse group was significantly higher than that of the control group ($P=0.001$) but not from that of the two-pulse group ($P=0.312$) and the three-pulse group ($P=0.439$). The data shown are means \pm SEM, $n=3$.

CHAPTER 4

DISCUSSION

4.1 CELL ATTACH ABILITY CHANGES AFTER nsEPS

The number of floating live, dead, and total cells after a single pulse did not significantly differ between the control group and single pulse groups ($P=0.511$, 0.736 , 0.828 , respectively) (Figure 10). This result indicates that the cells have no significantly different attachment abilities. The cells in the control group and single pulse groups had similar cell densities based on the cell micrographs at 6, 12, 18, and 24 h (Figures 15 and 16), which indicates that the number of attached cells in the control group did not significantly differ from those of the single pulse group. Therefore, a single pulse does not affect the attachment ability of the cells.

The results of the long-term cell viability test (Figure 22) after two, three, and four pulses indicated that the percentage of attached live cells in the control significantly differed from those of the two-, three, and four-pulse groups ($F=10.724$; $df=3, 32$; $P<0.00005$). The percentage of attached live cells at 24 h was significantly higher than at 6, 12, and 18 h (all $P<0.05$), which indicates that the cell attachment ability gradually recovered after 24 h. The two-, three-, and four-pulse groups significantly decreased the percentage of attached live cells ($P=0.014$, 0.004 , 0.00002 , respectively), which indicates that the two-, three-, and four-pulse treatments decreased the cell attachment ability within 24 h.

Therefore, the two, three, and four 300 ns 40 kV/cm pulses significantly inhibited the attachment of melanoma cells onto the plate surface. A single pulse did not change the cell attachment ability. This result is very promising for future clinical use to inhibiting melanoma metastasis. Cell attachment and cell adhesion plays an important role in spreading tumor cells through the circulatory system (cell migration) and in establishing new tumors. Inhibition of the melanoma cell attachment provides an opportunity to reduce new tumor formation and slow down the metastatic process.

This study explored a new field in the nsEPs effect on melanoma cells. We found that nsEPs has great potential in inhibiting the cell attachment ability,

especially that of cancer cells. However, the mechanism remains unclear. The role played by cell adhesion molecules (CAMs), such as integrins, in nsEP-induced inhibition of attachment is unknown. In the future, CAMs could be targeted to investigate the inhibitory effect of nsEPs on cell attachment or cell adhesion.

4.2 CELL MORPHOLOGY CHANGES AFTER nsEPS

The results of the cell morphology test after a single 300 ns 40 kV/cm pulse indicated that cells were spread out, formed spines, and became spindle-shaped in both the control group and the single pulse group (Figure 15). No significant morphologic differences were observed between the control group and the single pulse group, which is consistent with the cell attachment ability in the single pulse experiments. Therefore, single pulses do not affect cell attachment ability and morphology.

The results of the cell morphology test after multiple pulses (Figures 23 - 26) show significant decreases in cell spread area at 6, 12, 18, and 24 h after two-, three-, and four-pulse treatments. The two-, three-, and four-pulse treatments significantly decreased the frequency of nuclear division, based on the changes in nuclear shape. Furthermore, multiple pulses greatly slowed cell attachment.

Therefore, two, three, and four 300 ns 40 kV/cm pulses decrease the cell attachment area, slow down the attachment process, and inhibit nuclear division. Single pulse did not change the cell attachment area, the attachment process, and nuclear division. These results verify the cell attachment ability study shown above, wherein two-, three-, and four-pulse treatments significantly inhibited cell attachment and adhesion. Nuclear division occurs during cell proliferation. Thus, nsEPs could significantly inhibit cell attachment, cell adhesion, and cancer cell proliferation. These strong indications suggest that nsEPs have great potential for inhibiting melanoma metastasis.

The limitation of this morphologic study is the lack of quantitative results. Everything was examined through direct visualization. In the future, cell cycle markers, such as propidium iodide (PI) and 7-aminoactinomycin D (7-AAD), and cell proliferation markers, such as Violet Proliferation Dye 450 (VPD450), can be used to quantify the cell cycle distribution and cell proliferation through flow cytometry. CAMs can also be stained through immunohistochemistry (IHC),

which would provide location information for the attachment study.

4.3 LONG-TERM VIABILITY TEST AFTER nsEPS

The results of the long-term viability test after multiple pulses revealed that the total cell viability of the control group (around 90%) was significantly higher than that of the two-, three-, and four-pulse groups (all $P < 0.0001$; Figure 18). The total cell viability of the two-pulse group (around 40%) was significantly higher than those of the three-pulse and four-pulse groups (around 20%; all $P < 0.0001$). The total cell viability did not significantly differ between the three-pulse group and the four-pulse group.

Therefore, the two-pulse treatment significantly decreases the total viability of the cells; the three-pulse and four-pulse treatments further decrease the cell viability. This nsEPs-induced decrease in cell viability may be related to cell apoptosis or cell necrosis. Previous research revealed that nsEPs trigger apoptosis-like mechanisms to activate caspase release (Ford et al., 2010). The research found that B16-F10 melanoma cells released significantly high amounts of caspase within 1 h of ten 300 ns 40 kV/cm pulses compared with the control. The cell survivability of the 10-pulse group was significantly low compared with that of the control group. Therefore, nsEP-induced apoptosis can decrease cell viability. Our results are consistent with those of a previous study.

The inhibitory effect of nsEP on cell viability provides a new method for reducing tumor size and indirectly confining the tumor in its original location. Therefore, nsEPs may be a good choice for treating metastatic melanomas in clinical trials.

The limitation of our research is that we determined the cell density and the number of floating cells after a single 300 ns 40 kV/cm pulse, but not the corresponding cell viability. Although the cell density and the number of floating cells did not significantly differ between the single pulse group and the control group, we can only deduce that single pulses do not affect cell viability. Therefore, cell viability after single 300 ns 40 kV/cm pulse should be tested in future studies.

4.4 PCR EFFICIENCIES

The theoretical amplification efficiency ranged from 1 to 2. An efficiency of 1

indicates no amplification, whereas 2 indicates that the amount of double-stranded DNA doubled during each PCR cycle. Normal amplification efficiencies ranges from 1.8 to 2. Amplification efficiency is influenced by primer quality and design, PCR inhibitors in the PCR reagents or samples, and the availability of dNTPs, amplification enzymes, and other factors. Both LinRegPCR and qpcR provide amplification efficiencies and other important parameters.

The advantage of LinRegPCR is that it allows adjustment of the slope to a certain extent based on the raw data point. The resulting amplification efficiency still has some bias because the software does not allow free adjustment of the slope. The resulting mean efficiency was > 2 . The melting curves of β -actin and MIA both showed only one peak, which excludes the possibility of primer dimers or non-specific amplification. Therefore, calculating efficiency using LinRegPCR is still valid even though the mean efficiency was > 2 . LinRegPCR still has room for improvement, e.g., manual slope adjustment and support for Mac and Linux systems.

The advantage of the qpcR package is that it allows the use of different parameters in calculating efficiency at different points of the raw data curve. The slope of the curve cannot be adjusted manually, which introduces a bigger bias (efficiency is much greater than 2). However, the efficiency results remain valid because of 2 is within their $\text{mean} \pm \text{SEM}$ range. The other advantage of qpcR is support for all systems: Windows, Mac, and Linux.

The PCR efficiency of β -actin was slightly higher than that of MIA, which may be caused by the larger amount of β -actin than MIA in the sample. The C_q values of MIA are 10 cycles greater than that of β -actin. The PCR reagents may have less activity than that from the previous 10 cycles because the MIA reaction requires a longer period to reach the fluorescence threshold. Thus, the MIA PCR efficiency is slightly lower. However, the MIA PCR efficiency remains around 2; thus, a PCR efficiency of 2 is valid for both β -actin and MIA.

4.5 MIA MRNA EXPRESSION LEVEL AFTER nsEPS

The MIA mRNA expression levels in the single 300 ns 40 kV/cm pulse group did not significantly differ from those of the control group ($F=0.063$; $df=1, 15$; $P=0.8059$; Figure 37). Therefore, one 300 ns 40 kV/cm electric pulse does not inhibit or stimulate MIA mRNA expression in murine B16-F10 melanoma cells.

The MIA mRNA expression levels decreased with time, from 100% at 6 h to 29.5% at 12 h, to 23.0% at 18 h, and then to 27.3% at 24 h. Therefore, MIA mRNA expression has a sloped pattern.

This sloped pattern may be due to growth disturbance during the experiment such as the trypsin treatment, centrifugation, low nutrient concentrations in PBS, and room temperature exposure. When the cells are seeded into the plate and cultured in the incubator after those operations, the environment and nutrients are optimal for cell growth. Cells largely express growth regulators, such as MIA. Thus, the MIA mRNA expression levels were high at 6 h. MIA mRNA is translated into MIA protein after its transcription. MIA stimulates the expression of downstream growth-related genes. MIA mRNA was produced within a very short period. Thus, the MIA mRNA level decreased to 29.5% at 12 h. MIA mRNA degrades continuously. The MIA mRNA level further decreased to 23.0% at 18 h. The cells grew thereafter; thus, the MIA mRNA levels increased to 27.3%, but the change was not significant. Therefore, a sloped pattern formed.

The MIA mRNA expression levels in the three-pulse and the four-pulse groups were significantly higher than that in the control group (Figure 39; $P=0.041$, 0.001 , respectively). The MIA mRNA expression levels did not significantly differ between the control group and the two-pulse group ($P=0.070$). The MIA mRNA expression level at 6 h was significantly higher than those at 12, 18, and 24 h ($P=0.000044$, $P<0.000001$, and $P<0.000001$, respectively). The MIA mRNA expression level at 12 h was significantly higher than that at 18 and at 24 h (both $P<0.000001$). The MIA mRNA expression levels did not significantly differ between the 18 h and the 24 h time points ($P=0.447615$).

These results indicate that three-pulse and four-pulse treatments significantly increase the MIA mRNA expression levels, whereas one-pulse and two-pulse treatments do not. The MIA mRNA expression level gradually decreased from the 6 h time point to the 18 h time point. The MIA mRNA expression level did not significantly differ between the 18 h time point and the 24 h time point. These results indicate that the MIA mRNA expression level gradually decreases within 24 h. However, three-pulse and four-pulse treatments increase MIA mRNA expression, thereby increasing metastatic potential.

This research shows that three and four 300 ns 40 kV/cm electric pulses increase the MIA mRNA expression level. The MIA expression levels after three

or four pulses were only slightly different from that of the control group at 18 and 24 h. Therefore, the MIA mRNA expression level was significantly increased within 12 h but reduced almost to normal between 12 h and 24 h. Total cell viability was also significantly decreased (more than half), and the cell attachment ability and cell nuclear division were decreased. These results are encouraging for the treatment of metastatic melanomas because nsEPs inhibits the adhesion and proliferation of metastatic melanoma cells. The two-pulse treatment did not significantly increase the MIA mRNA expression levels, but significantly decreased cell attachment ability and nuclear division, as well as changed the cell morphology. Three-pulse and four-pulse increased the MIA mRNA expression levels within 12 h, which returned to normal after the next 12 h. Thus, two-, three-, and four-pulse treatments optimally inhibit melanoma metastasis and cell attachment.

The mechanism by which nsEPs stimulate MIA mRNA expression is still unknown. Furthermore, studies on nsEP-induced mRNA degradation are still unavailable. Thus, information regarding the effects of nsEPs on MIA mRNA expression is limited. More research should be done to explore the benefits of nsEPs.

More time points and replicates are needed to test the slope, such as at 6, 12, 18, and 24 h before the pulses and at 30, 36, 42, and 48 h after the pulses. These time points can also be closer together such as at 0.5, 1, 2, and 3 h after the pulses. The cells may also be grown on the cover slides or pulsing cuvette, to which the electric pulses could be directly applied, to reduce trypsin-EDTA treatment and other disturbances.

Our pilot study shows that the one-, two-, three-, and four-pulse groups and the control group do not significantly differ in lysozyme structure (data not shown). This finding indicates that some protein structures remain unchanged under nsEPs, which is very promising for nsEP treatment because normal proteins should be unaffected. Furthermore, methods for detecting the amount of protein, such as western blot and ELISA, can be used to measure MIA protein concentration.

This study opens a new field for treating metastatic melanomas using nanosecond high-voltage electric pulses. Further studies are needed to develop this new field and benefit humans and other organisms.

CHAPTER 5

CONCLUSIONS

We have demonstrated the changes in cell attachment ability within the 24 h after nsEP treatment. A single 300 ns 40 kV/cm pulse did not affect attachment ability and cell morphology. The two, three, and four 300 ns 40 kV/cm pulses significantly decreased cell attachment ability ($P=0.014$, 0.004 , 0.00002 , respectively), cell attachment area, as well as slowed down the attachment process, and inhibited nuclear division for 24 h. The cell attachment ability gradually recovered after 24 h, but it did not to its normal value. Treatment with more pulses more strongly inhibited the cell attachment ability.

We also demonstrated the changes in cell viability within 24 h after the nsEP treatment. A single 300 ns 40 kV/cm pulse did not affect cell viability. However, two, three, and four 300 ns 40 kV/cm pulses significantly decreased cell viability (more than half; all $P<0.0001$). More than half of the cells died after the two-, three-, and four-pulse treatments.

We determined the MIA mRNA expression levels within 24 h after the nsEP treatment. Treatment with one or two 300 ns 40 kV/cm pulses did not affect MIA mRNA expression, whereas three or four 300 ns 40 kV/cm pulses significantly increased the MIA mRNA expression levels within 6 and 12 h, but remained close to normal within 18 and 24 h ($P=0.041$, 0.001 , respectively). Considering MIA is a marker for melanoma metastasis, treatment with three or four pulses increases the risk of melanoma metastasis within the first 12 h of pulsing but only slightly after the following 12 h.

We conclude that a single 300 ns 40 kV/cm pulse does not change the attachment ability, morphology, and MIA mRNA expression levels of murine B16-F10 melanoma cells within 24 h. Three to four 300 ns 40 kV/cm pulses significantly decreased the cell attachment ability, cell viability, nuclear division, and the cell attachment area, but significantly increased the MIA mRNA expression levels within the first 12 h after pulsing. Treatment with two 300 ns 40 kV/cm pulses significantly decreased cell attachment ability, cell viability, and cell

attachment area, but did not significantly increase the MIA mRNA expression levels within the first 24 h after pulsing.

Therefore, treatment with two, three, or four 300 ns 40 kV/cm pulses reduces cell attachment ability, and cell viability. Although the MIA mRNA expression levels increased within the first 12 h, the increase during the second 12 h after the pulse treatments was not much. Treatment with two to four 300 ns 40 kV/cm pulses is optimal for treating metastatic melanomas.

REFERENCES

- Al-Sakere, B., André, F., Bernat, C., Connault, E., Opolon, P., Davalos, R.V., Rubinsky, B., and Mir, L.M. (2007), Tumor ablation with irreversible electroporation. *PLoS One* 2, e1135.
- Angres, B., Barth, A., and Nelson, W.J. (1996), Mechanism for transition from initial to stable cell-cell adhesion: kinetic analysis of E-cadherin-mediated adhesion using a quantitative adhesion assay. *The Journal of Cell Biology* 134, 549–557.
- Arunkumar, M.J., Ranjan, A., Jacob, M., and Rajshekhar, V. (2001), Neurocutaneous melanosis: a case of primary intracranial melanoma with metastasis. *Clin Oncol* 13, 52–54.
- Aung, P., Oue, N., Mitani, Y., Nakayama, H., Yoshida, K., Noguchi, T., Bosserhoff, A., and Yasui, W. (2005), Systematic search for gastric cancer-specific genes based on SAGE data: melanoma inhibitory activity and matrix metalloproteinase-10 are novel prognostic factors in patients with gastric cancer. *Oncogene* 25, 2546–2557.
- Bauer, R., Humphries, M., Fässler, R., Winklmeier, A., Craig, S.E., and Bosserhoff, A.K. (2006), Regulation of integrin activity by MIA. *Journal of Biological Chemistry* 281, 11669–11677.
- Beebe, S.J., Fox, P.M., Rec, L.J., Willis, E.L.K., and Schoenbach, K.H. (2003), Nanosecond, high-intensity pulsed electric fields induce apoptosis in human cells. *The FASEB Journal* 17, 1493–1495.
- Beebe, S.J., Schoenbach, K.H., and Heller, R. (2010), Bioelectric applications for treatment of melanoma. *Cancers* 2, 1731–1770.
- Blesch, A., Bosserhoff, A.K., Apfel, R., Behl, C., Hessdoerfer, B., Schmitt, A., Jachimczak, P., Lottspeich, F., Buettner, R., and Bogdahn, U. (1994), Cloning of a novel malignant melanoma-derived growth-regulatory protein, MIA. *Cancer Research* 54, 5695–5701.

Bogdahn, U., Apfel, R., Hahn, M., Gerlach, M., Behl, C., Hoppe, J., and Martin, R. (1989), Autocrine tumor cell growth-inhibiting activities from human malignant melanoma. *Cancer Research* 49, 5358–5363.

Bosserhoff, A. and Buettner, R. (2002), Expression, function and clinical relevance of MIA (melanoma inhibitory activity). *Histol Histopathol.* 17, 289–300.

Bosserhoff, A.K., Echtenacher, B., Hein, R., and Buettner, R. (2001), Functional role of melanoma inhibitory activity in regulating invasion and metastasis of malignant melanoma cells in vivo. *Melanoma Research* 11, 417–421.

Bosserhoff, A.K., Kaufmann, M., Kaluza, B., Bartke, I., Zirngibl, H., Hein, R., Stolz, W., and Buettner, R. (1997a), Melanoma-inhibiting activity, a novel serum marker for progression of malignant melanoma. *Cancer Research* 57, 3149–3153.

Bosserhoff, A.K., Kondo, S., Moser, M., Dietz, U.H., Copeland, N.G., Gilbert, D.J., Jenkins, N.A., Buettner, R., and Sandell, L.J. (1997b), Mouse CD-RAP/MIA gene: Structure, chromosomal localization, and expression in cartilage and chondrosarcoma. *Developmental Dynamics* 208, 516–525.

Bosserhoff, A.K., Moser, M., Hein, R., Landthaler, M., and Buettner, R. (1999), In situ expression patterns of melanoma-inhibiting activity (MIA) in melanomas and breast cancers. *The Journal of Pathology* 187, 446–454.

Bosserhoff, A.K., Stoll, R., Sleeman, J.P., Bataille, F., Buettner, R., and Holak, T.A. (2003), Active detachment involves inhibition of cell-matrix contacts of malignant melanoma cells by secretion of melanoma inhibitory activity. *Laboratory Investigation* 83, 1583–1594.

Buzbee, T.M. and Legha, S.S. (1992), Spontaneous rupture of spleen in a patient with splenic metastasis of melanoma. A case report. *Tumori* 78, 47–48.

Cemil, B., Emmez, H., Oztanir, N., Tokgoz, N., and Dogulu, F. (2008), A cystic amelanotic melanoma metastasis to the brain: case report. *Neurocirugia* 19, 365–367.

Chrissos, D.N., Stougiannos, P.N., Mytas, D.Z., Katsaros, A.A., Andrikopoulos, G.K., and Kallikazaros, I.E. (2008), Multiple cardiac metastases from a malignant melanoma. *Eur J Echocardiogr* 9, 391–392.

De Vries, T., Fourkour, A., Punt, C., Diepstra, H., Ruiter, D., and Van Muijen, G. (1999), Melanoma-inhibiting activity (MIA) mRNA is not exclusively transcribed in melanoma cells: low levels of MIA mRNA are present in various cell types and in peripheral blood. *British Journal of Cancer* 81, 1066.

Dietz, U.H. and Sandell, L.J. (1996), Cloning of a retinoic acid-sensitive mRNA expressed in cartilage and during chondrogenesis. *Journal of Biological Chemistry* 271, 3311–3316.

El Fitori, J., Kleeff, J., Giese, N.A., Guweidhi, A., Bosserhoff, A.K., Büchler, M.W., Friess, H., et al. (2005), Melanoma Inhibitory Activity (MIA) increases the invasiveness of pancreatic cancer cells. *Cancer Cell Int* 5.

Ford, W.E., Ren, W., Blackmore, P.F., Schoenbach, K.H., and Beebe, S.J. (2010), Nanosecond pulsed electric fields stimulate apoptosis without release of pro-apoptotic factors from mitochondria in B16f10 melanoma. *Archives of Biochemistry and Biophysics* 497, 82–89.

Guba, M., Bosserhoff, A., Steinbauer, M., Abels, C., Anthuber, M., Buettner, R., and Jauch, K. (2000), Overexpression of melanoma inhibitory activity (MIA) enhances extravasation and metastasis of A-mel 3 melanoma cells in vivo. *British Journal of Cancer* 83, 1216.

Hashemi, M., Stark, A., Hugo, H., and Mehdorn, M. (2009), Intracranial trigeminal nerve metastasis of a desmoplastic neurotropic melanoma: case report. *Cent Eur Neurosurg* 70, 91–94.

Hoang, M.T. and Eichenfield, L.F. (2000), The rising incidence of melanoma in children and adolescents. *Dermatol Nurs* 12, 188–189, 192–193.

Houmsse, M., Raman, S.V., Leier, C.V., and Orsinelli, D.A. (2004), Metastatic melanoma of the left ventricle: cardiac imaging in the diagnosis and surgical approach. *Int J Cardiovasc Imaging* 20, 523–528.

Howlader, N., Noone, A., Krapcho, M., Neyman, N., Aminou, R., Altekruse, S., Kosary, C., Ruhl, J., Tatalovich, Z., Cho, H., et al. (2012), SEER cancer statistics review, 1975–2009 (vintage 2009 populations). Bethesda, MD: National Cancer Institute .

Jemal, A., Siegel, R., Ward, E., Hao, Y., Xu, J., Murray, T., and Thun, M.J. (2008), Cancer statistics, 2008. *CA: A Cancer Journal for Clinicians* 58, 71–96.

Kopf, A.W., Rigel, D.S., and Friedman, R.J. (1982), The rising incidence and mortality rate of malignant melanoma. *J Dermatol Surg Oncol* 8, 760–761.

Kubota, Y., Tomita, Y., Tsukigi, M., Kurachi, H., Motoyama, T., and Mir, L.M. (2005), A case of perineal malignant melanoma successfully treated with electrochemotherapy. *Melanoma Research* 15, 133.

Kurul, S., Aykan, F., and Tas, F. (2006), Penile metastasis of cutaneous malignant melanoma: a true hematogenous spread?: Case report and review of the literature. *Melanoma Research* 16, 259–261.

Langley, R.R. and Fidler, I.J. (2011), The seed and soil hypothesis revisited—the role of tumor-stroma interactions in metastasis to different organs. *Int J Cancer* 128, 2527–2535.

Lesur, G., Bourgault, I., Longvert, C., El Hajjam, M., Dubreuil, O., Julié, C., Saiag, P., and Clerici, T. (2009), [Rectosigmoid junction metastasis from melanoma: a case report]. *Gastroenterol Clin Biol* 33, 93–96.

Loffeld, A. and Marsden, J.R. (2005), Management of melanoma metastasis to the breast: case series and review of the literature. *Br J Dermatol* 152, 1206–1210.

Luxman, D., Jossiphov, J., Cohen, J.R., Wolf, Y., and David, M.P. (1997), Uterine metastasis from vulvar malignant melanoma. A case report. *J Reprod Med* 42, 244–246.

Martel, F., Grundemann, D., and Schomig, E. (2002), A simple method for elimination of false positive results in RT-PCR. *Journal of Biochemistry and Molecular Biology* 35, 248–250.

Mostofi, F.K., Davis, C.J., Sesterhenn, I.A., and Sobin, L.H. (1999), *Histological typing of urinary bladder tumours* (Springer Berlin).

Mouawad, R., Sebert, M., Michels, J., Bloch, J., Spano, J.P., and Khayat, D. (2010), Treatment for metastatic malignant melanoma: old drugs and new strategies. *Critical Reviews in Oncology/Hematology* 74, 27.

Nuccitelli, R., Chen, X., Pakhomov, A.G., Baldwin, W.H., Sheikh, S., Pomicter, J.L., Ren, W., Osgood, C., Swanson, R.J., Kolb, J.F., Beebe, S.J., and Schoenbach, K.H. (2009a), A new pulsed electric field therapy for melanoma disrupts the tumor's blood supply and causes complete remission without recurrence. *Int J Cancer* 125, 438–445.

Nuccitelli, R., Chen, X., Pakhomov, A.G., Baldwin, W.H., Sheikh, S., Pomicter, J.L., Ren, W., Osgood, C., Swanson, R.J., Kolb, J.F., et al. (2009b), A new pulsed electric field therapy for melanoma disrupts the tumor's blood supply and causes complete remission without recurrence. *International Journal of Cancer* 125, 438–445.

Nuccitelli, R., Pliquett, U., Chen, X., Ford, W., James Swanson, R., Beebe, S.J., Kolb, J.F., and Schoenbach, K.H. (2006), Nanosecond pulsed electric fields cause melanomas to self-destruct. *Biochemical and Biophysical Research Communications* 343, 351–360.

Pakhomov, A.G., Bowman, A.M., Ibey, B.L., Andre, F.M., Pakhomova, O.N., and Schoenbach, K.H. (2009), Lipid nanopores can form a stable, ion channel-like conduction pathway in cell membrane. *Biochemical and Biophysical Research Communications* 385, 181–186.

Pakhomov, A.G., Kolb, J.F., White, J.A., Joshi, R.P., Xiao, S., and Schoenbach, K.H. (2007a), Long-lasting plasma membrane permeabilization in mammalian cells by nanosecond pulsed electric field (nsPEF). *Bioelectromagnetics* 28, 655–663.

Pakhomov, A.G., Shevin, R., White, J.A., Kolb, J.F., Pakhomova, O.N., Joshi, R.P., and Schoenbach, K.H. (2007b), Membrane permeabilization and cell damage by ultrashort electric field shocks. *Archives of Biochemistry and Biophysics* 465, 109–118.

Perret-Court, A., Fernandez, C., Monestier, S., Millet, V., and Tasei, A.M. (2010), Placental metastasis of melanoma: a new case and literature review. *Ann Pathol* 30, 143–146.

Piel, M., Nordberg, J., Euteneuer, U., and Bornens, M. (2001), Centrosome-dependent exit of cytokinesis in animal cells. *Science* 291, 1550–1553.

Punda, M., Franceschi, M., Rončević, S., Mateša, N., and Kusić, Z. (2010), Intrathyroid metastasis of malignant melanoma: a case report. In *Annual Congress of the European Association of Nuclear Medicine*, vol. 37, 452.

Ramakers, C., Ruijter, J.M., Deprez, R.H.L., and Moorman, A.F. (2003), Assumption-free analysis of quantitative real-time polymerase chain reaction (PCR) data. *Neuroscience Letters* 339, 62–66.

Rigel, D.S., Friedman, R.J., and Kopf, A.W. (1996), The incidence of malignant melanoma in the United States: issues as we approach the 21st century. *J Am Acad Dermatol* 34, 839–847.

Ritz, C. and Spiess, A.N. (2008), qpcR: an R package for sigmoidal model selection in quantitative real-time polymerase chain reaction analysis. *Bioinformatics* 24, 1549–1551.

Romeo, S., Sarti, M., Scarfi, M.R., and Zeni, L. (2010), Modified Blumlein pulse-forming networks for bioelectrical applications. *J Membr Biol* 236, 55–60.

Ruijter, J., Ramakers, C., Hoogaars, W., Karlen, Y., Bakker, O., Van den Hoff, M., and Moorman, A. (2009), Amplification efficiency: linking baseline and bias in the analysis of quantitative PCR data. *Nucleic Acids Research* 37, e45–e45.

Schmidt, J., Riechers, A., Stoll, R., Amann, T., Fink, F., Spruss, T., Gronwald, W., König, B., Hellerbrand, C., and Bosserhoff, A.K. (2012), Targeting Melanoma Metastasis and Immunosuppression with a New Mode of Melanoma Inhibitory Activity (MIA) Protein Inhibition. *PLoS One* 7, e37941.

Schoenbach, K.H., Hargrave, B., Joshi, R.P., Kolb, J.F., Nuccitelli, R., Osgood, C., Pakhomov, A., Stacey, M., Swanson, R.J., White, J.A., et al. (2007),

Bioelectric effects of intense nanosecond pulses. *Dielectrics and Electrical Insulation*, IEEE Transactions *14*, 1088–1109.

Shin, N.Y., Hong, Y.J., Kim, A.H., Shim, H.S., Nam, J.E., Lee, H.J., and Kim, M.J. (2011), Diffuse interstitial infiltrative lung metastasis of malignant melanoma: a case report. *Korean J Radiol* *12*, 252–255.

Siegel, R., Naishadham, D., and Jemal, A. (2013), Cancer statistics, 2013. *CA: A Cancer Journal for Clinicians* *63*, 11–30.

Stoll, R., Renner, C., Buettner, R., Voelter, W., Bosserhoff, A.K., and Holak, T.A. (2003), Backbone dynamics of the human MIA protein studied by ¹⁵N NMR relaxation: Implications for extended interactions of SH3 domains. *Protein Science* *12*, 510–519.

Stoll, R., Renner, C., Zweckstetter, M., Brüggert, M., Ambrosius, D., Palme, S., Engh, R.A., Golob, M., Breibach, I., Buettner, R., et al. (2001), The extracellular human melanoma inhibitory activity (MIA) protein adopts an SH3 domain-like fold. *The EMBO Journal* *20*, 340–349.

Takahashi, I., Sugimoto, S., Nunomura, M., Takahashi, A., Aida, T., Katoh, T., Abe, H., Kojima, H., and Inoue, K. (1990), [A case of cystic metastatic intracranial amelanotic melanoma—analysis of findings in CT and MRI]. *No To Shinkei* *42*, 1031–1034.

Thomas Vernier, P., Sun, Y., Marcu, L., Craft, C.M., and Gundersen, M.A. (2004), Nanoelectropulse-induced phosphatidylserine translocation. *Biophysical Journal* *86*, 4040–4048.

Toledano, H., Visée, C., Arroua, F., Rossi, D., and Bastide, C. (2009), Bladder metastasis of malignant melanoma: a case report and review of literature. *Prog Urol* *19*, 139–141.

Tscheudschilsuren, G., Bosserhoff, A., Schlegel, J., Vollmer, D., Anton, A., Alt, V., Schnettler, R., Brandt, J., and Proetzel, G. (2006), Regulation of mesenchymal stem cell and chondrocyte differentiation by MIA. *Experimental Cell Research* *312*, 63–72.

Turner, S. and Sherratt, J.A. (2002), Intercellular adhesion and cancer invasion: a discrete simulation using the extended Potts model. *Journal of Theoretical Biology* 216, 85–100.

van Groningen, J.J., Bloemers, H.P., and Swart, G.W. (1995), Identification of melanoma inhibitory activity and other differentially expressed messenger RNAs in human melanoma cell lines with different metastatic capacity by messenger RNA differential display. *Cancer Research* 55, 6237–6243.

Vinay, K., Abbas, A., and Fauston, N. (2004), Robbins and Cotran pathologic basis of disease. New York: Saunders , 623–625.

Xiao, S., Guo, S., Nesin, V., Heller, R., and Schoenbach, K.H. (2011), Subnanosecond electric pulses cause membrane permeabilization and cell death. *IEEE Trans Biomed Eng* 58, 1239–1245.

Yeung, R.S. (1994), Management of recurrent cutaneous melanoma. *Curr Probl Cancer* 18, 143–186.

Zhang, J., Blackmore, P.F., Hargrave, B.Y., Xiao, S., Beebe, S.J., and Schoenbach, K.H. (2008), Nanosecond pulse electric field (nanopulse): A novel non-ligand agonist for platelet activation. *Archives of Biochemistry and Biophysics* 471, 240–248.

Zhu, N., Eves, P.C., Katerinaki, E., Szabo, M., Morandini, R., Ghanem, G., Lorigan, P., MacNeil, S., and Haycock, J.W. (2002), Melanoma Cell Attachment, Invasion, and Integrin Expression is Upregulated by Tumor Necrosis Factor α and Suppressed by α Melanocyte Stimulating Hormone. *Journal of Investigative Dermatology* 119, 1165–1171.

APPENDIX

CONVERSION OF G TO RPM

Some centrifuge machines only allow the adjusting of RPM instead of RCF. Therefore, RCF was used to calculate the needed RPM (Equation 4).

$$RCF = 1.118 \times 10^{-5} \times R \times RPM^2 \quad (4)$$

where RCF is the Relative Centrifugal Force (g), R is the rotating radius (cm), and RPM is revolutions per minute.

1. The rotating radius of the low speed centrifuge machine was 16 cm. The required RCF was $125 \times g$.
 $\therefore 125 = 1.118 \times 10^{-5} \times 16 \times RPM^2$. $\therefore RPM = 836$.
2. The rotating radius of the Spectrafuge machine was 6 cm. The required RCF was $125 \times g$.
 $\therefore 125 = 1.118 \times 10^{-5} \times 6 \times RPM^2$. $\therefore RPM = 1365$.
3. The rotating radius of the Spectrafuge machine was 6 cm. The required RCF was $5000 \times g$.
 $\therefore 5000 = 1.118 \times 10^{-5} \times 6 \times RPM^2$. $\therefore RPM = 8634$

VITA

Hongxia Jia
 Department of Biological Sciences
 Old Dominion University
 Norfolk, VA 23529

- **Education**

- Ph.D. in Biomedical Sciences (August 2008 - December 2013)
 Old Dominion University, Norfolk, VA 23529
- M.D. in Clinical Medicine (September 2001 - June 2008)
 Nankai University Medical School, Tianjin, China, 300071

- **Awards**

- Recipient, Graduate Teaching/Researching Assistantship, Old Dominion University, Norfolk, VA, 2008 - 2013.
- Nominee, Outstanding GTA-laboratory, Old Dominion University, Norfolk, VA, 2013
- Nankai University, Tianjin, China
 - * Recipient, Jieping Wu Outstanding Medical Graduate Award, 2008.
 - * Recipient, First Prize, "100 projects" of Creative Research for the Undergraduates Award, 2004.
 - * Recipient, Specialized Scholarship of Excellent Achievement, 2004.
 - * Recipient, Basic Disciplines Scholarship, 2003.
 - * Recipient, The Third Prize Scholarship, 2002.
 - * Recipient, The Second Prize Scholarship, 2001.
 - * Recipient, Merit Student Award, 2001.

- **Publications and Presentations**

- Guo, X., Zhang, L., Jia, H., He, E. and Che, Y. "The Role of Hyperlipidemia in Insulin Resistant Beagle Dog Multi-Organ Injury." Chinese Journal of Cardiovascular Review 2006, 4: 292-294.
- Jia, H., Tan, P., Xiao, S., Pakhomov, R.A. and Swanson, R.J. "High-Voltage Nanosecond Pulsed Electric Fields Induce both Muscular Facilitation and Inhibition in Rats." Bioelectrics 2010, 7th International Bioelectrics Symposium, Norfolk, VA, 2010.